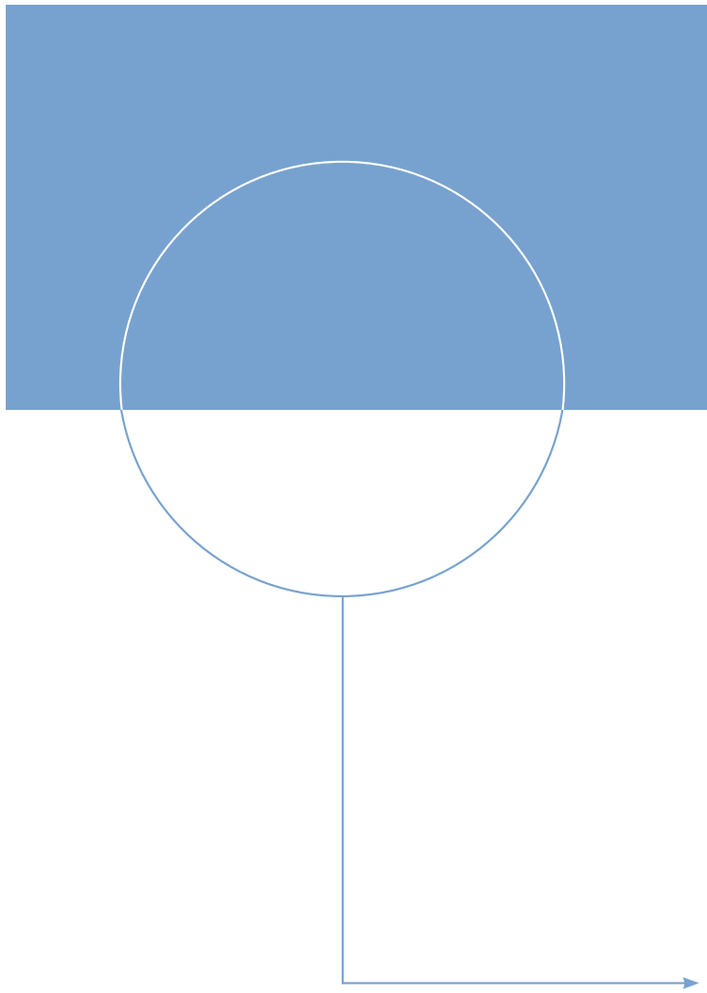

Master's thesis

2019

Espen Sinding-Larsen

NTNU
Norwegian University of
Science and Technology
Faculty of Engineering
Department of Civil and Environmental Engineering

Espen Sinding-Larsen

Runout modelling

Strain softening of landslide debris

June 2019

NTNU
Norwegian University of
Science and Technology

NTNU
Norwegian University of
Science and Technology

NTNU

Norwegian University of
Science and Technology

Runout modelling

Strain softening of landslide debris

Espen Sinding-Larsen

Submission date: June 2019
Supervisor: Jean-Sebastien L'Heureux
Co-supervisor: Zhongqiang Liu

Norwegian University of Science and Technology
Department of Civil and Environmental Engineering

Preface

This study is a Master thesis in TBA4900 as a 30 ECTS course as a part of MSc in Geotechnics in Civil and Environmental Engineering at NTNU. The thesis is carried out in the spring semester in 2019. The project is given by NGI (Stiftelsen Norges Geotekniske Institutt), with main supervisor Dr. Jean-Sebastien L'Heureux at NTNU and Zhongqiang Liu at NGI. Z. Liu was main supervisor for the program BingClaw while L'Heureux was the supervisor for the general task in hand. The aim of this thesis was to find out if the remoulding parameter Γ, can be derived from the post peak behaviour from the triaxial test.

Trondheim, June 12, 2019

Espen Sinding-Larsen

Acknowledgment

I would like to thank my main supervisor Jean-Sebastien L'Heureux for the technical discussions within geotechnics, and the provision of the necessary data needed to do the research done in this thesis. I would also thank NGI for letting me use their database and the modelling tool BingClaw. A big thank to Zhongqiang Liu and Suzanne Lacasse from NGI for this thesis and with access and introduction to BingClaw and access to the database used. We had many interesting discussions that gave insight into the problem in hand.

E.S-L

Abstract

Landslides are a serious problem that must be considered when constructing new infrastructure. There are danger both in front and behind of a initial slide. Even though the terrain is relatively flat. For sensitive clays, the landslide can move retrogressively backwards and sideways and impact large areas behind the initial sliding pit. Depending on the characteristic of the material, the debris can also affect large areas in front of the sliding pit.

This paper will focus on the latter. Specifically the strain softening behaviour of clay studied from curves derived from triaxial tests. If the strain softening behaviour happens fast, the runout distance can be expected to be large. With slow to none strain softening the runout is expected to be short. Different ways to approximate the strain softening behaviour of the clay are pursued. It was found out that the strain softening behaviour the triaxial test shows is most likely only valid for small strains, when comparing the shear stress against the shear strain. Of that reason the best approximation of Γ was derived when the clay was less remoulded than 20%. The remoulding process is in this thesis describe by a remoulding parameter Γ. The different approximations of the Γ -parameter found, was correlated to index parameters. The best correlation found was to the liquidity index. Here Γ was almost constant for liquidity index under 1.2 and nonlinear increasing for liquidity index over 1.2.

Sammendrag

Skred er et alvorlig problem som må vurderes når man bygger ny infrastruktur. Det er fare både foran og bak et innledende skred, selv om terrenget rundt er relativt flatt. For sensitive leirer kan jordskredet bevege seg retrogressivt bakover og sidelengs og påvirke store områder bak den innledende skredgropen. Avhengig av egenskapene til materialet, kan skredmaterialet også påvirke store områder foran skredgropen.

Denne oppgaven vil fokusere på det sistnevnte. Spesielt studere progressivt brudd eller "strain softening" av leire. Treaksiale test er benyttet for å studere denne oppførselen. Hvis "strain softening" oppførselen oppstår raskt, kan utløpsavstanden forventes å være stor. Med langsomt til ingen "strain softening", forventes utløpsavstanden å være kort. Forskjellige måter å tilnærme denne oppførselen er forfulgt. Det ble funnet ut at oppførselen treaksial testen viser er mest sannsynlig bare gyldig for liten tøyning, når man sammenligner skjærspenningen mot skjærtøyning. Av den grunn ble den beste tilnærmingen av Γ avledet da leiren var mindre omrørt enn 20 %. Omrøringsprosessen er i denne oppgaven beskrevet av en omrøringsparameter Γ. De forskjellige tilnærmingene til Γ -parameteren som ble funnet, var korrelert med indeksparametere. Den beste korrelasjonen funnet var flyteindeksen. Her var Γ nesten konstant når flyteindeksen var under 1.2 og ikke-lineære økende når flyteindeksen er over 1.2.

Contents

Chapter 1

Introduction

1.1 Background

A serious problem with debris flows are that it is difficult to calculate the range, velocity and the force. This applies especially for sensitive clays such as quick clay, since the quick clay changes characteristic when being shared. In Norway, quick clay slides is a serious problem. It can be difficult to estimate the magnitude because they many times have a retrogressive nature. BingClaw is made for better calculation of risk in hazard zones, by calculating velocity, runout distance and height.

In a runout model like this there are many uncertainties in the input. This thesis will mainly focus on how BingClaw describes the remoulding process of a clay. BingClaw does this through the parameter Γ.

1.2 Problem Formulation

The paramount problem is to find out if the remoulding coefficient in BingClaw can be decided through index tests. To manage to study the remoulding behaviour, a test which shows how the clay gets remoulded must be chosen. In this thesis the triaxial test is chosen. The subordinate problem would then be to find out if the triaxial test is a trustworthy test to study this behaviour.

1.3 Objectives

The main objectives for this thesis are:

1. Find a suitable model to represent Γ
2. Determine a relationship between index parameter and Γ
3. How good does the triaxial test represent the remoulding process.

1.4 Limitations

Many of the limitations in this thesis are related to uncertainties. First of all the Γ-parameter is to this point an empirical value, derived from parametric studies. Further is the behaviour of the remoulding process at this point not related to shear strain before, and unknown for large strain. The analysis is done from the assumption that the remoulding process can be described by a given equation. The database used in this thesis is not created with this thesis in mind. Thus some triaxial tests are taken with eg. different strain rate.

It may be a big difference in the results if strain localization happens or not. Strain localization is not well documented in the database used, and can not directly be considered.

1.5 Structure of the Report

The rest of the report is structured as followed: Chapter 2 is general theory with regard to the problem in hand. Chapter 3 describes the raw data and how it is processed. Chapter 4 presents the results from the analysis with some interpretations. Chapter 5 discuss the result and compare them to each other. Chapter 6 concludes the study.

Chapter 2

Theory

This chapter will give the basis understanding of quick clay, debris flow, rheology, the program BingClaw and energy calculation. The theory is written with the modelling program BingClaw in mind. The equations in the rheology section is of that reason equations from the BingClaw model.

2.1 Quick Clay

Quick clay or sensitive clay are serious problem in Scandinavia, eastern Canada and some places north in Russia. Quick clay slides have a flow like behaviour which gives the debris the possibility to run long distances. Since quick clay slides also can be retrogressive it can increase risk and endanger lives both in front of and behind the slide. Retrogression is a phenomenon that makes it possible for the slide to dig itself backwards or sideways after an initial slide. The initial slide can uncover a new slope that is not stable which further can lead to a new slide. This behaviour can continue until the sliding pit comes to bedrock or firmer ground, or till a stable slope is established.

Norwegian quick clay is defined as clay with remoulded shear strength S_{ur} under 0.5kP and often a sensitivity S_t over 30. Clay from different places are distinguished from each other because of slightly differently behaviour. For example eastern Canadian clay tend to need more shear before remoulding than Norwegian clay. It has been a cementation effect in the Canadian clay which makes it stiffer (Karlsrud et al., 1985). Cementation of the clay can happen for old clays when the mineralogy in the clay is right. This effect has not happened to Norwegian clay. Quick clay in Norway comes from after the last big ice age and the following rising of the continental plate. Under this time period, the start of the Holocene, sedimentation happened in salt water. The particles flocculated because of the salt, giving the the sediment like a "house of cards" like structure. After the rising of the continental plate some marine clay got above sea level, in Trondheim in Norway this is up to about 180 meters above sea level. Here the salt gets washed out of the clay by rainwater, loosing up the bindings made by salt in the clay. Clay with less salt than 5g/l will exhibit quick behaviour (Sandven et al., 2014). Figure 2.1 shows where water flows interferes with the clay and makes quick clay possible.

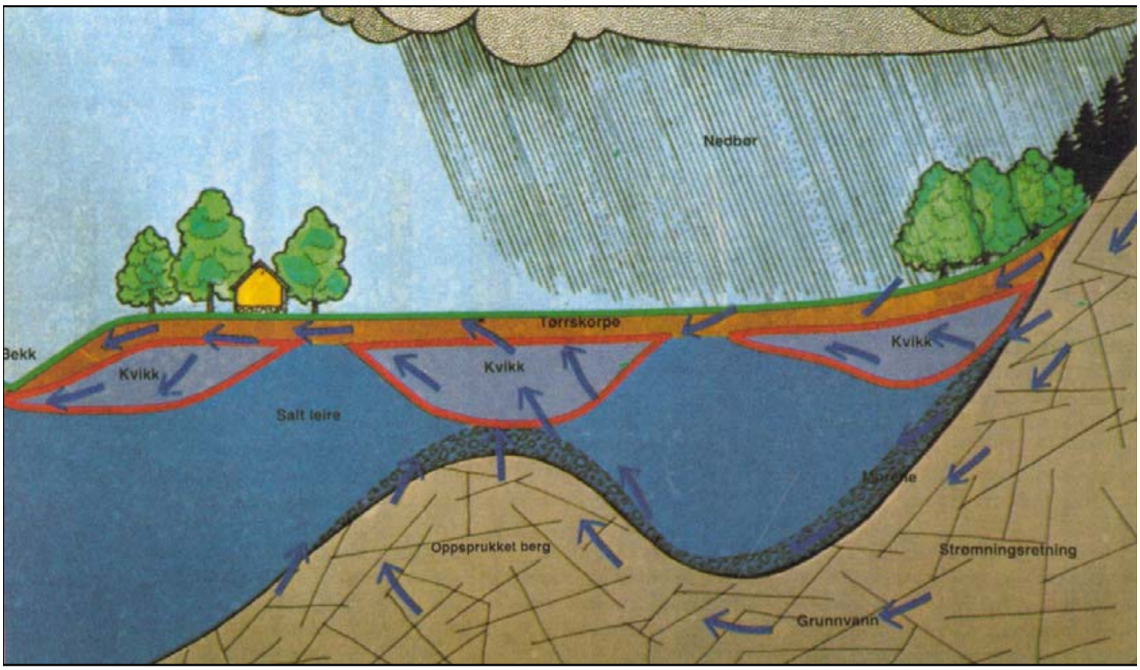

Figure 2.1: Possible places to find quick clay, figure from Løken (1983). The dark blue is salty clay, light blue shows quick clay, orange is the dry crust and the grey is cracked bedrock. The blue arrows shows the flow path

2.2 Debris Flow

Takahashi (2014) defines debris flow as; "a flow of sediment and water mixture in a manner as if it was a flow of continuous fluid driven by gravity, and it attains large mobility from the enlarged void space saturated with water or slurry". He further classify debris flow into three groups: Stony-type, Turbulent-muddy-type and viscous debris flow. Only the viscous debris flow will be discussed here. Viscous flow can best be described as a Herschel-Bulkley fluid as discussed above. The debris will then flow down a slope with a plug layer and a shear layer as shown in figure 2.2. In the plug layer, with a height of $h - h_s$ the material could be undisturbed and will move with uniform velocity. The shear layer will have a parabolic velocity distribution. and it is in this layer the remoulding happens.

The debris flow can either run on top of a rigid bed or in soft deposits. When running on top of a rigid bed Takahashi (2014) describes that the particles on the blunt nose is transported around to the bottom of the nose. In comparison to a quick clay layer this will mean that more of the material will be remoulded and that the slide will become slower. When running on softer deposit the front will erode the bed and mix with it, and the front will not rotate in the same matter as with deposits running on a rigid bed (figure 2.3). The velocity and runout distance is shown to be greater for debris on soft deposits. Even though Takahashi (2014) mostly describes debris flows in rivers, an analogy can be taken from this to a submarine case, where the runout often runs on a soft sea bed deposit.

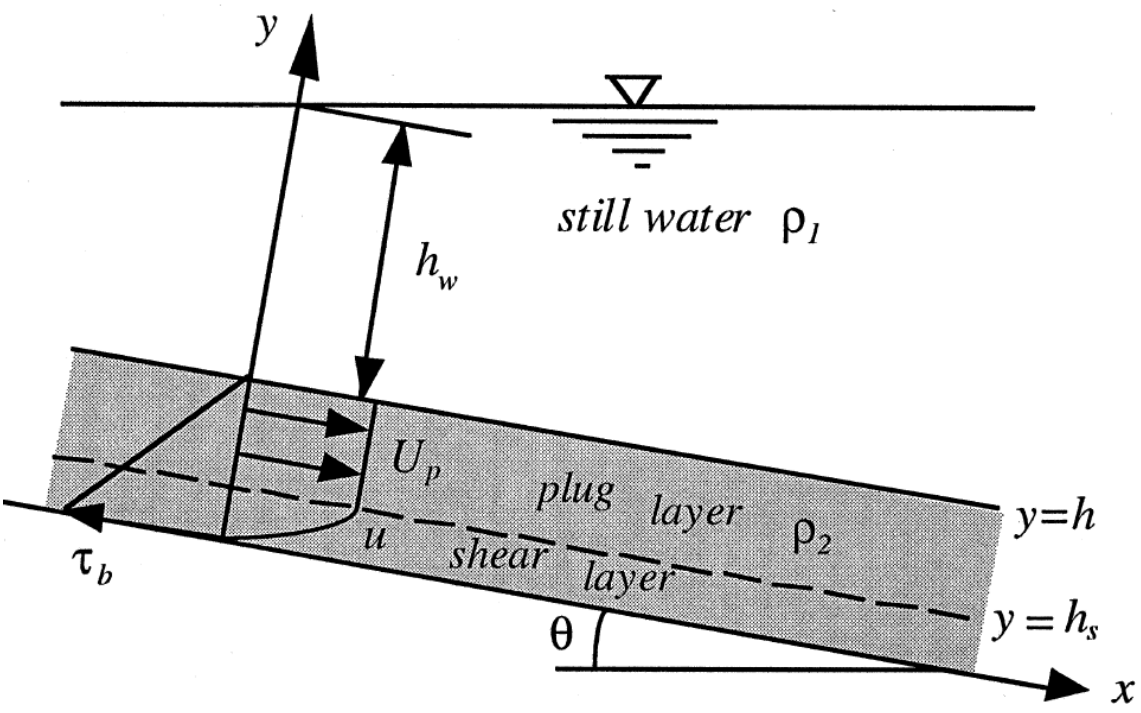

Figure 2.2: The velocity field of a viscoplastic fluid as Herschel-Bulkley fluid, with shear and plug layer. Figure from Huang and Garcia (1999)

2.3 BingClaw

BingClaw is is a numerical model using a deformable mesh within a Lagrangian framework in a Eulerian system to manage to solve the differential equations. It uses the Visco-Plastic, Herschel-Bulkley rheology, with a parabolic form of the debris. From this the moment balance of both the plug and shear layer is solved as shown under.

$$\frac{\delta}{\delta t} \cdot h + \nabla \cdot (h\vec{\mathbf{u}}) = 0 \tag{2.1}$$

$$\frac{\delta}{\delta t}\vec{\mathbf{u}}_p + \vec{\mathbf{u}}_p \nabla \vec{\mathbf{u}}_p + \left(1 - \frac{\rho_w}{\rho_d}\right) \cdot g\nabla (h+b) = \frac{\tau_y sgn\left(\vec{\mathbf{u}}_p\right)}{h_p \rho_p} \tag{2.2}$$

$$\frac{\delta}{\delta t} \cdot (h\vec{\mathbf{u}}) + \left(\left(h_p + \alpha_2 h_s\right)\vec{\mathbf{u}}_p \cdot \nabla\right)\vec{\mathbf{u}}_p + \vec{\mathbf{u}}_p \left(\nabla \cdot \left(h_p + \alpha_2 h_s\right)\vec{\mathbf{u}}_p\right) + \left(1 - \frac{\rho_w}{\rho_d}\right) \cdot gh \cdot \nabla (h+b) \tag{2.3}$$

$$= -\frac{\tau_y sgn\left(\vec{\mathbf{u}}_p\right)}{\rho_p} - \frac{\tau_y \alpha_3}{\rho_d}\vec{\mathbf{f}}_s$$

$$|\vec{\mathbf{u}}| = \frac{h_p + \alpha_1 h_s}{h} \cdot \left|\vec{\mathbf{u}}_p\right| \tag{2.4}$$

Here subscript p refers to the plug layer and subscript s the shear layer. h= $h_s + h_p$ is the height of the slide, u and v is the average velocity. Equation 2.4 describes the average velocity. ρ_w andρ_d denotes the dencity of water and the

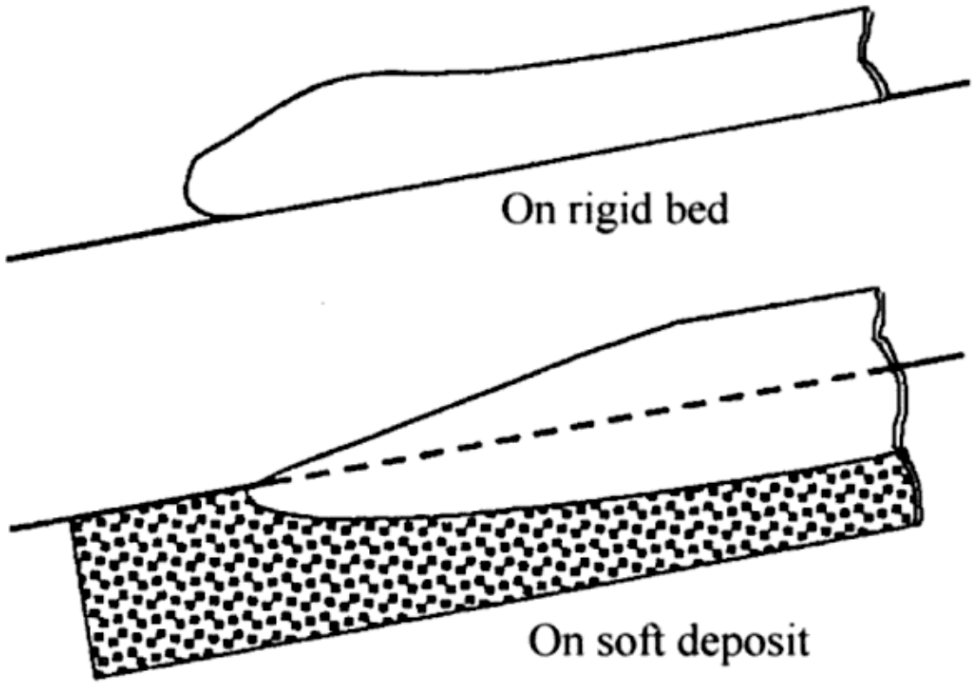

Figure 2.3: Shows how debris flow on rigid bed and on soft bed. Figure from Takahashi (2014)

debris

Løvholt et al. (2017) described the solution of the equation set as following:

> This system of equations is solved in three steps: first, by checking that the Earth pressure exceeds the shear strength, then by solving for the terms without friction numerically using a finite volume formulation [LeVeque (2002)], and finally, using a fractional step method for the frictional terms. The terms α_1, α_2, and α_3 are functions of the Herschel-Buckley parameters n [see, e.g., Huang and Garcia (1997)].

A more thorough discussion of the governing equations is discussed in Imran et al. (2001), and will therefore not be further discussed here.

Clawpack is added to the old program Bing to create BingClaw. Bing is already tested on multiple slides and tested on e.g. the 1978 Rissa slide in Norway byL'Heureux et al. (2012). The Bing model was extended from a quasi-2D model to a quasi-3D model and needed a new software to solve the PDEs in this framework. Therefore the Clawpack software was added. Clawpack is a PDE solver "of the conservation laws with adaptive mesh refinements" (Kim, 2015). and is mainly made by LeVeque (LeVeque, 2002).

Some other enhancements form the Bing model is that hydrodrag is now accounted for. The model also accounts for added mass, which makes it possible for the debris to gain mass while sliding. This makes BingClaw better to model submarine slides than Bing. BingClaw does also take the remoulding effect as described earlier into consideration. See Kim (2015) for a more detailed description.

2.4 Rheology

The rheology of a viscous medium is different in different fluids or soils. While water have a rheology equal to a Newtonian fluid, sensitive clay will have a thinning effect with strain and therefore behave more like a Bingham fluid or Herschel-Bulkley fluid, figure 2.4. The Bingham plastic model may overestimate the true yield stress significantly due to the shear thinning at low shear rates (Zhaohui, 1982; O'Brien and Julien, 1988). Huang and Garcia (1998) describes that the Herschel-Bulkley better fits rheological data well over a wide range of strain. For that reason the Herschel-Bulkley model might be better for modelling debris flow. The Herschel-Bulkley model says that the soil must reach a specific capacity before the shearing starts, the strain rate will thereafter considerately increase with a small increase of stress. From equation 2.5 it is shown how the yield strength is dependent on the shear rate. This means that shear strength will decrease with bigger shear rate. The equivalent of this is to move line 4 in figure 2.4 vertical down. A direct result from this is that the shear rate will increase if shear stress is held constant.

$$\tau_y(\gamma) = \tau_{y,\infty} + (\tau_{y,0} - \tau_{y,\infty}) \cdot e^{-\Gamma\gamma} \tag{2.5}$$

$$\gamma = \int_0^t \left|\left| \frac{\delta \vec{\mathbf{u}}}{\delta z} \right|\right|_{z=0} dt = \frac{n+1}{n} \int \frac{||\vec{\mathbf{u}}_p||}{h_s} dt \tag{2.6}$$

In equation 2.5 $\tau_{y,0}$ is the initial shear strength, $\tau_{y,\infty}$ is the residual shear strength, γ the total shear strain described by Eq.2.6 and Γ the coefficient to decide remoulding speed. Γ is usually between 0.01 and 0.1 for medium sized slides such as for Rissa and Kattmarka slide, and even smaller for bigger slides such as Storegga. For bigger landslides Γ is normally between $5 \cdot 10^{-4}$ and $5 \cdot 10^{-3}$ (Jihwan, 2017).

The Herschel-Bulkley rheology can be described as

$$\left|\frac{\dot{\gamma}}{\dot{\gamma}_r}\right|^n = \begin{cases} 0 & \text{if } |\tau| \leq \tau_y, \\ \dfrac{\tau}{\tau_y \cdot sgn(\dot{\gamma})} - 1 & \text{if } |\tau| > \tau_y \end{cases} \tag{2.7}$$

where $\dot{\gamma}$ is a strain rate, $\dot{\gamma}_r$ is a reference strain rate defined as $\dot{\gamma}_r = (\tau_y/\mu)^{1/n}$ with a dynamic viscosity μ and an exponent n (Jihwan, 2017). n is a parameter between 0 and 1 where as for n=1 the model is equal to Bingham fluid.

2.5 Calculation of Energy in Debris Flow

In a energy perspective of debris flow the potential energy (E_P) of the debris masses gives the driving energy while friction (E_F) and remoulding energy (E_R) contributes to dissipation. The total energy(E_T) can be described through equation 2.8 (Vaunat and Leroueil, 2002), with kinetic energy as E_k.

$$\Delta E_T = \Delta E_P(t) + \Delta E_F(t) + \Delta E_R(t) + \Delta E_k(t) = 0 \tag{2.8}$$

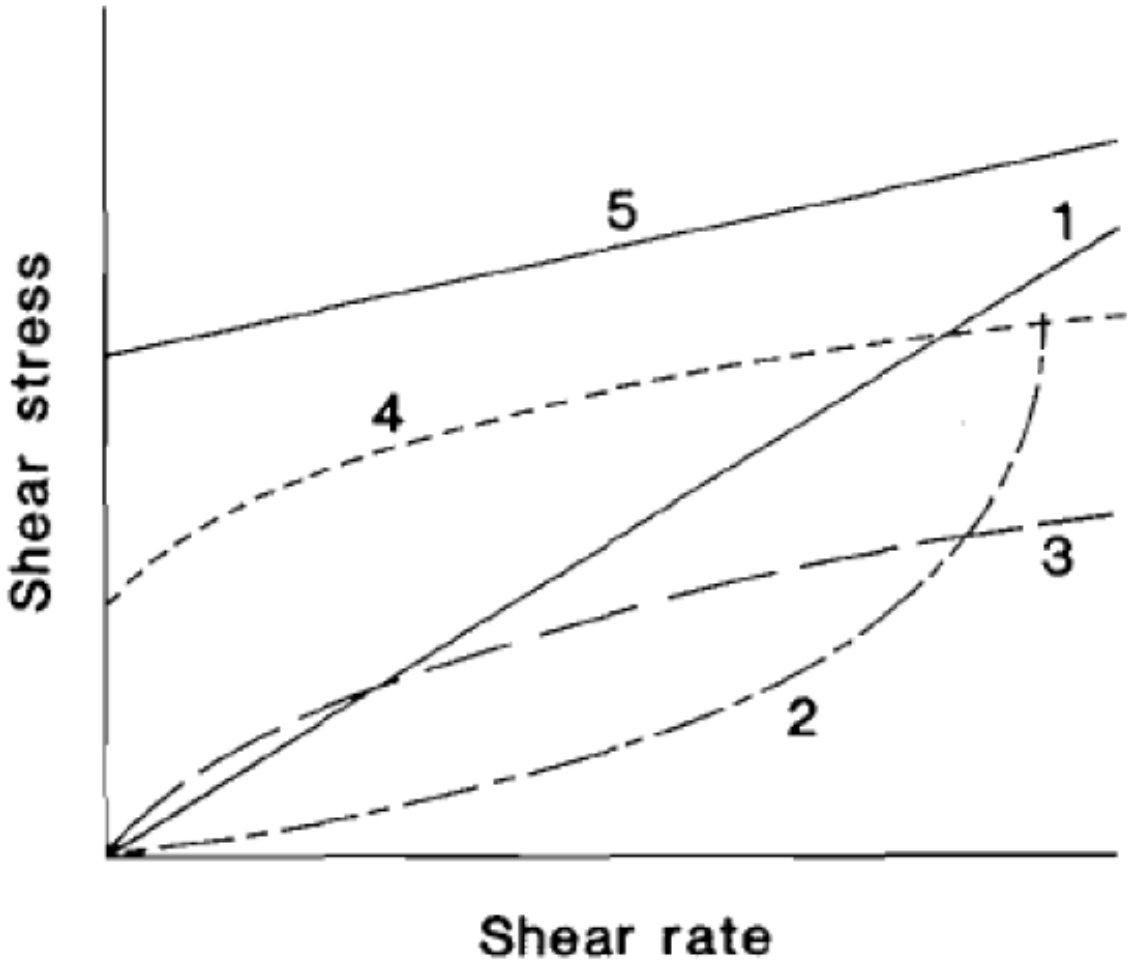

Figure 2.4: Representation of the relationship between shear rate and shear stress for different type of fluids: (1) Newtonian, (2) shear-thickening, (3) shear-thinning, (4) Herschel-Bulkley and (5) Bingham, figure collected from Issler et al. (2013)

The potential energy is further described as

$$E_P = H_G \cdot \gamma \cdot V \tag{2.9}$$

where γ is the average unit weight, H_G is the vertical displacement and V is the total volume of the landslide.

The remoulding or disintegration energy is the energy used to change the strength of the material from initial to remoulded state. It is different ways to find this energy. Tavenas et al. (1983) tested different methods to find this energy by simulating processes the sample could encounter in a landslide. The processes could be shear along a surface, extrusion and squeezing between intact soil or rock, impact of falling objects or impact along the surface. These processes were simulated by lab experiments shown in figure 2.5

Tavenas et al. (1983) recommended that simple shear test was best suited to investigate the disintegration process

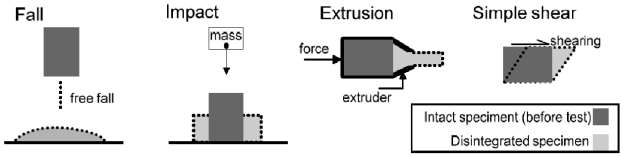

Figure 2.5: Shows different lab testes Tavenas et al. (1983) did to find the disintegration energy

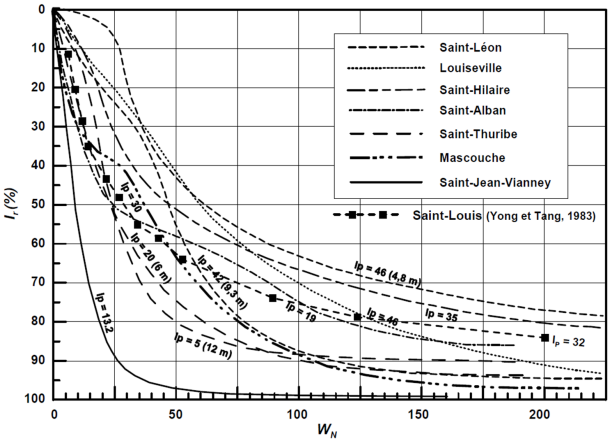

Figure 2.6: Modified figure of remoulding energy, from Locat et al. (2008).

of sensitive clay. To describe in what degree the clay was remoulded he used the remoulding index equation 2.10.

$$I_R = \frac{S_u - S_{ux}}{S_u - S_{ur}} \tag{2.10}$$

Where S_u is the shear strength, S_{ur} is the remoulded shear strength of the material and S_{ux} is the shear strength at a given strain.

Tavenas et al. (1983) represented the energy by taking the remoulded energy defined as the integrated area under $\tau - \gamma$ graph from max shear strength and divided it on a reference energy $0.013 \cdot \sigma_P$ (Tavenas et al., 1979). The reference energy is the energy to reach maximum shear strength for Canadian clays. Locat et al. (2008) continued with this idea and modified a figure from Tavenas et al. (1983) with a representation of the plasticity index seen in Figure 2.6

Thakur et al. (2015) tried to recreate some similar results by using an electric field vane by analysing the shear stress vs vane rotation graph. The domain used was only a rotation up to 90 degrees. The area under this graph is equal to the disintegration energy. He found that the electronic vane test gave significant results in explaining the disintegration energy, and shows that an unconventional use of the vane apparatus can give information of the disintegration energy.

Turmel et al. (2018) has also done similar work. He calculated the remoulding energy in a triaxial domain, and used the result to find an Energy Reduction Factor. This factor is used to take the remoulding effect into consideration in the software InterFOAM. This thesis has tried to recreate some of this work, and will be presented in 4.1.

Chapter 3

Data processing

This chapter presents the data, and how the data is processed.

3.1 Sample data

The data used is gathered by Karlsrud and G. Hernandez (2012). All of the samples used in the analysis is high quality samples. They are extracted using a Shearbrook block sampler with sample diameter of 250mm and sample height equal to 350mm. Some of the reasons that this sample method is superior to for example 54mm, 72mm and 95mm sampler, is that it better keeps the in situ properties. The smaller samplers disturb the material more, and during storing and transporting the smaller sample sizes looses more water content and strength properties. This may also change the structure of the material (Karlsrud and Hernandez-Martinez, 2013). Figure 3.1 describes the difference between the response curve for different sample sizes for both a triaxial test and an oedometer test. The block sample gives a more sharp response, and makes it easier to interpret the result than the smaller samples. From the triaxial test it is also shown that the block sample goes faster to remoulded state. This fact may make it easier to estimate remoulded energy.

From their study all parameter from triaxial and oedometer tests can be extracted plus the following index parameters: water content (w), Atterbergs limit (w_P and w_L), liquidity index (IL), plasticity index (I_P), clay content (cc), peak shear strain (γ_{peak}, peak strain from triaxial test), maximum undrained share stress (S_u), remoulded shear stress (S_{ur}), effective stress (σ'), preconsolidation pressure (p_c) and over consolidation ratio (OCR). These are the parameters mainly used in this thesis.

3.1.1 Missing Values

All values or index parameters were not recorded from every site. These sites were excluded from the analysis, if an analysis required missing values from these given sites. See Table A.1 in Appendix A.

In some cases the sensitivity were decided using vane test instead of fall cone test. The vane test will in many

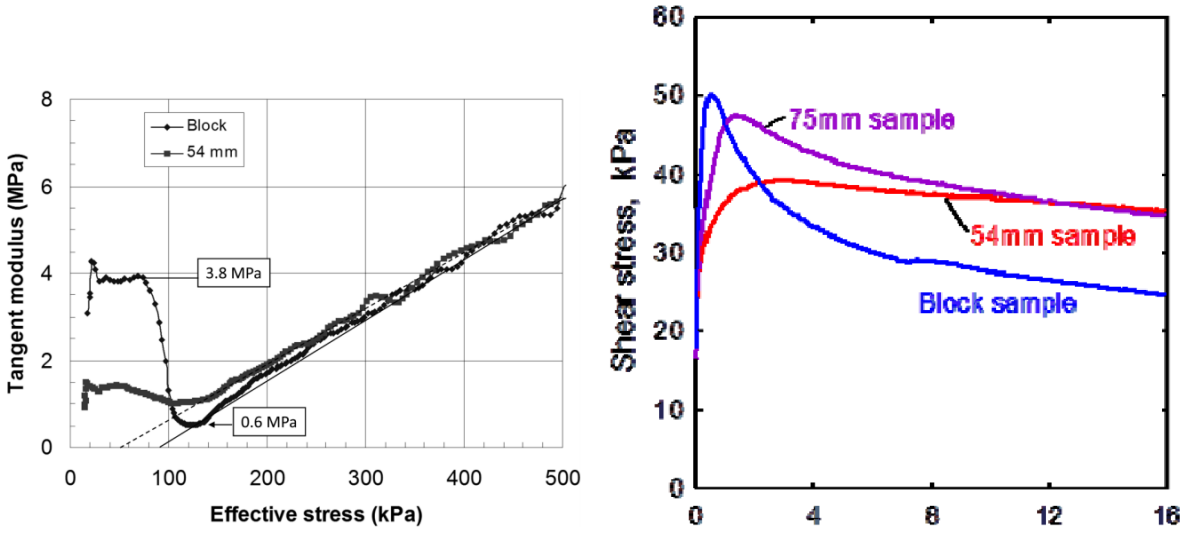

Figure 3.1: Figure to the left shows the response curve for an oedometer test for both a block sample and 54mm sample (Karlsrud and Hernandez-Martinez, 2013). Figure to the right shows response curves for a triaxial test for block sample, 75mm sample and 54mm sample. (Lunne et al., 1997)

cases give a higher value for remoulded shear strength than the fall cone test, especially for high sensitive materials. This is mainly because the vane does not record strength under 0.5kPa and the rod friction may also contribute to an error in the recorded strength (Karlsrud and Hernandez-Martinez, 2013). From some of the cases where the vane test was used to decide sensitivity, the shear strength and remoulded shear strength was not necessary given. Thus the shear strength was calculated from triaxial test, and the remoulded shear strength was further derived from the sensitivity and the maximum shear strength.

3.1.2 Variation of Data

The data in the high quality database form Karlsrud and G. Hernandez (2012) includes both sensitive and non-sensitive clays. In Table 3.1 an overview of the range of the different index parameters is shown. More detailed information is shown in appendix A.

3.2 Triaxial Test

Triaxial test is one of the best laboratory test to find the in situ maximum shear stress (S_u) the clay can resist. Compared to uniaxial test the triaxial test has a confining pressure greater than zero, $\sigma_3 > 0$. A common triaxial test is the CAU_C test (Consolidated Anisotropic Undrained Compression test). CAU_C has been preformed on all samples used in this study. It exists other types of triaxial tests which is loaded and consolidated differently, but they will not be further discussed since they are not used in this study. Anisotropic consolidation means that the axial pressure is greater than the confining pressure, $\sigma_1 > \sigma_3$. This is to reflect the in situ stresses in a best possible way.

When a sample is taken from the soil the stress situation of the sample will change due to unloading. Samples

Table 3.1: Shows max, and mean for the parameters used further in the study

	Max	Mean	Min
pc [kPa]	475	225.48	86.4
γ_{peak}	6.1 %	1.3 %	0.2 %
OCR	6.49	2.57	1.1
w_L	74.0 %	34.5 %	22.5 %
w_P	33.3 %	20.7 %	9.9 %
I_P	41.5 %	13.7 %	3.9 %
LI	3.0815	1.5423	0.5797
w	64.3 %	37.5 %	25.3 %
cc	64.5 %	37.8 %	21.5 %
σ' [kPa]	227	100.69	28.9
S_u [kPa]	100.8	48.338	14
S_{ur} [kPa]	20.16	3.3453	0.144
St	240	55.801	4
Quality, Δ e/ei	0.0643	0.0262	0.0013

that initially are experiencing high stress levels, can change structure when unloaded. This may give the test some errors. The consolidation brings the sample back to its in situ stress condition, and removes some of the error made from unloading. After the consolidation process the area of the sample must be correlated, since the consolidation will squeeze the sample together and therefore increase the area in the axial direction. This is done by Eq. 3.1. Since the sample will bulge out when being sheared, the area must in this phase be corrected more. This is done with Eq. 3.2. This correction is especially important with regard to large strain. (Sandven et al., 2014; Karlsrud and G. Hernandez, 2012)

$$A_a = A_0 \left(\frac{1 - \frac{\Delta V}{V_0}}{1 - \frac{\Delta V}{3V_0}} \right) \tag{3.1}$$

$$A_S = \frac{A_a}{1 - \epsilon} \tag{3.2}$$

Where A_a is area after consolidation, A_0 initial build-in area, V_0 initial build-in volume, ΔV expelled water volume in the consolidation phase and ϵ is the axial strain in the shear phase.

Thakur (2007) describes in his PhD how the thickness of the shear band depends on the post peak behaviour. In undrained conditions the rate of shear strength reduction will increase with a small shear band thickness and decrease with a larger shear band thickness. Thakur (2007) also defines three different failures from the triaxial test. Strong discontinuity localized failure, weak discontinuity localized failure and diffuse failure, see Figure 3.2. Strong discontinuity localized failure describes a very brittle material behaviour with a thin shear band, with shear band thickness close to zero. This failure is locally undrained. For the sample this means that the excess pore pressure will build up in the shear band and decrease in the rest of the sample, which will experience elastic unloading. Therefore the shear strength reduction will increase fast with axial displacement. The weak discontinuity localized failure have a thicker shear band. This is defined as locally drained. Dependent on how much pore pressure build up and how much pore water that can dissipate. In other words; rate of displacement vs permeability. By letting some pore

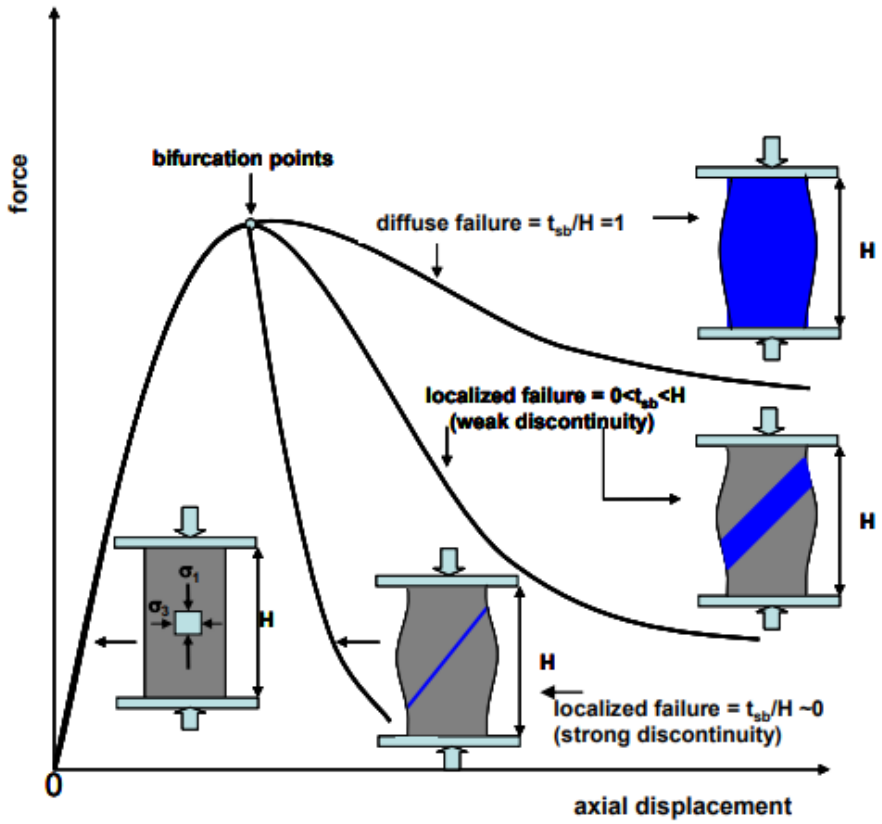

Figure 3.2: Shear band thickness dependent post peak behaviour, Thakur (2007)

pressure dissipate, a thicker shear band will form. Even though a thick shear band initially is induced it will often shrink.

A diffuse failure to a triaxial specimen can happen when loading at a so slow rate that the pore pressure can equalize through the whole specimen. Thus no localization happens due to pore water flow.

When talking about landslides it is the strongly discontinue localized failure that is most relevant. In a landslide the initial fracture will not happen so slow that pore water has the possibility to dissipate. The landslide is instead subjected to a large strain rate right after the initial failure.

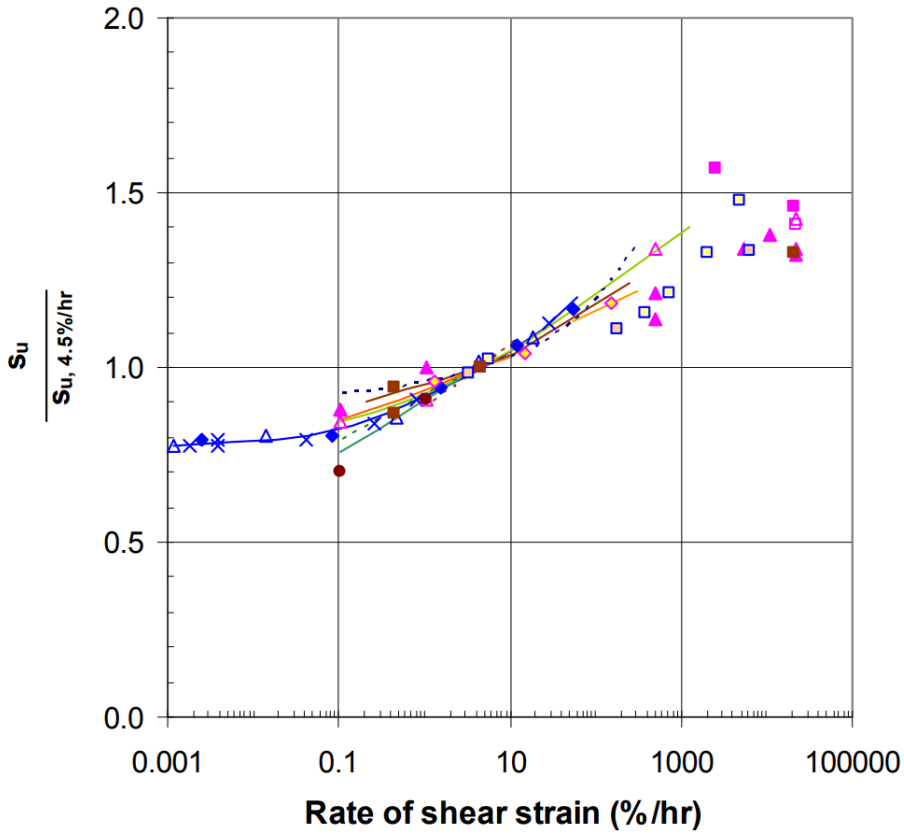

Figure 3.3: Strain rate dependent shear strength (Lunne et al., 2007)

The wanted result from a triaxial test is to find the shear strength when the pore pressure is equal in the whole sample, and not locally build up pore pressure. This is a reason to run the triaxial test with a slow rate. Also when increasing the strain rate, the shear resistance of the clay increases as seen in Figure 3.3. In the database presented all of the triaxial tests are done with a strain rate between 0.7 and 1.5 %/hr. Within this range there are no significant change in the undrained shear strength, and the errors induced by this will be small. The shear strength is therefore not corrected due to strain rate, but at the same time it could explain some of the errors in the result.

The localization is not taken direct into consideration in this study because it is difficult to determine the thickness of the shear band, and will be a subject to error. But it will be discussed in relation to the results in Chapter 5.

3.3 Multivariate regression

A method to correlate parameters to each other is by regression analysis. With this, Γ can possibly be correlated to index properties, or other correlations can be found. A multivariate regression is a linear regression with one dependent variable (**Y**), the response which is wanted from the regression, and more than two predictors (**X**), or also called independent variables. If it is only one predictor it can be called a simple regression. In Chapter 4 curve fit analysis were done to estimate the dependent variable, Γ. This parameter was then correlated to index parameters by multivariate analysis. The method is described below. The software used for multivariate analysis is Minitab.

The best combination of the independent variables is first to be found. Of that reason a best subset analysis is conducted. From this values for R^2, $R^2(adj)$, $R^2(pred)$, Mallows Cp and S were given for every subset. The ranking of the different subset goes in the following order:

1. Find the highest value of R^2
2. Find the highest value of $R^2(adj)$
3. Find the highest value of $R^2(pred)$
4. Find out if is is a large drop between R^2(adj) and R^2(pred)
5. Find the Cp closest to the number of predictors plus the constant 1

R^2 describes how much of the variance in the dependent variable that can be described by the independent variables. R^2(adj) is the adjusted value of R^2, with regards to number of independent variables in the expression. This is because an increase in independent variables can increase R^2, but not necessary increase the quality of the model. When a new predictor is added and the R^2(adj) increases, indicates a better model. The R^2(pred) says how well the model behaves and can predict response by adding new observations. A large drop from R^2(adj) to R^2(pred) indicates overfitting. Overfitted models are "models that contain more unknown parameters than can be justified by the data" (Everitt and Skrondal, 2010). The mallows C_P gives an indication of the bias of the model and can be helpful when choosing the right regression model, when choosing a low value close to the number of predictors. Mallows C_P compares the different subset of predictors to each other and will with confident help to find the better model (Mallows, 1973).

3.3.1 Correlations

Multicollinearity and overfitting can be a problem for multivariate regression. These problems are based from the fact that some variables can describe the same thing and the regression does not necessary become better from including more independent variables. When eg. an independent variable goes up another could go equally down and reset the problem. Therefore it is wise to choose the variables that describes different aspects in the problem.

The goal with multivariate regression is that the independent variables used does not correlate to each other, but correlate to the dependent variable. It is of that reason wise to check if any of the independent variables correlate

to each other. This is done by finding the correlation coefficient and the representative P-value. The correlation coefficient describes the linear dependency between two variables. The P-value says how well the null hypothesis is rejected. The null hypothesis in this case is that there are no correlation. If the P-value is less than 0.05 we say that the correlation is statistical significant. Rephrasing: It is a correlation.

Table B.2 in the appendix shows if the correlations is statistical significant and B.1 show shows the corresponding correlation coefficient. In some cases this will not be sufficient, since it might be multiple trends eg. two different linear trends. It is also possible that correlation is dependent in a different pattern, eg. in a non-linear pattern that this type of analysis can not find significant. A check of the scatter plots can therefore be done to check if there are any other correlations that could be interesting before starting a regression analysis.

3.3.2 Curve Fitting

MATLABs curve fitting toolbox makes it possible to find the best linear/nonlinear fit to a problem using regression. The advantage of this toolbox is that it gives the possibility to implement custom equations eg. Eq.2.5. The curves are fitted by the fit curve function, and it uses least square method that will give the curve with highest R^2 value. The R^2 value gives the sum of squared residual over the sum of the squared residual to the mean.

This toolbox is used when trying to find a correlation for different curve forms. Further discussion about this is done in section 4.1.2 and 4.2.

From a subset analysis a regression analysis with the most suitable parameter can be made. A check of the P-value and the VIF gives a good control to if the coefficients are accurate and if there are multicollinearity. The P-value tells if the coefficient is significant to the model. P-Value less than 0.05 is usually set as the level a coefficient is significant. P-value under 0.1 is often set as a slight significance and can be used, and a P-value above 0.1 is most likely not significant. Then the coefficient should be removed from the model. The VIF, or variance inflation factor, is a factor that says how much the variance increases because of collinearity. A strong indication of high multicollinearity is when the VIF is above 10. When this happens one or multiple parameters in the regression should be removed Neter et al. (1996).

Chapter 4

Results and Interpretation

This chapter presents and discuss all obtained results section wise. Comparison between the results will first be discussed in Chapter 5. In this chapter the triaxial curve is only studied from peak shear strength as shown in Figure 4.1 below. This part of the curve is defined as the remoulding curve.

4.1 Normalization of Specific Energy

The specific energy, the area under $\tau - \gamma$-graph $[J/m^3]$ from the triaxial test, is normalized to get a denomination free parameter at the x-axis, Eq. 4.1. The intention is to include just the remoulding energy. The energy used to reach shear strength of the clay is for that reason not included. In this thesis γ is defined from the peak shear stress. $\gamma = \gamma^* - \gamma_{peak}$, see Figure 4.1. After the remoulded energy (E_R) is calculated it is normalized and plotted against the remoulding index (I_R), see Equation 4.1 and 2.10. Form this plot between a normalized energy (E_N) and I_R. A check

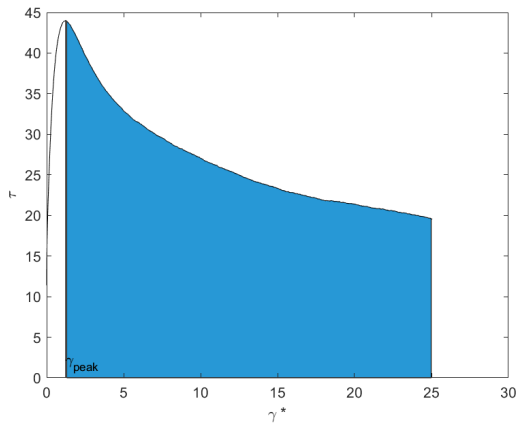

Figure 4.1: Sketch over the domain used from the triaxial tests

is done to find if there are any correlation, which will be presented in Section 4.1.1. E_N can be described as:

$$E_N(\gamma) = \frac{E_R(\gamma)}{N} \tag{4.1}$$

Where N is a normalization parameter consisting of either [1 atm= 100kPa, S_u, C_{ur}, p_c (pre consolidation pressure) or σ' (in situ effective stress)] multiplied (or divided) with none, one or multiple of the following index parameter [OCR, w, w_P, w_L, I_P, LI, cc (clay content) or γ_{peak}(shear strain at peak for triaxial tests)]. The numbers in percent is represented as numbers between zero and one. This gives a unitless parameter, $\frac{kJ/m^3}{kPa} = []$

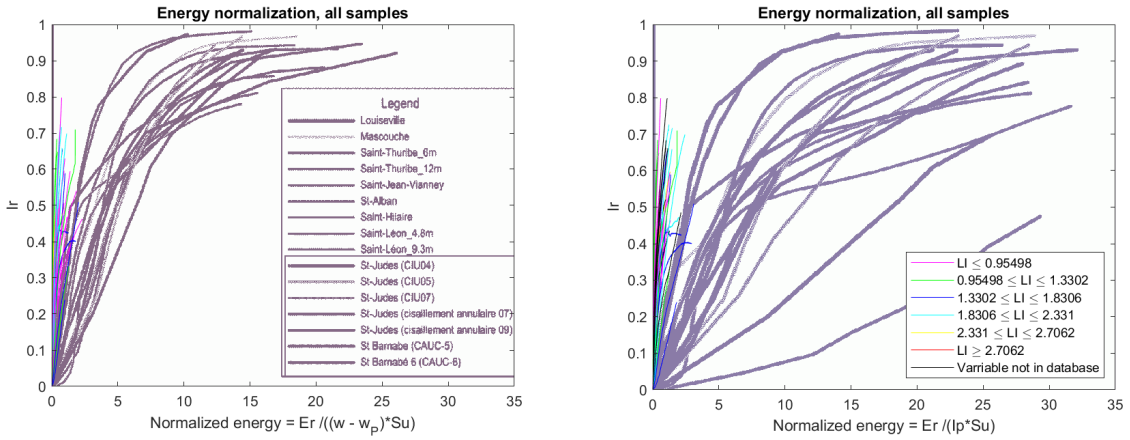

Figure 4.2: Normalization done by Turmel et al. (2018) in gray, included Norwegian clays in colours

As previous mentioned Turmel et al. (2018) did some work with normalization of the remoulding energy from the triaxial test. Figure 4.2 shows the normalization Turmel did, with a comparison with the Norwegian clays described in section 3.1. One difference between the methods used to find I_R for triaxial tests is that the Canadian clays used an residual strength interpreted from the triaxial test instead of remoulded strength in Eq. 2.10. The interpreted residual was found when the shear stress from the triaxial test reaches a "plateau". The Norwegian clay in this study uses either remoulded strength obtained from fall cone or vane test, which gives a much smaller strength. Because of this, I_R from the Norwegian clay is lower than I_R for the Canadian Clay

The Canadian triaxial samples used, from Figure 4.2, was not block samples. They will of that reason most likely show a less brittle behaviour. If the Canadian clay was taken with a block sampler the samples would accumulate more remoulding energy at small strain but the later energy response would be lower, see Figure 3.1. With this in mind Figure 4.2 shows that all of the Norwegian clays behave more brittle than the Canadian clay, and that it needs less energy to remould. A reason could be the cementation effect in Canadian clay as mentioned in Section 2.1.

4.1.1 Method to get optimal normalization

From this section on, only Norwegian clay will be considered.

The spread of the Norwegian clay using the normalization in Figure 4.2 was quite large, see Figure 4.3. For that reason an attempt to make a better normalization was made. First the $I_R - E_N$ graph was represented without any

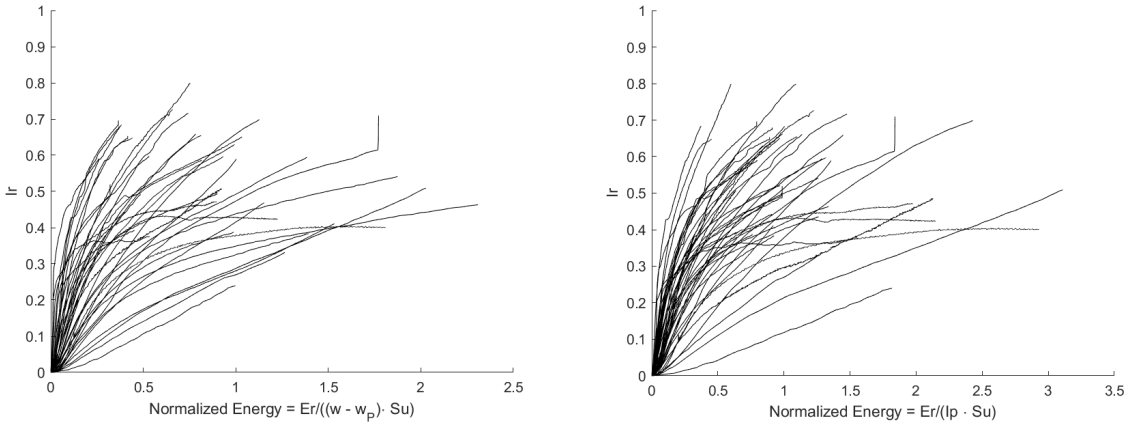

Figure 4.3: Normalization done by Turmel et al. (2018), for only Norwegian clay

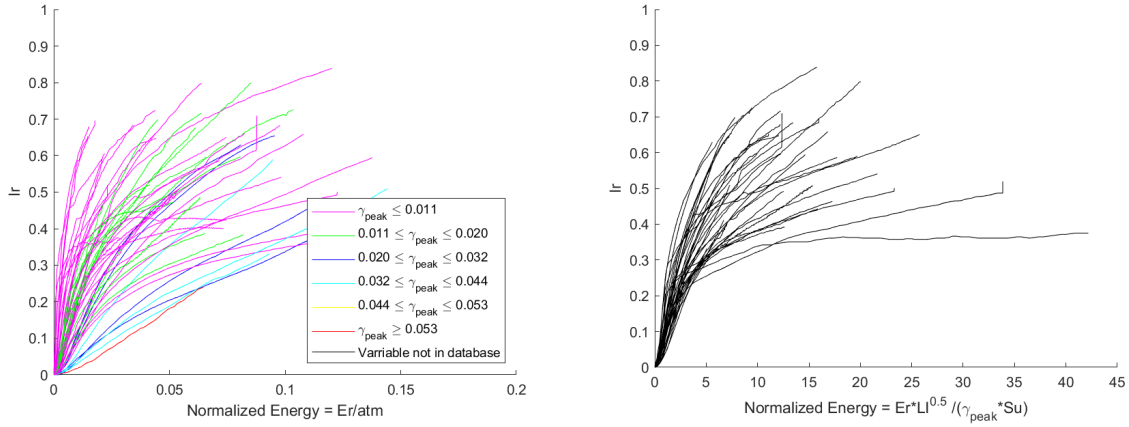

(a) No normalization

(b) Best found normalization

Figure 4.4: Difference between no normalization an a potentially best normalization

variable normalization, $N = 1atm = 100kPa$. A third parameter is represented by colours depended on the size of the third parameter to the given triaxial plot. An example is shown in Figure 4.4a. Here the order of size for γ_{peak} is emphasized with colour. The same normalization is shown with all the different index parameters in the legend, which can be seen in Appendix C.1. The parameter that showed the best increasing trend was then included to the normalization parameter N (Eq. 4.1). A new printout was done, Appendix C.2, and a new parameter to be included to the parameter N was chosen. This was done until no new trends could be seen, see Appendix C.2 - C.5 for details. A possibly best normalization was found, see Figure 4.4b. The reason there are fewer number of lines in Figure 4.4b than in Figure 4.4a, is that for some samples not all parameters (eg. LI) was added to the database.

4.1.2 Curve fitting in I_R domain

It is possible to describe the curve of a triaxial test by fitting a chosen curve to the remoulding curve. Equation 4.2 to 4.5 gave a very good fit to the remoulding curve in the $I_R - \gamma$ domain.

$$I_R = a + b \cdot ln\left(c \cdot \gamma\right) \tag{4.2}$$

$$I_R = a + b \cdot \gamma^c \tag{4.3}$$

$$I_R = \frac{a + b \cdot \gamma}{c + \gamma} \tag{4.4}$$

$$\gamma = a * e^{b \cdot I_R} \tag{4.5}$$

In equation 4.2 to 4.5 a, b and c is constants, γ is the shear strain and I_R is the remoulding index. The curve fitting constants were saved for every triaxial test and compared to the index properties to the clay to see if there were any correlations. The goal was that the constants could be described by index properties. In general the constants a,b and c did not correlate to the index parameters. (Correlation coefficient around zero and random skater around this line). There were one exception, which was that constant a in equation 4.4 and 4.5 correlated to γ_{peak}. The b- and c-coefficient did also highly correlate to each other. This could lead to a multicollinear problem when interpreting I_R. Since the other constants b and c could not be sufficient described by other index parameters, the equations were discarded.

4.1.3 Concluding Energy and Ir-domain

In Section 4.1.2 a regression between the remoulding curve in the I_R-γ domain was done. The idea was to find an equation that fits the remoulding curve in this domain, find index parameters that correlated to the coefficients in the equations and then find a relation to Γ. This analysis ended when the index parameters did not correlate sufficient to the coefficients in the equations. It could still be interesting to see if there are an equation where the coefficients correlates sufficient to the index parameters.

There is also a problem regarding the relation to Γ. This was not studied due to time restrictions with the thesis.

4.2 Curve Fitting of Triaxial Plot

As seen in the previous section, curve fitting of curves in $I_R - \gamma$ domain did not give any sufficient results. Another more direct approach was therefore studied. BingClaw implements the strain softening as explained from equation 2.5. By comparing this equation to the triaxial curve with Γ as the unknown constant, every fit will get an unique Γ dependent on the inclination to the triaxial test. This may further be compared and correlated to the index properties. Two different models were developed to describe the strain softening behaviour. The models does only describe the remoulding process to the clay, by a remoulding curve.

$$Mod1: \quad \tau_y(\gamma) = \tau_{y,\infty} + (\tau_{y,0} - \tau_{y,\infty}) \cdot e^{-a1\gamma}, \quad \Rightarrow \quad \Gamma = a1 \tag{4.6}$$

$$Mod2: \quad \tau_y(\gamma) = \tau_{y,\infty} + (\tau_{y,0} - \tau_{y,\infty}) \cdot e^{-a2\gamma^{b2}}, \quad \Rightarrow \quad \Gamma = \frac{a2}{\gamma^{1-b2}} \tag{4.7}$$

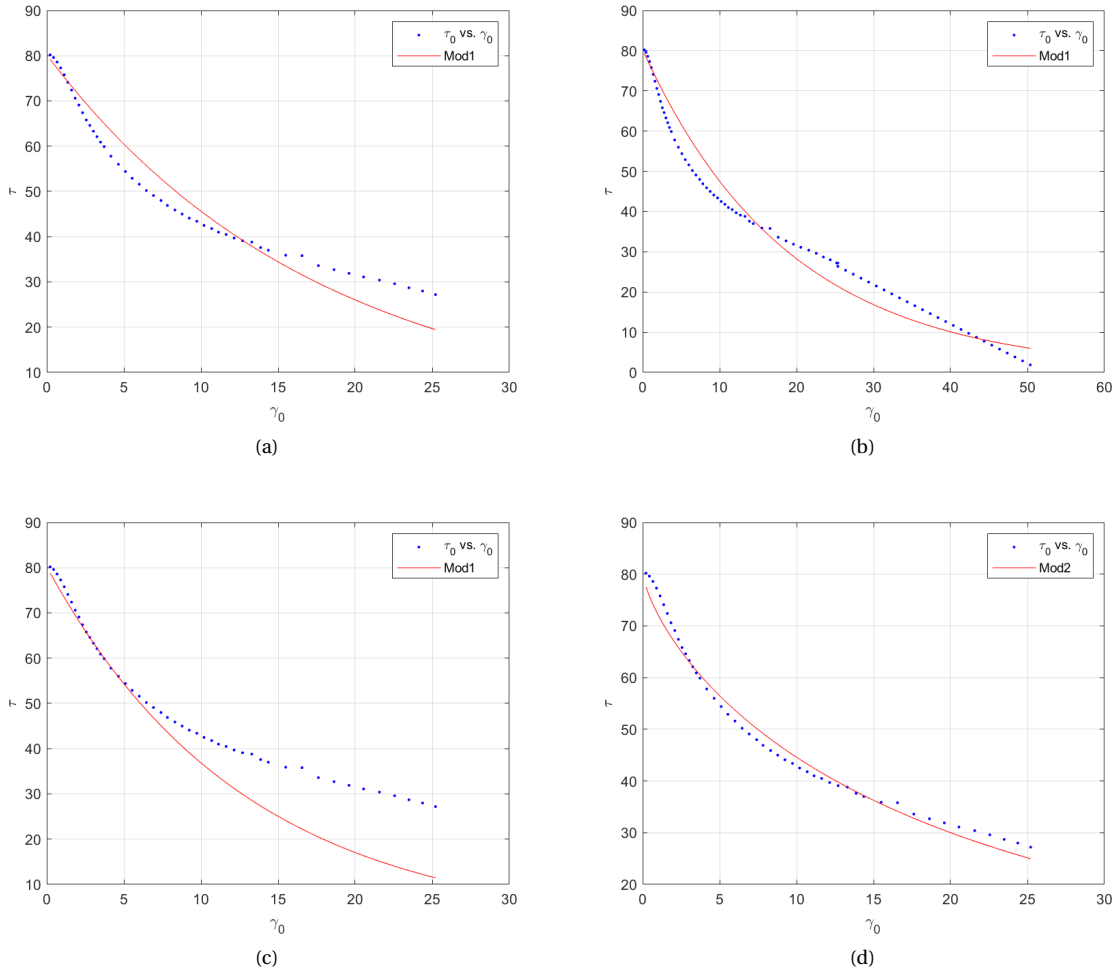

Figure 4.5: Curve fitting of triaxial test from peak stress for model 1, at the top and model 2, at the bottom. All form a triaxial test from Gardermoenbanen with sensitivity 240

Model 1 and model 2 are derived by substituting Γ in equation 2.5 with a- and b-coefficients showed in Eq. 4.6 and 4.7. The difference between the two models is that the Γ in model 2 is nonlinear and dependent on the strain. Further in this study a1 denotes the coefficient to model 1. The coefficients a2 and b2 denotes the coefficients to model 2. Then Γ will denote the coefficient obtained from BingClaw.

In figure 4.5 both models are shown with a fit to the strain softening part for one triaxial test from Gardermoenbanen with St = 240. The y-axis is shifted so that $\gamma_0 = \gamma^* - \gamma_{peak}$, as explained in Section 4.1. The blue dotted line is the path of the triaxial test and the red curve is the fitted curve. Figure 4.5a to 4.5c are fits to model 1. Figure 4.5a is

a fit over the domain given from the triaxial test. Figure 4.5b shows a fit over a linearly extrapolated triaxial curve. Figure 4.5c is the curve only fitted to low strain. Figure 4.5d on the other hand is a fit with model 2. These different fits and their correlation to index parameters are all presented sectionally below.

Figure 4.5 shows that Eq. 4.7 gives a much better fit than Eq. 4.6 and describes the inclination change in the start of the strain softening process from the triaxial test much better. An important question is if the triaxial test is a representative model for representing the strain softening behaviour. It is not given that large strain gives correct shear strength values for the remoulding process, and in what magnitude the shear band development affects the results as mentioned in 3.2. Different approaches and domains may for that reason make the some curve fit representations wrong. Index properties may also correlate differently to the different approaches, since they describe slightly different behaviours. In Section 4.2.1, 4.2.2 and 4.2.4 it is assumed that the whole domain to triaxial test is a representative model to describe the remoulding process. Every point from the triaxial test in these sections are weighted equally in the curve fitting. In Section 4.2.3 only the point at $I_R = 20\%$ is considered, to simulate the behaviour to this point

In the following sections each curve fit model is also related to the index properties by eg. multivariate regression. The last section, Section 4.2.5 gives an approximated solution where the a- and b2-coefficient are only dependent on one index parameter. With this it might be possible to predict the strain softening behaviour without doing a triaxial test.

4.2.1 Curve Fitting Model 1

Curve fitting of model 1, Eq. 4.6, is the strain softening model used in the current BingClaw program. From Fig. 4.5a this equation is tried to be fitted to the triaxial curve, by least square method. The a1-coefficient derived gives then the curve with least squared residual to the triaxial points.

The range of a1 for this curve fit approach spans between: a1$\in$[0.0176 , 0.151]. The a1-coefficient is correlated to different index parameters and visualized through scatter plots in Figure 4.6. Generally the trends are very weak and there are much scatter. At the same time there are some patterns within the scatter plots. In the correlation to OCR, S_u and S_{ur}, Fig. 4.6c-4.6e, the scatter seems to decrease with increasing OCR, S_u and S_{ur}. From Fig. 4.6a a weak dependency between a1 to OCR and LI can be seen. Where a1 decreases with increasing OCR and increasing with increasing LI. This gives sufficient correlation to preform a multivariate regression using MINITAB. The regression line Eq. 4.8 was acquired.

$$a1 = 0.0119 + 0.01879 \cdot LI - 0.00791 \cdot OCR - 0.1505 \cdot w_L + 0.438 \cdot w_P \tag{4.8}$$

Regression line Eq. 4.8 gives a R-sq of 46.9%. The scatter seems to be clustered within max and min borders in OCR, S_u and S_{ur} to a1 domains, see lines in Figure 4.6c - 4.6e. The regression could for that reason be restricted within these limits, by saying that the regression is maximum the maximum limit or minimum the minimum limit. When restricting the regression line Eq. 4.8 the R-sq becomes 50.44%. The results are shown in Table 4.1a

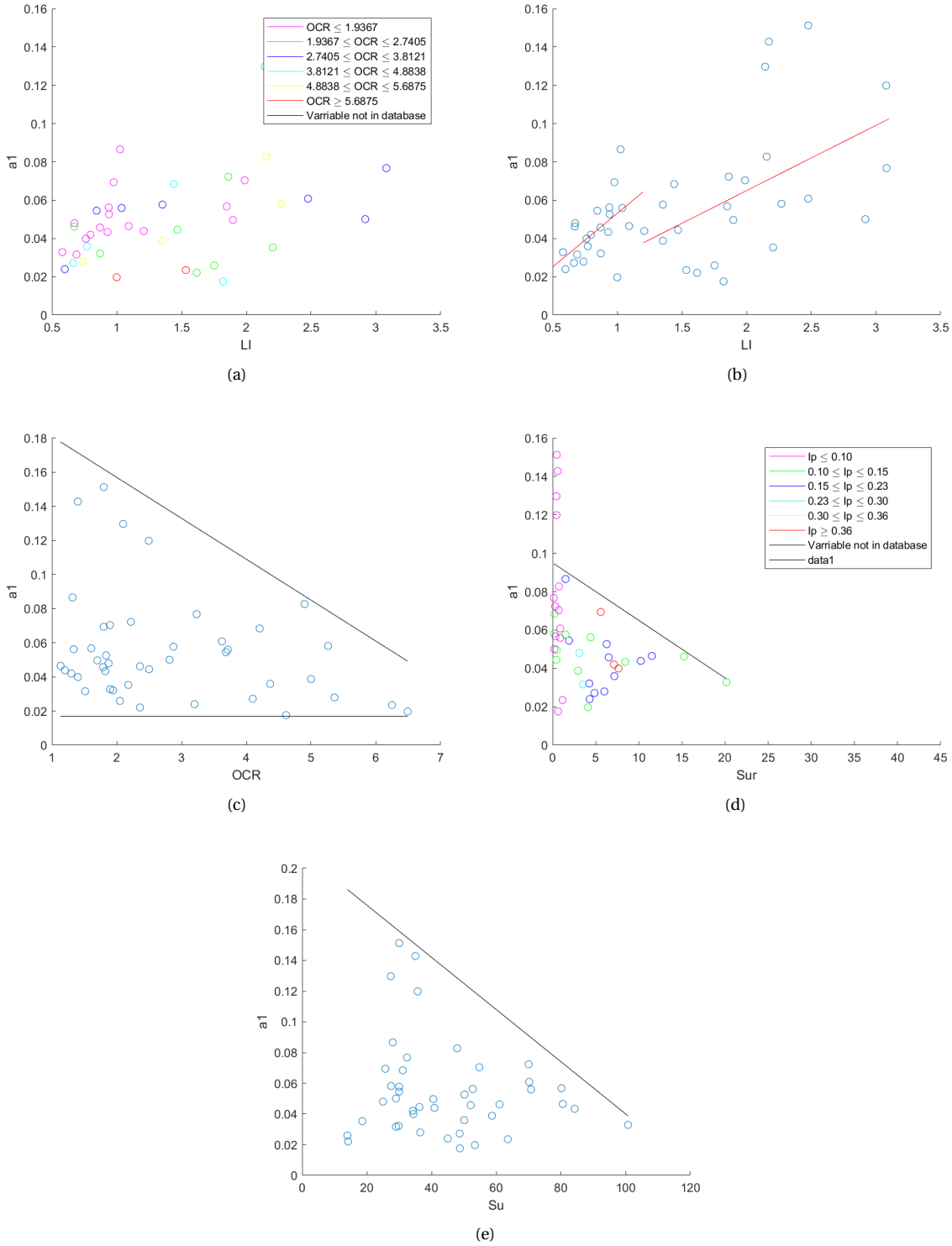

Figure 4.6: Scatter plots for coefficient a1 in model 1.

Table 4.1: Regression summary for Eq. 4.8

(a) Summary of regression to a1

Model Summary			
S	R-sq	R-sq(adj)	R-sq(pred)
2.38 %	46.91 %	41.46 %	31.09 %
	50.44%*	* With limit restrictions	

(b) Summery of coefficients

Term	Coef	SE Coef	P-Value	VIF
LI	0.01879	0.007	0.011	1.89
OCR	-0.00791	0.00269	0.005	1.15
w_L	-0.1505	0.0788	0.064	7.12
w_P	0.438	0.19	0.026	4.96

Table 4.1b shows how the different parameters fits to the model. Most of the parameters have a P-value under 0.05 which shows that they are significant to the model. The VIF is also under 10 for all coefficients which says that there are no high multicollinearity. But for w_L the P-value is higher than the usual threshold at 0.05. But that does not mean it is not significant. w_L does also have a VIF equal to 7.12 which is lower than the threshold to high multicollinearity, but it is still relatively high and indicates some multicollinearity. The reason for this is most likely that w_L, w_P and LI correlates, but since they explains different properties of the clay they are all included. By removing one of the coefficients, R-sq will decrease.

In general the bigger the a1 coefficient is the steeper the remoulding curve will be. The material will also go faster to remoulded state. When the liquidity index LI increases more water are in the pores, and when LI goes above 1, the water content is higher than the liquid limit. The latter gives clay the possibility to act as a fluid when remoulded. When the liquidity index increases a more brittle material is expected. This means most likely a faster remoulding, thus a higher a1 for higher LI.

By increasing the consolidation of the clay, more water will be pushed out of the material. The structure in the clay will also more tight since a load has pushed the clay together. Therefore it may be expected a slower remoulding process. Thus a negative coefficient for increasing OCR makes sense.

When the liquid limit increases the clay can handle a higher water content. The plasticity index will also increase since it is a strong positive correlation between these parameters. This makes it possible for the clay to better deal with deformations in the plastic regime. Thus a smaller a1 constant with an increase of the liquid limit. On the other hand an increase of the plasticity limit will decrease the plasticity index, and increase a1.

The coefficients changes a1 as expected and have reasonable values. This makes Eq. 4.8 credible.

4.2.2 Curve Fitting of Extrapolated Triaxial Plots

By extrapolating the triaxial curves an approximation of how the triaxial curves could look like all the way to remoulded state. The easiest extrapolation is to linearly extrapolate the curve to remoulded state. This is done by taking the average inclination between $\gamma = 15 - 20\%$, and continued with a line tangent to $\gamma = 15$ % from point $\left(\gamma = 15\%, \tau\left(\gamma = 15\right)\right)$. The extrapolated line is first added to the triaxial line after the maximum shear strain to the given triaxial data. The extrapolated data points are added to the triaxial data with the same shear strain distance between the points as the average shear strain distance in the interval $\gamma \in [15\%, 20\%]$. The reason for this is to have

the same weight to the extrapolated line as the triaxial line when using the curve fitting function in MATLAB.

Some triaxial plots does only go to $\gamma < 20\%$ in these cases the the inclination is calculated from $\gamma = 15\%$ to $\gamma = 17\%$. If the shear strain from a site is lower than this the measurement is not taken into consideration.

By extrapolating, the scatter plots seems to be more scattered, see Fig. 4.7. There are still some trends that can be commented. In Figure 4.7a a weak inclining trend is still present, but a trend line is difficult to draw here since there are to much scatter. The best trend line can be seen in Figure 4.7b. It is still much scatter, but a regression line with $IL \cdot w_L$ as the independent variable will make a little improvement from the mean.

In Figure 4.7c to 4.7e there are also some clusters and max and min limits that can be drawn. The biggest variation of a1 lies where OCR and S_{ur} are small. From there it will be less scatter with increasing OCR and S_{ur}.

Figure 4.7c shows the same trend as the scatter with OCR and S_{ur}. This restriction misses on some values outside the max limit. These values are from sites that are very little sensitive. For a model only interested in sensitive clay this values should be neglected, but as a general description of all clay they must be included. From this figure it is also possible to determine an other relationship. The clays with preconsolidation pressure under 200kPa has an upper restriction drawn with a red line. In the cases where the preconsolidation pressure is above 200kPa, the scatter is to big so no interpretation can be made.

A multivariate regression was tried for this case to approximate a1, and is shown in equation 4.9. The range of the extrapolated a1 is: a1 $\in$ [0.0111 , 0.1232]

$$a1 = -0.0026 + 0.00005 \cdot pc + 0.0705 \cdot LI \cdot w_L \tag{4.9}$$

Table 4.2: Regression summary for Eq. 4.9

(a) Summary of regression to extrapolated a1

Model Summary			
S	R-sq	R-sq(adj)	R-sq(pred)
0.0132	29.55%	25.15%	15.61%
	37.6% *	*With limit restrictions	

(b) Summery of coefficients

Term	Coef	SE Coef	P-Value	VIF
pc	0.00005	0.0000204	0.02	1.12
$LI \cdot w_L$	0.0705	0.0209	0.002	1.12

From Table 4.2a the R-sq becomes 29.55%. With restricting the regression within the clusters defined in Figure 4.7c and 4.7d it is possible to achieve a R-sq equal to 37.6%. So if a1 is bigger than the max limit or smaller than the min limit, a1 is brought to the limit line. There are also two outliers seen in Figure 4.7, which disturbs the result.

The a1 coefficient in the extrapolated case says mostly something about γ_r (shear strain at remoulded state), in correlation with the steepness of the remoulding curve. The coefficients in Eq. 4.9 has both a P-value under 0.05 and a VIF under 5, see Table 4.2b. Thus the coefficients both are significant and not multicollinear.

A linear extrapolation will give an underestimation of the remoulded shear strain. Even though the remoulding curve is approximately linear at the end, it has a slight inclination change towards a lower inclination. This would

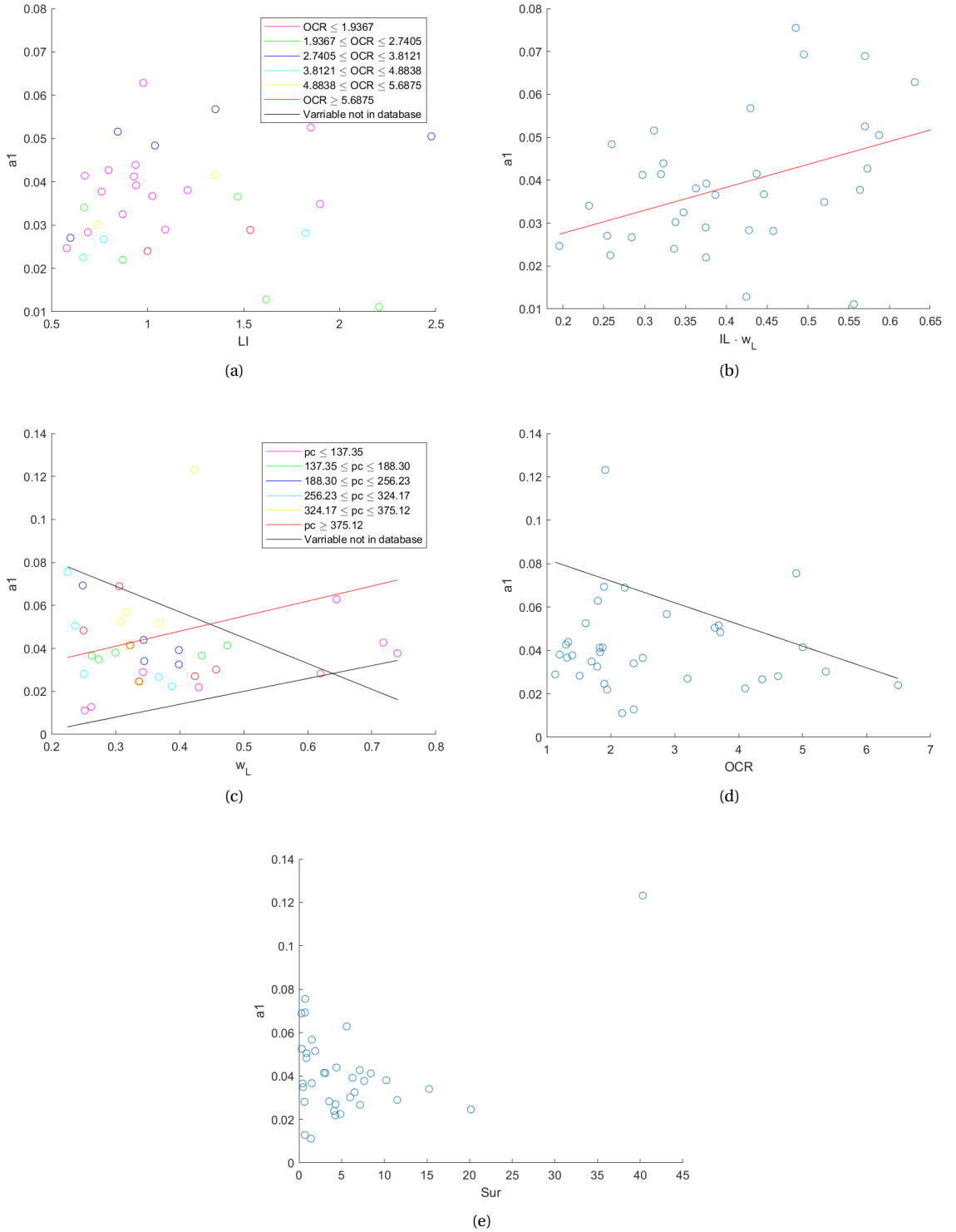

Figure 4.7: Scatter plots for coefficient a in extrapolated model 1.

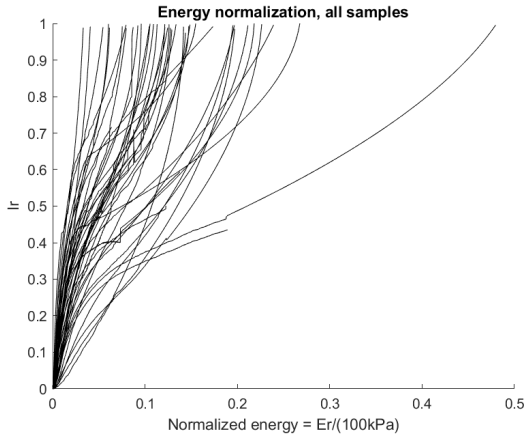

Figure 4.8: Energy plot of linear extrapolated triaxial curves

make the remoulded shear strain larger than estimated.

Another point that makes an error is the assumption that the inclination form $\gamma = 15\% - 20\%$ would be the best interval to describe the inclination to remoulded state. This is mainly done to avoid some irregularities at the end of some data sets and that they have the same starting point. The slope of the later part of the triaxial curve is also subject to bigger errors, since the triaxial test is not built to study large strain. The rubber membrane around the sample in the triaxial test could be subject to some errors since it gives a radial force when expanding. The top and bottom pistons will give friction that could also influence the results at high strain behaviour.

Extrapolating the results seems to give a worse result. The correlations to the index parameter is lower and the area to restrict the parameters is with more scatter.

Figure 4.8 shows that by extrapolating the triaxial curve linearly, the energy curves upwards at large I_R. The Energy curves should logically bend asymptotic against a horizontal asymptote at $I_R = 1$ (Tavenas et al., 1983). This indicates that the remoulded shear strength is highly underestimated, and a nonlinear extrapolation may be wise to preform.

4.2.3 Curve fitting for low shear strain

The two previous sections has tried to find an average a1-coefficient by weighting the regressed line over different domains. In reality a1 can be decided if two points on the remoulding curve are known. Equation 4.10 is derived by combining a set of equations, with two different points inserted in Equation 2.5. Then solve it in regards to a1.

$$a1 = \frac{ln\left(\frac{\tau(\gamma_1)}{\tau(\gamma_2)}\right)}{(\gamma_2 - \gamma_1)} \tag{4.10}$$

Where $\gamma_1 = 0$, $\tau(\gamma_1) = S_u$ and $\tau(\gamma_2)$ is the shear strength at the chosen shear strain level γ_2.

The first point is easy to choose, since the start point is fixed. Choosing a second point is not straight forward. If a wrong point is chosen the a1-coefficient can describe different fractions of different triaxial curve. The author

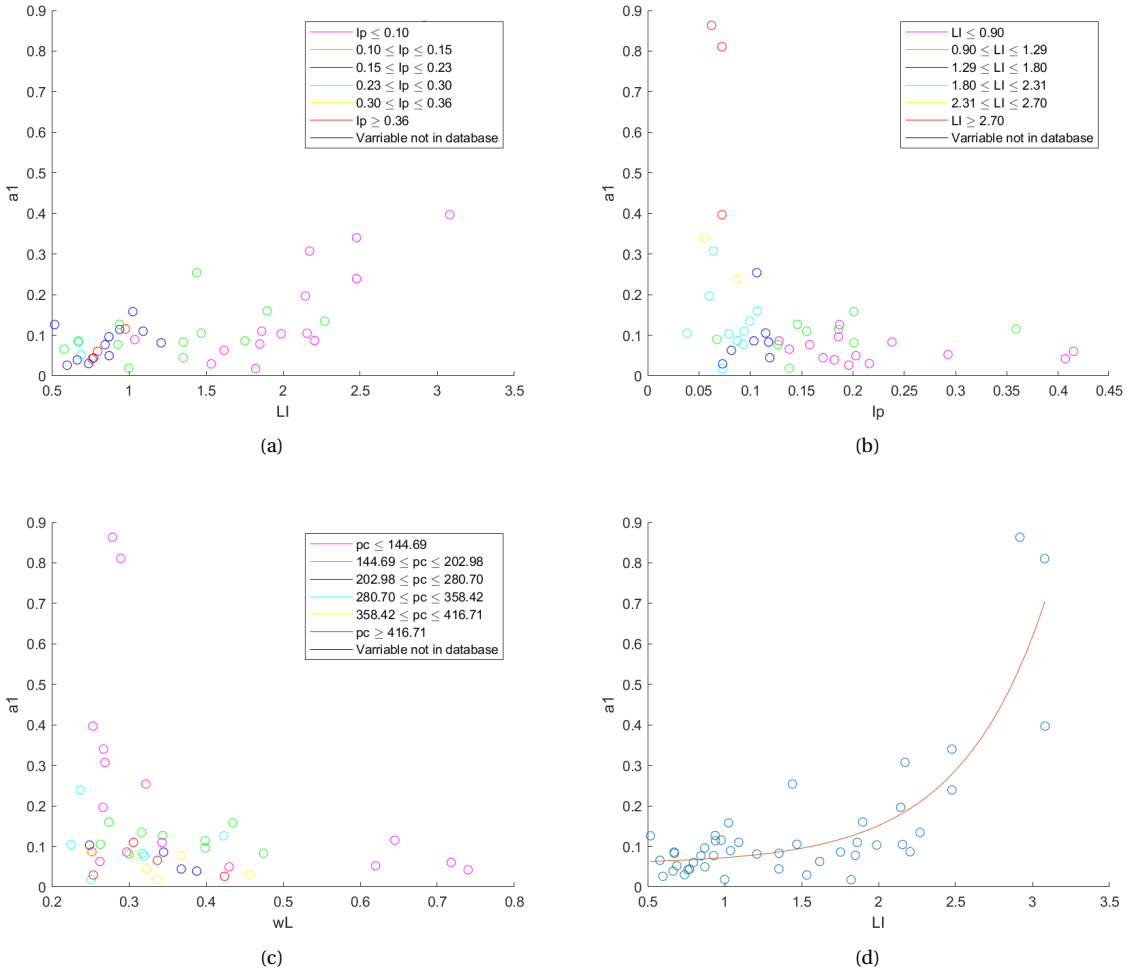

Figure 4.9: Scatter plots for Γ - coefficient in model 1.

chose the second point when I_R, the remoulding index, was equal to 0.2, or 20%. The approximation of the curve will then be as shown in Figure 4.5c.

When obtaining a1 from every triaxial test scatter plots can be made to show the correlation, Figure 4.9. The range of a1 is: a1∈[0.0177, 0.8633].

In Figure 4.9a and 4.9b it is possible to see that there is not much variation of a1 before the liquidity index exceeds 1.5, or the plasticity index is lower than approximately 12%. In for example Figure 4.9a, an average value of a1 could be used when LI<1.5. From there a linear increasing line could be used. Figure 4.9d shows a nonlinear trend between a1 and LI. This will be further presented in Section 4.2.5. From the figure a relation to sensitive clay can be made. L'Heureux (2013) describes that large retrogressive slides can happen when LI>1.2. From Figure 4.9d large values of a1 is first observed when LI is approximate 1.5. Large a1 indicates rapid remoulding. With rapid remoulding more material can be expected to be influenced since the sliding mass will move faster early, and a larger force and turbulence will react at the sliding scar. This may result in a steeper sliding pit, thus a new slide is more likely to happen.

An other observation can be made in Figure 4.9c. It looks like a1 only has a large value when the preconsolidation pressure is low. From the results presented it is shown that a1 is dependent on multiple variables. A quick multivariate regression was done and Equation 4.11 was derived.

$$a1 = -0.0080 + 0.1519 \cdot LI - 0.000291 \cdot \ pc \tag{4.11}$$

Table 4.3: Regression summary for Eq. 4.11

(a) Summary of regression of a1

S	R-sq	R-sq(adj)	R-sq(pred)
0.122902	51.73 %	49.43 %	40.01 %

(b) Summary of regression of a1

Term	Coef	SE Coef	P-Value	VIF
LI	0.1519	0.027	0.000	1.10
pc	-0.000291	0.000164	0.083	1.10

Table 4.3a shows that the regression has a R-sq of 51.73%. That a1 increases with LI makes sense as mentioned in Section 4.2.1. The pre consolidation pressure has a negative sign, and this makes sense as discussed in Section 4.2.2. The significance of LI is high since the P-value is under 0.05, but pc has a P-value of 0.083, which makes it a little significant but not much. It influences the regression mostly when pc is high. The coefficients have a VIF of 1.1. This indicates that the coefficients are not multicollinear.

4.2.4 Curve Fitting Model 2

Curve fitting model 2 Eq. 4.7 was introduced since the fit of model 1 did not show a good representation of the triaxial plot for every triaxial test. Model 1 and model 2 is equal when b2=1. Thus model 1 may be seen as a special case of model 2. Model 2 manages to describe both the steep inclinations in the start of the remoulding curve and the more flat bit at large strains, see Figure 4.5d. The b2-coefficient describes mainly the transition from a steep curve with high inclination to low inclination. The lower b2 the higher the derivate will be. The a2-coefficient manages to describe how large the strain at fully remoulded state is. But both parameters correlates some to each other, and describe partial both properties. Just as for model 1 in section 4.2.1, the curve fitting is in the available domain from the triaxial test, $\gamma \in [\gamma_{peak}, \gamma_{max}]$.

No extrapolation of the triaxial result is done for this model. Since the initial curve fitting fits relatively good, Fig. 4.5. By extrapolation more error might also be introduced. There is one outlier in the data that is shown very clear in model 2. For one of the triaxial test the curve is only concave, when usually it is convex. This is rare when doing triaxial tests, especially for sensitive samples, and therefore there is done one analysis without this outlier. Table 4.4 shows how the coefficient a2 and b2 in model 2 changes the behaviour of the remoulding curve.

Correlation to a2 - coefficient

As previous mentioned the a2 coefficient describes mostly the later response of the remoulding curve. The range of a2 parameter lies between 0.0102 and 0.4019. In Figure 4.10 some of the relationship between a2 and the index

Table 4.4: Responses of coefficients from model 2

Coeff.	Order of Magnitude	Inclination Response	γ_r Response
a2	high	Higher inc.	lower
a2	low	Lower inc.	higher
b2	high	Lower inc.	higher
b2	low	Higher inc	lower

parameters can be seen. In Figure 4.10b and 4.10f a clear linear trend can be seen. a2 is increasing with LI, Fig. 4.10b and decreasing with increasing $pc \cdot w_L$, Fig. 4.11f.

Further in Fig. 4.10a the size of OCR is emphasised with colours. In this scatter plot it looks like points where OCR is low lies at the top of the scatter and points with big OCR lies at the bottom of the scatter, and therefore a2 is most likely a function of both OCR and LI.

Further in the other scatter plots in Fig. 4.10 there are some clear cluster to restrict the spread within. In Figure 4.10d a2 is only varying between 0.01 and 0.23 for the cases with liquid limit under 0.3. The residual of b2 is also decreasing with increasing S_{ur}.

Figure 4.10c shows some of the same relations as Fig. 4.10a. This scatter plot shows that there are a relation between w_L OCR and a2. Low liquid limit and low OCR gives high a2. a2 will form there decrease with OCR. Similarly for samples with high liquid limit. They will start on a lower a2 value and decrease with increasing OCR. The product of pc and w_L did also show a linear trend with a2 shown in Figure 4.10f. Some residuals in this plot were relative big. By comparing the box drawn in Fig. 4.10b and 4.10f, the box in drawn in Fig. 4.10f is slightly bigger, which indicates a worse correlation. A subset analysis showed that a regression to the liquidity index and OCR provided a better answers. Therefore a multivariate regression with these index parameters was made in MINITAB, and Eq. 4.12a was derived. Equation 4.12b is a regression with same parameter only an outlier is removed.

$$a2 = 0.1186 + 0.0865 \cdot LI - 0.02962 \cdot OCR \tag{4.12a}$$

$$a2 = 0.1112 + 0.0884 \cdot LI - 0.02688 \cdot OCR \tag{4.12b}$$

Table 4.5: Regression summary for Eq. 4.12a

(a) Summary of regression of a2

Model Summary			
S	R-sq	R-sq(adj)	R-sq(pred)
0.05	66.47 %	64.83 %	61.49 %
	68.92%*	*With limit restrictions	
0.049	69.62%	68.10 %	65.02%
	72.37%**	**With limit restrictions, and removing an outlier	

(b) Summery of coefficients

Term	Coef	SE Coef	P-Value	VIF
LI	0.0865	0.0113	0.000	1.01
OCR	-0.02962	0.00558	0.000	1.01
LI*	0.0884	0.0105	0.000	1.00
OCR*	-0.02688	0.00529	0.000	1.00
*Coefficients when removing an outlier				

The regression analysis shows that it can predict the a2 coefficient with relative good accuracy. Table 4.5a shows

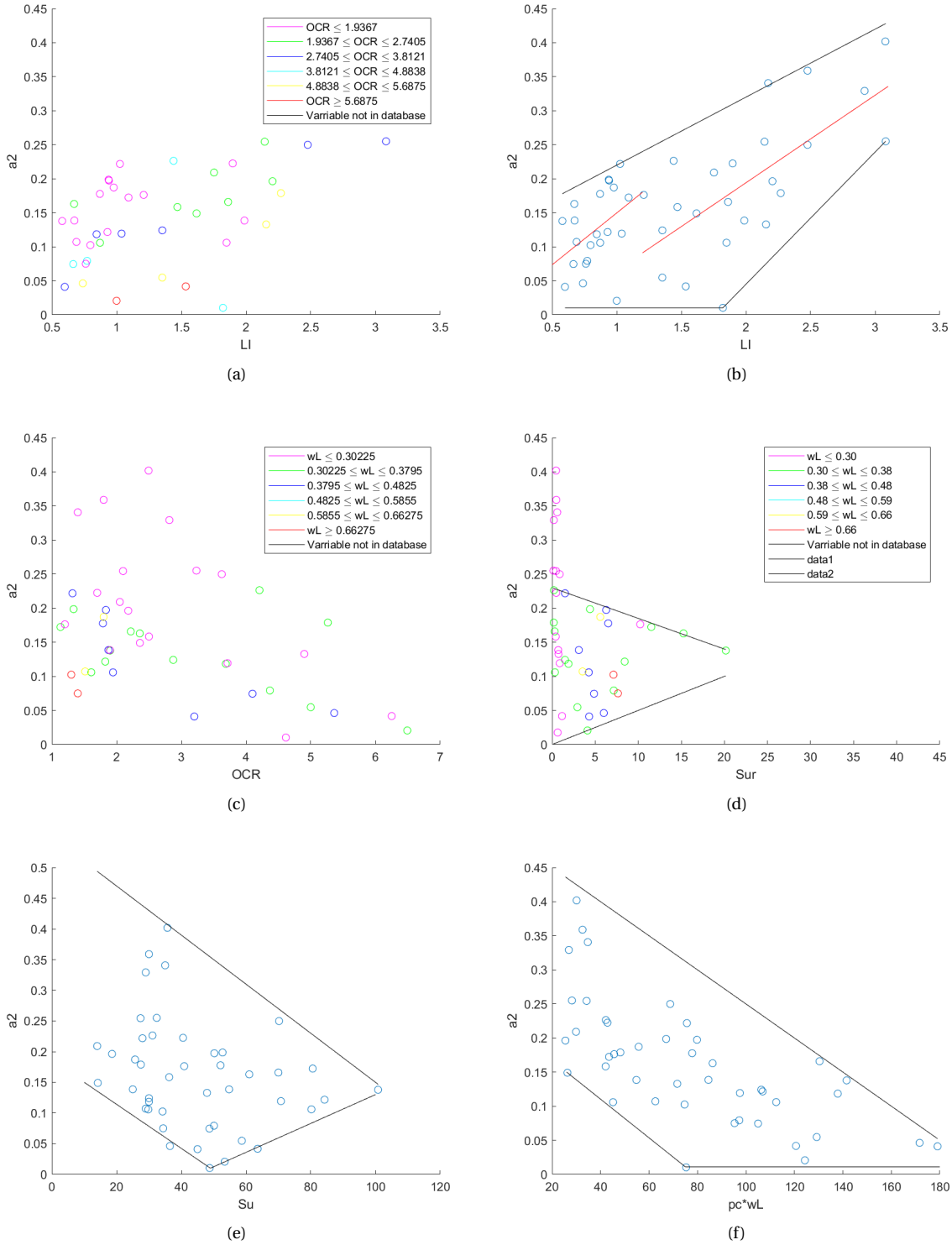

Figure 4.10: Scatter plots for coefficient a in model 2.

that the R-sq of the original regression is 66.47%. By removing one outlier the R-sq is increased with three percent, and even three more percent when restricting a2 within the limits drawn in Figure 4.10. This increases R-sq to 72.37%.

Further the coefficients used in the regression is significant with a P-value under 0.0005. There is also no indication of multicollinearity since the VIF is 1. The sign of the coefficients can be described as discussed in section 4.2.1, and with the same analogy the signs to the coefficients makes sense. In total Eq. 4.12b gives the best result.

Correlation to b2 - coefficient

The b2-coefficient tries to describe the early part of the remoulding curve, and says something about how big the change of inclinations or the derivate is. The range of b2-coefficient is between 0.1419 and 0.983. This is then when excluding the one outlier which has the value 1.23.

The correlations between b2 and some index parameters are shown in Figure 4.11. The b2-coefficient has a linear trend with both the liquidity index and the preconsolidation pressure, shown in Figure 4.10b and 4.11c. There seems to also be a linear trend between b2 and OCR (Fig. 4.11f), but it seems to be more scatter compared to LI and pc, see Fig. 4.11a and 4.11c.

Much of the variation of the b2-coefficient can be described from the clay content. Figure 4.11b shows that with high clay content less variation in b2 is found, and that b2 ends on a value around 0.7-0.75 for rich clays. Much of the variation can also be seen Figure 4.11d, which shows that low S_{ur} gives high variation and high S_{ur} gives a b2 coefficient around 0.5. The last scatter plot, Figure 4.11e, shows how b2 changes in relation to shear strength.

The scatter plot shows that the biggest variance is around shear strength equal to 50 kPa, and then decreasing with lower and higher shear strength. If the lowest value of b2 is considered as a outlier the lower bound can be described as a single linear line. If not it looks like that b2 has a linear trend of the scatter for S_u<40.

From the analysis of the scatter plots a subset analysis was preformed. From the best combination of the parameters a multivariate regression analysis was preformed, and regression Equation 4.13 was derived.

$$b2 = 0.2774 + 0.001265 \cdot pc - 0.00196 \cdot S_u + 0.722 \cdot I_P \tag{4.13}$$

Table 4.6: Regression summary for Eq. 4.13

(a) Summary of regression of b2

Model Summary			
S	R-sq	R-sq(adj)	R-sq(pred)
0.10953	61.56%	58.60%	52.19%
	0.7441%*	With limit restrictions	

(b) Summery of coefficients

Term	Coef	SE Coef	P-Value	VIF
pc	0.001265	0.000186	0.000	1.74
S_u	-0.00196	0.00111	0.085	1.72
I_p	0.722	0.194	0.001	1.05

Table 4.6 shows result of the multivariate regression analysis of the best subset. The least significant parameter in regression Equation 4.13 is the shear strength with a P-value 0.085. By excluding the shear the R-sq(adj) will go from 58.6% to 56.4%.This shows that S_u does not influence the regression much, but improves the regression some.

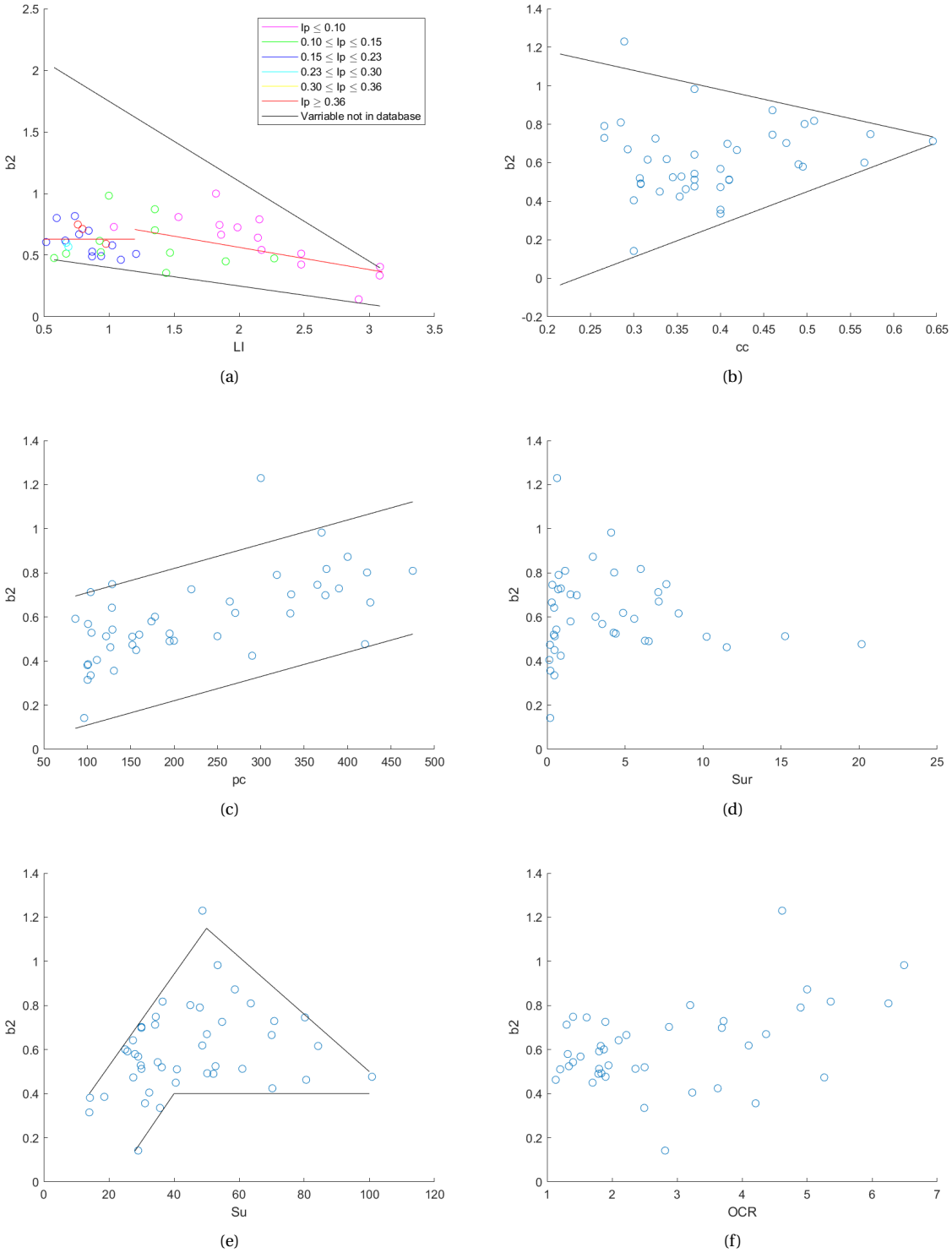

Figure 4.11: Scatter plots for coefficient b2 in model 2.

The P-vale to both pc and I_P is both under 0.05 and shows that they are significant. Further none of the parameters have a VIF above 5, and indicates low multicollinearity. It is also possible to do a multivariate regression analysis with w_L instead of I_P which will give approximately the same R-sq. The accuracy of b2 can be increased by bringing b2 to either the max or the min limit drawn in Figure 4.11 when b2 from Eq. 4.13 exceeds the limits. When restricting b2 to the max and min limits R-sq increases to 74.4%.

The preconsolidation pressure has a positive sign. When pc goes up b2 goes up. This can be explained from the structure of the clay. When the preconsolidation is high, there are more contact forces between the clay. It is with other words more compact. The clay will therefore probably have less pore pressure builds up. A higher b2-coefficient with increasing pc can for that reason be expected.

With a high I_P more plastic movement is possible. It can therefore make sense that the remoulding process goes slower. If this is the case, b2 would be higher with increasing I_P.

From the discussion above the sign of the coefficients in Tab. 4.6 makes sense.

4.2.5 One parametric models

BingClaw has at the moment a quite simple input. It is not possible with layering. The values chosen must therefore be an representative average for the whole slide. Choosing this average can be a demanding task, especially when parameters vary in three dimensions. A one-parametric interpretation of all models are for that reason done, seen in Table 4.7 and Equations 4.14a to 4.14h.

$$a1 = -0.00300 + 0.05612 \cdot LI \tag{4.14a}$$

$$a1 = -0.00325 + 0.03411 \cdot LI \tag{4.14b}$$

$$a1 = \quad 0.01693 + 0.05353 \cdot LI \cdot w_L \tag{4.14c}$$

$$a1 = \quad 0.0560638 + 0.00276222 \cdot e^{1.77156 \cdot LI} \tag{4.14d}$$

$$a2 = -0.00292 + 0.1526 \cdot LI \tag{4.14e}$$

$$a2 = -0.06350 + 0.1288 \cdot LI \tag{4.14f}$$

$$b2 = \quad 0.6536 - 0.0285 \cdot LI \tag{4.14g}$$

$$b2 = \quad 0.9257 - 0.1810 \cdot LI \tag{4.14h}$$

In Table 4.7 the referred equations are corresponding to the red line in the referred figures.

Each coefficient to the models presented earlier in this chapter are divided into two domains, with the division at LI=1.2, except the extrapolated model 1 in Sec. 4.2.2 and the low shear strain model (Sec. 4.2.3). The division at LI=1.2 is because for clays with liquidity index higher than 1.1 - 1.2 large retrogressive slides can be expected

Table 4.7: The result of one parameter regression

Domain	Mod. Coef.	S	R-sq	R-sq(adj)	Ref. Eq.	Ref. Fig.
LI < 1.2	a1	0.0136	29.52 %	25.81 %	4.14a	4.6b
LI > 1.2	a1	0.0340	23.46 %	19.82 %	4.14b	4.6b
	a1	0.0143	16.29 %	13.75 %	4.14c	4.7e
	a1	0.0894	74.4%		4.14d	4.9d
LI < 1.2	a2	0.0525	17.23 %	12.87 %	4.14e	4.10b
LI > 1.2	a2	0.0747	47.46 %	44.96 %	4.14f	4.10b
LI < 1.2	b2	0.1377	0.11 %	0.00 %	4.14g	4.11a
LI > 1.2	b2	0.2194	17.15 %	13.20 %	4.14h	4.11a

(L'Heureux, 2013). The extrapolated model 1 from Section 4.2.2 is not divided at liquidity index = 1.2, since the only linear trend found was when a1 was plotted against $LI \cdot w_L$, Figure 4.7. A division in the $LI \cdot w_L$ domain for determining large retrogressive slides are previously not done before. Equation 4.14d is a nonlinear model for its whole domain and it was not necessary to divide the domain in two.

Table 4.7 shows that R-sq are much lower than the values presented earlier in this chapter. The R-sq varies between 17% and 30% for every regression line, except for a2-coefficient when LI>1.2, which seems to be much more reliable with a R-sq =47.5%. These equations could of that reason be seen as bad approximations.

For the b2-coefficient when LI<1.2, the R-sq is almost zero. In this case the mean value b2=0.63 would be just as good.

Equation 4.14d has a standard deviation of 0.089 which is much better compared to the multivariate regression done in Section 4.2.3, which had a standard deviation of error of 0.1229. The R - sq for a non linear model is not a valid value, but it is in the table to give an indication of the quality of the model compared with the other models. This is the only case in this study that the one parametric model gives a better fit than the multivariate linear model. This indicates that Eq. 4.14d gives the best correlation to the index parameters.

Chapter 5

Discussion

The aim for this thesis was to find the remoulding coefficient Γ from BingClaw. Different regressions of the remoulding curve are done and approximate solutions are derived.

If the curve of the triaxial test is a good representation of the the remoulding process for a clay sample. The simplest way to find Γ is by doing a regression of an actual triaxial test from a block sample. Then random scatter from the analysis of the regression can then be ignored. The only error will be the quality of the sample and quality of the test procedure.

There are still cases where a good model to find Γ will be better than actually doing the lab test. In early design an approximate model will give an idea of the magnitude of an eventual slide. Thereafter if further studies are needed, detail design can be done to restrict the runout with better accuracy.

There are also other factors that can make the approximated model just as good as a lab test. Some relevant research areas are very remote and have a long transportation to the closest laboratory. Samples with high overburden has a big chance of changing structure when it is completely unloaded. This is compensated with the consolidation process in the triaxial test, but it still disturbs the sample. Further high quality samples are needed to find the best representation of the remoulding curve, see Fig. 3.1. The 75mm and 54mm sampler are not sufficient. A block sampler is needed to find the most correct representation. The block sampler is at least in Norway a not so common sampling method as the 74mm and 54mm sampler. Not every geotechnical drilling rigs has the possibility to take block samples, and not all drillers has the experience to take block samples. This is a minor problem if the contractor is willing to invest in high quality samples. At the same time the model presented might give a good enough coefficient. It may also five an indication of the quality of the sample

5.1 Model Comparison

The point or points on the triaxial curve that best represent the remoulding curve has to be chosen before calculating the remoulding coefficient. Which point is the most trustworthy point? Two least square regressions models were done, Section 4.2.1. This is by assuming that the whole domain of the triaxial curve is trustworthy. Overall the result becomes much worse when trying to linearly extrapolate the triaxial curve, as discussed in section 4.2.2. The extrapolated energy plot Figure 4.8 does also show that the a linear extrapolation is wrong.

The strain recorded from the triaxial test will be the average strain for the whole sample, and not the actual strain in the shear layer, which the calculations in BingClaw assume. Since it is not known if there are any shear band localization from the triaxial test taken, the strain must be seen as a global strain. By seeing this as global strain the steepness of the start of the remoulding curve can indicate how well the sample will localize a shear band. Thakur (2007) describes that if a localization happens the shear band thickness will go towards zero with higher strain. This is under a small strain and strain rate condition.

The strain rate may in fact make the clay react differently. For high strain rate the rheological properties to the clay must be taken to consideration. The strain rate will then contribute to higher strength. In a real slide the strain rate will be so great that the strength of the clay will increase as presented in Section 2.4. Further when the clay is exposed to a landslide, the flow will be greater, and the clay will be exposed to other factors such as turbulent flow. Turbulent flow will remould a bigger area and increase the shear band thickness.

By assuming that the whole domain from the triaxial test is valid to describe the remoulding process. Model 1, Eq. 4.6, is not the best representation as previous mentioned in Chapter 4. First of all the initial regression does not fit very good to the remoulding curve as seen in Figure. 4.5. Further as seen in Table 5.1, the correlations to the index parameters is in general much better for Model 2 than Model 1, with one exception (Eq. 4.14d). From the regression lines, the R-sq is improved approximately 20% with regards to the correlation to the index parameter between these models. And almost 10% more by restricting the regression to the max and min limits seen in the scatter plots i Section 4.2. It is therefore clear which model that describes the triaxial test best, but the assumption that the triaxial test represent the remoulding process might be wrong, therefore model 1 could still be valid.

Table 5.1: Summary of regression analysis from Chapter 4

Model	Coefficient	R - sq	R-sq (Lim Restricteons)	R-sq (adj)
Model 1	a1	46.91 %	50.44 %	41.46 %
Model 1 Extrapolated	a1	29.55 %	37.59 %	25.15 %
Model 1 Low Strain	a1	74.4%*		
Model 2	a2	69.62 %	72.37 %	68.10 %
Model 2	b2	61.56 %	74.41 %	58.61 %
*R-sq not representative for nonlinear model, just an indication.				

5.2 Model Test

As mentioned in Section 4.2.5 it can be difficult to decide one average for the Attenberg limits, OCR, pc and S_u. The models and approaches from this thesis uses one or multiple of these parameter to decide the coefficients a1, a2, and b2. The uncertainties when choosing these values could be just as big as if the model only was dependent on one variable (Section 4.2.5). To do this comparison, the values for the coefficients from the regression models must be compared to the values derived from the BingClaw analysis.

Table 5.2: Left table: Index Parameters as input to the presentation of the different models used, Figure 5.1 and 5.2. Values gathered from Natterøy (2011); Kummeneje (1996); Gregersen (1981). Right table: shows derived coefficients form the index parameters

(a) Used index to find a- and b-coefficients. OCR are guessed values

	Rissa	Finneidfjord
OCR	1.2	1.2
LI	2.4	2.5
w_L	0.23	0.36
w_P	0.18	0.3
I_p	0.05	0.06
pc	206.4	105.6
S_u	15	9.2
w	0.3	0.45
σ'	103.2	88
S_{ur}	0.24	0.08

(b) Generated Coefficients from Eq in Chapter 4.2

Coeff	Rissa	Finneidfjod
a_1	0.0917	0.1266
a_{1_1}	0.1317	0.1373
a_{1_expol}	0.0466	0.0661
a_{1_1Expol}	0.0465	0.0651
$a_{1\_1NonLin}$	0.2500	0.2876
a_2	0.2911	0.2999
a_{2_2}	0.2456	0.2585
b_2	0.6391	0.6096
b_{2_2}	0.4913	0.4732

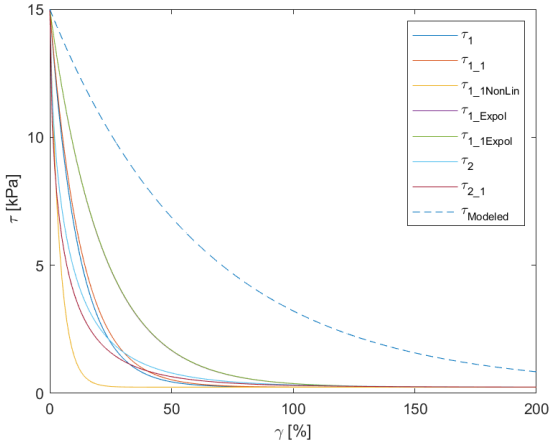

Figure 5.1: Summary of every model produced with index from Rissa

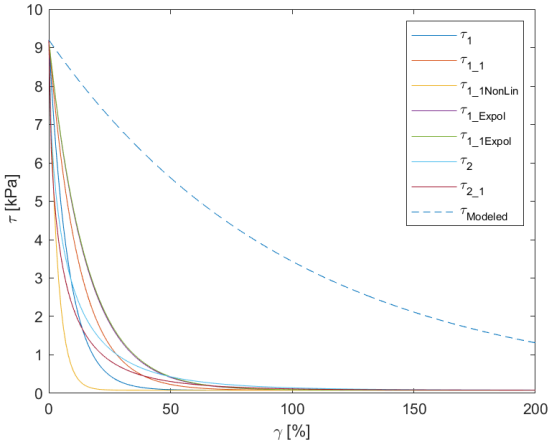

Figure 5.2: Summary of every model produced with index from Finneidfjord

In Figure 5.1 and 5.2 all the results from Section 4.2 are shown graphically with use of index parameters gathered from the Rissa and the Finneidfjord slide, see Table 5.2a. The coefficients derived are shown in Table 5.2b. In the figures the shear strength are plotted against shear strain. In the legend, the first number in the subscript is a reference to the model used. If there are two numbers in the subscript the second denotes that the model has a

coefficient derived from a one variable regression. "NonLin" in the subscript denote the the model is nonlinear. "Expol" in the subscript denotes that coefficient is derived from triaxial curves that are extrapolated. $\tau_{Modeled}$ is the reference curve derived from parametric studies in BingClaw. The subscript notation in Figure 5.1 to Figure 5.4 corresponds with Table 5.2b.

Liu et al. (2018) found that Γ should be approximately 0.016 to match the runout distance for the Rissa landslide. The author found in earlier project work (fall 2018) that Γ for Finneidfjord should be larger than 0.01 based on the shape of the slide. A final Γ was not possible to find since the runout distance was far to large with the chosen parameters. The factor that contributed most to change in runout distance was the added mass coefficient. In his study this factor was set equal to zero, no added mass.

In the Figure 5.1 and 5.2, the remoulding curves derived from this study does not match the remoulding curve found from from parametric studies, $\tau_{Modeled}$. One of the reasons for this is that $\tau_{Modeled}$ and the curves from this study uses different γ. This study has only looked at a global strain for the whole triaxial test, while BingClaw uses the actually, or local shear strain. The global and local strains from the triaxial test are not equal, since a localisation of shear band most likely is developed, as previous discussed.

5.2.1 Correcting for Shear Band Thickness

Thakur et al. (2017) found from a plane strain uniaxial apparatus that the shear band was in average 5mm thick. This is 5% of the total thickness of the triaxial sample. The local shear strain of the triaxial test would therefore be approximately 20 times larger than the global strain. For model 1 this would result in that the a1-coefficient is reduced to 5% of the original value. This reduction will only be correct for model 1. For model 2 this reduction of the a2-coefficient gives an indication but a new analysis must be done to find the new and correct coefficient. The result for model 2 in Figure 5.3 and 5.4 is therefore not trustworthy. The a2-coefficient in model 2 should be even smaller than the reduction when calculating the coefficient again. This will result in a lower inclination at large strain, when correcting for a 5mm shear band. The b2-coefficient will not change by this correction. Since the comparison curve $\tau_{Modeled}$ uses model 1 and that it is unknown which model that is best to describe the remoulding curve. Model 2 will not be further discussed.

In Figure 5.3 and 5.4 a factor of 0.05 is multiplied to the a1- and a2-coefficients to correct them to be dependent on local strain instead of global strain. The closest curve to the derived curve from BingClaw is the $\tau_{1\_1NonLin}$-curve. The τ_1-curve which uses an a1-coefficient from a multivariate regression averaging over the whole triaxial domain, Eq. 4.8, and the one parametric version of this curve and τ_{1_1} is almost at the same spot. At the same time they are quite far away from $\tau_{Modeled}$ when comparing in the figures. Further the extrapolated curves which lies over each other is even further away form the result derived from BingClaw. This supports the possibility that only the start of the triaxial test can represents the remoulding curve, and at large strain other factors influences the remoulding process showed in the triaxial test.

When only considering a 5mm shear band and only considering low shear strain from the triaxial results (to

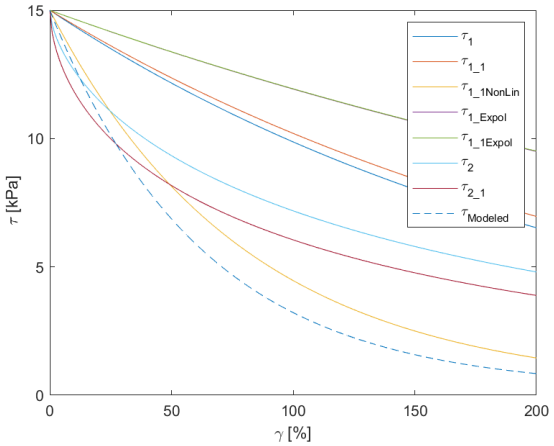

Figure 5.3: Remoulding curves where global shear strain are converted to local shear strain, "$a1 \cdot 0.05$", for Rissa

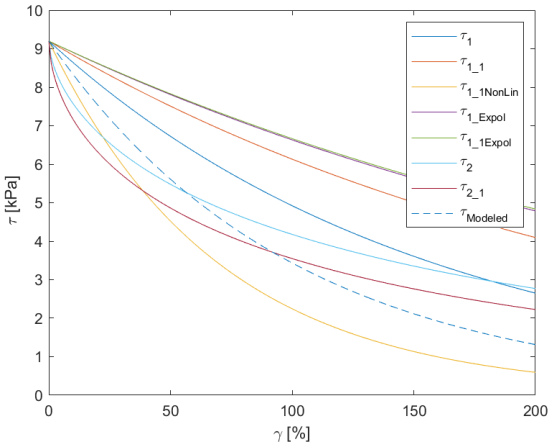

Figure 5.4: Remoulding curves where global shear strain are converted to local shear strain, "$a1 \cdot 0.05$", for Finneidfjord

$I_R = 0.2$), and then converting to local strain. The $a_{1\_1Nonlin}$-coefficient from Table 5.2b for Rissa will be 0.0125, and for Finneidfjord 0.01438. Rissa which has a Γ of 0.016 modelled from BingClaw is then not far from a1 achieved from this study. In fact by increasing by one standard deviation a1 becomes 0.1697. The modelled Γ form BingClaw is within one standard deviation of a1 derived from the low strain approach in this study. The same with Finneidfjord which had a Γ larger than 0.01 modelled from BingClaw, does also fit for the case of $\tau_{1\_1NonLin}$ from this study Γ in Figure 5.4

The result of a 5mm shear band (Thakur et al., 2017) can not directly be implemented to the triaxial test, without more supporting results or studies. It is a possibility that a shear band from a triaxial test is a different size, since it has a confining pressure and not plane strain. It is also a possible that the shear band is sample size dependent. The coefficient could therefore change when scaling from a triaxial test to an actual slide.

5.3 Validity of Triaxial Test

A way to check the validity of the triaxial test would be to compare remoulded shear strain (γ_R) from the models produced with the actually remoulded shear strain. A problem is that there are from the authors knowledge no previous study of this theme. The triaxial test does also not give any actually shear strain. This depends on how many and how thick the shear bands are. Further the triaxial test goes very slow, so the assumptions of locally undrained might be wrong in some cases (especially for silty clays). When the test goes slow, the clay might then have time to get volume strain. Contrary when an actual slide happens there will not be time for volumetric strain, it will be fully undrained, and the strain rate will be large. When the strain rate is large other effects not studied in this study might come to light.

A way to solve these problems might be to go back to the energy consideration. Then a consideration of the total remoulded energy for Norwegian clay could be found, as Locat et al. (2008) did. When studying the energy it might

give better results if real energy instead of specific energy is studied.

From the comparison of remoulding energy Turmel et al. (2018) did in Figure 4.2, both simple shear and triaxial gives answers in the same range. Compared to the Canadian clay the Norwegian clay are much more brittle. At the same time the Norwegian clay tend to behave in the same matter as the Canadian clay. It has the same form of the energy curve. It only require less energy to remould, which Thakur et al. (2015) also confirmed. This shows that the triaxial test at least is close to previous studies.

On the other hand the slow stress strain curve that the triaxial test gives could be used for the strain softening behaviour in some models inside modelling tools as eg. NGI ADP-model. In this model the peak shear strength is achieved at different times for passive and active site. Then the fracture propagation may be easier to describe.

A source of error when using the triaxial test at large strain would be the effect of the rubber membrane, and the interaction forces between the clay and the pistons. The rubber membrane is necessary to divide the confining water pressure and the pore pressure in the sample. The membrane has little interference at low strain since it then will be little radial strain. When the sample expands radially at large strain, the rubber membrane will try to resist and make a bigger radial pressure inwards, which is not accounted for.

At large strain the friction forces from the pistons to the sample will also interfere. This is because the sample wants along the failure surface at 45 degree angle. When the friction from the pistons restrict this, the sample will produce new shear bands or activate larger volume of the sample. Then the recorded share strength will not be accurate for one single shear band.

Given these aspects discussed, the triaxial curve could only be assumed to be valid for small strains when considering remoulding studies.

Chapter 6

Summary and Recommendations for Further Work

6.1 Summary and Conclusion

This thesis has discussed the remoulding process of Norwegian clays. This is done through both an energy consideration and through a strain softening equation from the program BingClaw. The motive was to find the remoulding parameter Γ, so that BingClaw with greater accuracy could calculate the remoulding behaviour of the clay, hence the runout distance, velocity and runout height. To study this behaviour, triaxial test taken from block samples was used. An energy normalization consideration was tried to find Γ, but no correlation was found.

Γ was thereafter approximated by comparing the strain softening curve from the triaxial test and the strain softening equation from BingClaw. The equation from BingClaw did not fit perfect to the remoulding part of the triaxial curve. Two different models, or equations was tried fitted to the remoulding curve. Model 2 did fit good to the triaxial curve. Both coefficients in the model had a R-sq over 70%. As mentioned in the discussion large shear strain from the triaxial test does probably not represent how the material is remoulded. Model 1 supported this when tried over different domains. When including large shear strain more scatter and uncertainties were introduced.

The Γ-parameter found from model 1, was in the end found by fitting it to a triaxial curve that was only remoulded 20% ($I_R = 20\%$). Further from the regression a nonlinear trend between Γ and the liquidity index was found with a R-sq over 70%. The behaviour of this relationship is comparable to quick clay. For the non sensitive clays, the coefficient is constant. For a more sensitive clay, a more brittle behaviour was given, with that Γ will increase with increasing LI. A confidence that the parameter can be described from the liquidity index was therefore given.

When correcting the Γ-parameter to local strain, correction for an average 5mm thick shear band. The nonlinear relationship between Γ and the liquidity index gave the most probable answer. The correction would be to multiply Γ found derived from global strain with 0.05.

6.1.1 Concluding remarks

- Γ can be found from index parameters with some significance when interpreting a triaxial curve from a bloc sample when the remoulding index is under 20%.
- A scaling factor to scale Γ derived from the global shear strain to a Γ valid for local strain from the triaxial test must be used. A suggested factor is 0.05.
- Γ can be correlated to index parameters. The best correlation is with the liquidity index
- It is found that the triaxial test possibly gives more error when interpreting it for large strains. The cause of this could be interaction forces between the pistons in the triaxial apparatus or the membrane around the sample. But the triaxial test seems to be valid for low strains after peak shear strength.

6.2 Further Work

Even though this study showed some promising results there are still a lot to control and study. First of all, more parametric studies in BingClaw for other slides should be done to have a broader comparison basis between lab data and modelled data.

The uncertainty from the triaxial test has to be studied if triaxial test further is going to be used for large strain. This is with regard to eg. the effect of both the friction from the pistons to the triaxial apparatus, and the rubber membrane. If the triaxial test further is going to be applied for remoulding studies, the effect of these at large strain must be taken into consideration to see in what degree they inflict error.

The triaxial test should be better controlled against other known models or tests. This could be done by comparing different tests, that may describe the strain softening process, eg. vane test, simple shear, plane strain compression test and so on. Important then is to do the comparison from the same block sample, to exclude variance because of index properties, and under the same conditions, eg. strain rate. The comparison may then give areas where the tests behave equally, or a correlation between the tests. From this a decision of which model, and which test presented in this study, that could be best.

Further more block sample data from other slides should be included to give the database a better statistical ground.

Bibliography

Everitt, B. and Skrondal, A. (2010). Standardized mortality rate (smr). *The Cambridge Dictionary of Statistics*, 409.

Gregersen, O. (1981). The quick clay landslide in rissa, norway. *Norwegian Geotechnical Institute Publication*, 135:1–6.

Huang, X. and Garcia, M. H. (1997). A perturbation solution for bingham-plastic mudflows. *Journal of hydraulic Engineering*, 123(11):986–994.

Huang, X. and Garcia, M. H. (1998). A herschel–bulkley model for mud flow down a slope. *Journal of fluid mechanics*, 374:305–333.

Huang, X. and Garcia, M. H. (1999). Modeling of non-hydroplaning mudflows on continental slopes. *Marine Geology*, 154(1-4):131–142.

Imran, J., Parker, G., Locat, J., and Lee, H. (2001). 1d numerical model of muddy subaqueous and subaerial debris flows. *Journal of hydraulic engineering*, 127(11):959–968.

Issler, D., Cepeda, J. M., Luna, B. Q., and Venditti, V. (2013). Back-analyses of run-out for norwegian quick-clay landslides.

Jihwan, K. (2017). Tutorial for bingclaw v.0.1.0. Technical report, NGI.

Karlsrud, K., Aas, G., and Gregersen, O. (1985). *Can we predict landslide hazards in soft sensitive clays? Summary of Norwegian practice and experiences*. Norges geotekniske institutt.

Karlsrud, K. and G. Hernandez, F. (2012). Summary of compressibility, strength and deformation parameters in relation to index properties. Technical Report 20051014-00-1-R, NGI.

Karlsrud, K. and Hernandez-Martinez, F. G. (2013). Strength and deformation properties of norwegian clays from laboratory tests on high-quality block samples. *Canadian Geotechnical Journal*, 50(12):1273–1293.

Kim, J. (2015). Extension of the bing model to two horizontal space dimensions. Technical report, NGI.

Kummeneje (1996). Grunnundersøkelser datarapport. Technical report, Kummeneje.

LeVeque, R. J. (2002). *Finite volume methods for hyperbolic problems*, volume 31. Cambridge university press.

L'Heureux, J.-S. (2013). Characterisation of historical quick clay landslides and input parameters for q-bing.

L'Heureux, J.-S., Eilertsen, R. S., Glimsdal, S., Issler, D., Solberg, I.-L., and Harbitz, C. B. (2012). The 1978 quick clay landslide at rissa, mid norway: subaqueous morphology and tsunami simulations. In *Submarine mass movements and their consequences*, pages 507–516. Springer.

Liu, Z., Lacasse, S., F., N., L'HeureuxJ.S., Kim, J., and Thakur, V. (2018). Modelling of landslide runout in sensitive clays.

Locat, P., Leroueil, S., and Locat, J. (2008). Remaniement et mobilité des débris de glissements de terrain dans les argiles sensible de l'est du canada. In *Proceedings of the 4th Canadian conference on geohazards: from causes to management. Presse de l'Université Laval, Québec*, pages 97–106.

Løken, T. (1983). Kvikkleire og skredfare-hvor og hvorfor. *Forskningsnytt*, 3:7–12.

Løvholt, F., Bondevik, S., Laberg, J. S., Kim, J., and Boylan, N. (2017). Some giant submarine landslides do not produce large tsunamis. *Geophysical Research Letters*, 44(16):8463–8472.

Lunne, T., Andersen, K. H., et al. (2007). Soft clay shear strength parameters for deepwater geotechnical design. In *Offshore site investigation and geotechnics, confronting new challenges and sharing knowledge*. Society of Underwater Technology.

Lunne, T., Berre, T., and Strandvik, S. (1997). Sample disturbance effects in soft low plastic norwegian clay. In *Symposium on Recent Developments in Soil and Pavement MechanicsCAPES-Fundacao Coordenacao do Aperfeicoamento de Pessoal de Nivel Superior; CNPq-Conselho Nacional de Desenvolvimento Cientifico a Tecnologico; FAPERJ-Fundacao de Ampora a Pesquisa do Estado do Rio de Janeiro; FINEP-Financiadora de Estudos e Projetos*.

Mallows, C. L. (1973). Some comments on c p. *Technometrics*, 15(4):661–675.

Natterøy, A. (2011). Skredkatalog om kvikkleire. *Semester Project, NTNU*.

Neter, J., Kutner, M. H., Nachtsheim, C. J., and Wasserman, W. (1996). *Applied linear statistical models*, volume 4. Irwin Chicago.

O'Brien, J. S. and Julien, P. Y. (1988). Laboratory analysis of mudflow properties. *Journal of hydraulic engineering*, 114(8):877–887.

Sandven, R., Senneset, K., Emdal, A., Nordal, S., Janbu, N., Grande, L., and Kornbrekke, H. (2014). Geotechnics, field and laboratory investigations. *Norwegian University of Science and Technology (NTNU), Geotechnical Division, Trondheim. Lecture notes: Part*, 1.

Takahashi, T. (2014). *Debris flow: mechanics, prediction and countermeasures*. CRC press.

Tavenas, F., Des Rosiers, J.-P., Leroueil, S., La Rochelle, P., and Roy, M. (1979). The use of strain energy as a yield and creep criterion for lightly overconsolidated clays. *Geotechnique*, 29(3):285–303.

Tavenas, F., Flon, P., Leroueil, S., and Lebuis, J. (1983). Remolding energy and risk of slide retrogression in sensitive clays. In *Proceedings of the Symposium on Slopes on Soft Clays, Linköping, Sweden. SGI Report*, number 17, pages 423–454.

Thakur, V. (2007). Strain localization in sensitive soft clays. *NTNU, Trondheim*.

Thakur, V., Gylland, A., Degago, S., Oset, F., and Sandven, F. (2015). In-situ determination of disintegration energy for soft sensitive clays. *Proceedings of GEOQuébec2015–challenges from North to South, Canadian Geotechnical Society*.

Thakur, V., Nordal, S., Viggiani, G., and Charrier, P. (2017). Shear bands in undrained plane strain compression of norwegian quick clays. *Canadian Geotechnical Journal*, 55(1):45–56.

Turmel, D., Locat, A., Locat, J., Leroueil, S., Locat, P., and D., D. (2018). Sensitive clay flowslides: from rupture to propagation.

Vaunat, J. and Leroueil, S. (2002). Analysis of post-failure slope movements within the framework of hazard and risk analysis. *Natural Hazards*, 26(1):81–107.

Zhaohui, W. (1982). Bed material movement in hyperconcentrated flow. *INST. HYDRODYN. & HYDRAULIC ENG., TECH. UNIV. DENMARK, DENMARK, 1982, 79*.

Appendix A

Data

In this appendix, data from all sites used in this study are shown. All index parameters are listed in Table A.1. The column "row" is the row from the excel sheet the parameters are taken from. (Database-high_quality_data-clay-SP8version.xlsm, provided from NGI). Further information about the direct triaxial raw data are linked in this sheet.

Table A.1: All gathered data

Site	S_u	S_{ur}	St	w_L	w_P	I_P	LI	γ [kN/m^3]	σ'	OCR	row	w	cc	quality	γ_{peak}	$w - w_P$
'Nybakk-Slomarka'	25	3.1	8.0645	0.4746	0.2365	0.2381	0.674	18.18	95	1.8743	291	0.397	0.566	0.012	0.0123	0.1605
'Nybakk-Slomarka'	28	1.5	18.667	0.4347	0.2338	0.2009	1.0259	17.78	132	1.3182	293	0.4399	0.495	0.0191	0.0076	0.2061
'Nybakk-Slomarka'	36.5	6	6.0833	0.457	0.241	0.216	0.7389	18.11	70.05	5.3623	285	0.4006	0.508	0.014	0.0281	0.1596
'Nybakk-Slomarka'	45	4.3	10.465	0.424	0.227	0.196	0.5995	18.83	131.95	3.2008	286	0.3445	0.497	0.0254	0.0208	0.1175
'Nybakk-Slomarka'	70	0.3	233.33	0.306	0.211	0.094	1.8617	18.44	191.98	2.2193	287	0.386	0.419	0.0391	0.0166	0.175
'Nybakk-Slomarka'	30	1.9	15.789	0.3684	0.2105	0.1579	0.8454	18.75	101.5	3.6877	289	0.344	0.408	0.0252	0.0218	0.1335
'Nybakk-Slomarka'	30	1.5	20	0.3174	0.1995	0.1178	1.3533	18.6	116.5	2.8755	290	0.359	0.476	0.0218	0.0202	0.1595
'Stjordal. parsell Trondheim'	61.536	NaN	NaN	0.293	0.192	0.101	0.7624	19.6	150	2	76	0.269	0.215	0.0388	NaN	0.077
'Stjordal. parsell Trondheim'	83.32	NaN	NaN	0.347	0.201	0.146	0.7055	19.4	214	1.4953	77	0.304	0.389	0.0457	NaN	0.103
'Stjordal. parsell Trondheim'	57.973	NaN	NaN	0.284	0.201	0.083	2.6867	17.8	110	1.5	78	0.424	0.382	0.0247	NaN	0.223
'Stjordal. parsell Trondheim'	68.188	NaN	NaN	0.252	0.185	0.067	2.1642	19.1	200	1.2	79	0.33	0.37	0.0643	NaN	0.145
'Rissa'	18.6	1.4	13.286	0.2522	0.1648	0.0874	2.2048	19.4	46.36	2.18	295	0.3575	NaN	0.0282	0.0179	0.1927
'Rissa'	14.2	0.69	20.58	0.2624	0.1808	0.0816	1.6176	19.13	42.52	2.36	294	0.3128	NaN	0.029	0.0088	0.132
'Rissa'	14	1	14	0.2972	0.1937	0.1035	1.7527	18.9	49.04	2.05	296	0.3751	NaN	0.0394	0.0022	0.1814
'Gardermobanen'	76.5	NaN	NaN	0.398	0.225	0.173	0.9653	18.2	190	2.1053	7	0.392	0.49	0.047	NaN	0.167
'Gardermobanen'	80.2	0.3342	240	0.308	0.215	0.093	1.8495	18.2	227	1.6087	8	0.387	0.46	0.0506	0.0109	0.172
'Hvalsdalen'	53.4	4.1077	13	0.336	0.198	0.138	1	18.9	57	6.4912	9	0.336	0.37	0.0294	0.0346	0.138
'Hvalsdalen'	58.7	2.935	20	0.323	0.204	0.119	1.3529	18.5	80	5	10	0.365	0.46	0.0329	0.0326	0.161
'Eidsvoll'	61	15.25	4	0.345	0.217	0.128	0.6719	19.2	106	2.3585	11	0.303	0.41	0.0191	0.0061	0.086
'Eidsvoll'	100.8	20.16	5	0.337	0.199	0.138	0.5797	19.6	221	1.9005	13	0.279	0.37	0.0362	0.0081	0.08
'Glava'	50.1	7.1571	7	0.368	0.197	0.171	0.7719	18.91	60.5	4.3682	14	0.329	0.293	0.0059	0.0167	0.132
'Glava'	48.7	4.87	10	0.388	0.206	0.182	0.6648	18.93	66	4.1	15	0.327	0.338	0.0209	0.0173	0.121
'Barkåker'	36.245	0.4264	85	0.263	0.148	0.115	1.4696	18.9	64	2.5	16	0.317	0.307	0.0148	0.0068	0.169
'Barkåker'	40.542	0.477	85	0.274	0.167	0.107	1.8972	18.4	92	1.7	18	0.37	0.33	0.024	0.0053	0.203
'Lierstranda'	29.815	4.2593	7	0.43	0.227	0.203	0.8719	18.07	54	1.9444	19	0.404	0.355	0.026	0.017	0.177
'Lierstranda'	50.2	6.275	8	0.399	0.213	0.186	0.9409	18.2	109	1.8349	20	0.388	0.308	0.025	0.0078	0.175
'Lierstranda'	52.116	6.5145	8	0.399	0.213	0.186	0.871	18.34	109	1.789	21	0.375	0.308	0.0236	0.0097	0.162
'Lierstranda'	52.748	4.3957	12	0.344	0.198	0.146	0.9384	18.89	146	1.3356	22	0.335	0.345	0.039	0.0053	0.137
'Drammen'	80.6	11.514	7	0.343	0.188	0.155	1.0923	18.6	111.9	1.133	30	0.3573	0.36	0.0274	0.0068	0.1693
'Drammen'	100.8	14.4	7	NaN	NaN	0.149	NaN	18.6	111.9	1.133	31	0.3515	NaN	0.0267	0.0081	NaN
'Emmerstad'	27.5	0.1858	148	0.3167	0.2172	0.0995	2.2693	NaN	28.9	5.2632	32	0.443	0.4	0.0015	0.0086	0.2258
'Emmerstad'	31.1	0.2101	148	0.3222	0.2158	0.1064	1.4401	18.1	31.1	4.2071	33	0.369	0.4	0.0028	0.0066	0.1532
'Emmerstad'	29	0.1959	148	0.2787	0.2165	0.0622	2.918	NaN	34.3	2.815	34	0.398	0.3	0.0013	0.0039	0.1815
'Emmerstad'	32.4	0.144	225	0.2533	0.1809	0.0724	3.0815	NaN	34.4	3.2333	35	0.404	0.3	0.0034	0.0037	0.2231
'Emmerstad'	35.7	0.4636	77	0.2895	0.2171	0.0724	3.0787	17.6	41.7	2.4943	37	0.44	0.4	0.0042	0.0051	0.2229
'Ellingsrud'	27.4	0.4492	61	0.2664	0.2064	0.06	2.144	18.6	61.2	2.1	39	0.335	0.37	0.0167	0.0071	0.1286
'Ellingsrud'	30	0.4918	61	0.2672	0.2118	0.0554	2.4765	18.6	67.7	1.8	41	0.349	0.37	0.0194	0.0065	0.1372
'Ellingsrud'	35	0.5932	59	0.269	0.205	0.064	2.1719	18.7	92.2	1.4	42	0.344	0.37	0.0187	0.0047	0.139
Daneviksgt.'	29	3.5366	8.2	0.62	0.3273	0.2927	0.6898	16.93	66.7	1.5142	51	0.5292	0.4	0.0234	0.0101	0.2019
Daneviksgt.'	40.9	10.225	4	0.3	0.099	0.201	1.209	18.74	126.5	1.2016	53	0.342	0.41	0.0407	0.0039	0.243
'Nykirke'	47.929	0.7374	65	0.225	0.1864	0.0386	2.1554	19.66	65	4.9	55	0.2696	0.266	0.0253	0.0177	0.0832
'Nykirke'	70.202	0.8775	80	0.237	0.1497	0.0873	2.4765	18.34	80	3.625	56	0.3659	0.353	0.0212	0.0149	0.2162
'Nykirke'	70.782	0.8848	80	0.25	0.1826	0.0674	1.0386	19.75	105	3.7143	57	0.2526	0.266	0.0189	0.0102	0.07
'Kvenild/Tiller'	31.7	1.4279	22.2	NaN	NaN	0.1357	NaN	18.33	61.8	3.5599	58	0.3693	0.31	0.0264	0.0134	NaN
'Kvenild/Tiller'	29.6	0.5382	55	NaN	NaN	0.1005	NaN	18.66	65.1	1.5054	59	0.3553	0.36	0.0195	0.0118	NaN
'Kvenild/Tiller'	34.5	0.552	62.5	NaN	NaN	0.1296	NaN	18.2	72.7	0.8941	60	0.3108	0.467	0.0194	0.0084	NaN
'Onsøy2 (2001)'	25.7	5.587	4.6	0.645	0.286	0.359	0.9777	15.9	48	1.8	61	0.637	0.49	0.0126	0.0098	0.351
'Onsøy2 (2001)'	34.2	7.125	4.8	0.718	0.303	0.415	0.7976	15.97	80	1.3	62	0.634	0.645	0.0205	0.0111	0.331
'Onsøy2 (2001)'	34.4	7.6444	4.5	0.74	0.333	0.407	0.7617	15.98	92	1.4	63	0.643	0.573	0.0266	0.0105	0.31
'Klett-Bårdshaug-111'	48.755	0.6415	76	0.251	0.178	0.073	1.8219	19.55	65	4.6154	64	0.311	0.289	0.0275	0.0614	0.133
'Klett-Bårdshaug-111'	63.581	1.156	55	0.254	0.181	0.073	1.5342	19.7	76	6.25	65	0.293	0.285	0.0332	0.0385	0.112
'Klett-Bårdshaug-138'	54.767	0.7113	77	0.249	0.17	0.079	1.9873	19	116	1.8966	66	0.327	0.325	0.0387	0.0134	0.157
'Klett-Bårdshaug-138'	84.257	8.4257	10	0.32	0.193	0.127	0.9291	19.3	183	1.8251	67	0.311	0.316	0.0432	0.0108	0.118
'Kløfta-Nybakk'	52.911	6.6139	8	NaN	NaN	0.184	NaN	18.2	98	2.602	68	0.386	0.459	0.021	0.0111	NaN
'Kløfta-Nybakk'	58.609	8.3727	7	NaN	NaN	0.124	NaN	18.9	155	1.5806	69	0.322	0.332	0.0334	0.0105	NaN
'Kløfta-Nybakk'	74.249	0.55	135	NaN	NaN	0.079	NaN	18.8	213	1.3146	70	0.366	0.457	0.0494	0.0079	NaN
'OSBS (2004)'	16.468	3.58	4.6	NaN	NaN	NaN	NaN	15.95	36.4	1.4835	71	0.66	NaN	0.0074	0.01	NaN
'OSBS (2004)'	14.563	3.1659	4.6	NaN	NaN	NaN	NaN	15.94	36.6	1.4754	72	0.6579	NaN	0.0261	0.0181	NaN
'OSBS (2004)'	30.922	6.7222	4.6	NaN	NaN	NaN	NaN	15.65	59.8	1.6167	73	0.705	NaN	0.0083	0.0108	NaN
'OSBS (2004)'	33.565	7.4589	4.5	NaN	NaN	NaN	NaN	15.91	89.5	1.2626	74	0.6529	NaN	0.0258	0.0118	NaN
'OSBS (2004)'	42.47	3.8609	11	NaN	NaN	NaN	NaN	16.3	116	1.3362	75	0.5903	NaN	0.0329	0.0105	NaN

Appendix B

Correlations

This appendix shows the correlation between the different parameters (Tab. B.1), with the respective P-value (Tab. B.2). These tables are used in the assessment of the different regression models in Chapter 4.

Table B.1: The correlation coefficient is shown in a colour scale, where dark green shows strong relationship, while light green to white shows moderate to no relationship

Corr Coeff	pc	γ_{peak}	OCR	w_L	w_P	Ip	LI	w	cc	σ'	S_u	S_{ur}	w-w_P	Qualitiy, Δe/ei	a1	a2	b2	Γ	St	$pc \cdot w_L$	$LI \cdot w_L$
pc	1.00	0.56	0.44	-0.18	-0.17	-0.17	-0.36	-0.49	-0.07	0.53	0.65	0.20	-0.57	0.39	-0.23	-0.54	0.65	-0.39	0.04	0.88	-0.54
γ_{peak}	0.56	1.00	0.66	-0.08	-0.07	-0.07	-0.12	-0.18	-0.07	-0.10	0.12	-0.15	-0.21	0.18	-0.42	-0.67	0.74	-0.38	-0.09	0.46	-0.22
OCR	0.44	0.66	1.00	-0.20	-0.14	-0.22	0.03	-0.23	-0.18	-0.47	-0.10	-0.22	-0.23	-0.35	-0.29	-0.44	0.45	-0.12	0.13	0.32	-0.08
w_L	-0.18	-0.08	-0.20	1.00	0.87	0.97	-0.57	0.79	0.69	-0.05	-0.20	0.28	0.54	-0.17	-0.19	-0.27	0.18	-0.26	-0.42	0.25	-0.12
w_P	-0.17	-0.07	-0.14	0.87	1.00	0.73	-0.34	0.75	0.60	-0.08	-0.21	0.16	0.40	-0.23	0.03	-0.12	0.14	-0.04	-0.19	0.21	0.08
Ip	-0.17	-0.07	-0.22	0.97	0.73	1.00	-0.63	0.74	0.66	-0.03	-0.18	0.32	0.55	-0.12	-0.27	-0.32	0.17	-0.34	-0.49	0.25	-0.20
LI	-0.36	-0.12	0.03	-0.57	-0.34	-0.63	1.00	0.02	-0.25	-0.31	-0.23	-0.53	0.24	-0.16	0.44	0.59	-0.38	0.69	0.66	-0.62	0.87
w	-0.49	-0.18	-0.23	0.79	0.75	0.74	0.02	1.00	0.66	-0.28	-0.41	-0.04	0.90	-0.30	0.00	0.03	-0.06	0.08	-0.06	-0.16	0.49
cc	-0.07	-0.07	-0.18	0.69	0.60	0.66	-0.25	0.66	1.00	0.08	-0.22	0.22	0.53	-0.07	0.01	-0.12	0.19	-0.18	-0.23	0.30	0.10
σ'	0.53	-0.10	-0.47	-0.05	-0.08	-0.03	-0.31	-0.28	0.08	1.00	0.78	0.46	-0.34	0.76	0.04	-0.13	0.22	-0.29	0.02	0.50	-0.40
S_u	0.65	0.12	-0.10	-0.20	-0.21	-0.18	-0.23	-0.41	-0.22	0.78	1.00	0.49	-0.44	0.56	-0.06	-0.20	0.27	-0.20	0.08	0.51	-0.39
S_{ur}	0.20	-0.15	-0.22	0.28	0.16	0.32	-0.53	-0.04	0.22	0.46	0.49	1.00	-0.17	0.10	0.06	0.01	0.02	-0.20	-0.41	0.38	-0.50
w-w_P	-0.57	-0.21	-0.23	0.54	0.40	0.55	0.24	0.90	0.53	-0.34	-0.44	-0.17	1.00	-0.27	-0.02	0.13	-0.19	0.15	0.05	-0.35	0.63
Qualitiy, Δe/ei	0.39	0.18	-0.35	-0.17	-0.23	-0.12	-0.16	-0.30	-0.07	0.76	0.56	0.10	-0.27	1.00	-0.28	-0.38	0.32	-0.51	-0.13	0.26	-0.30
a1	-0.23	-0.42	-0.29	-0.19	0.03	-0.27	0.44	0.00	0.01	0.04	-0.06	0.06	-0.02	-0.28	1.00	0.78	-0.20	0.50	0.25	-0.29	0.42
a2	-0.54	-0.67	-0.44	-0.27	-0.12	-0.32	0.59	0.03	-0.12	-0.13	-0.20	0.01	0.13	-0.38	0.78	1.00	-0.74	0.78	0.26	-0.60	0.57
b2	0.65	0.74	0.45	0.18	0.14	0.17	-0.38	-0.06	0.19	0.22	0.27	0.02	-0.19	0.32	-0.20	-0.74	1.00	-0.60	-0.15	0.66	-0.38
Γ	-0.39	-0.38	-0.12	-0.26	-0.04	-0.34	0.69	0.08	-0.18	-0.29	-0.20	-0.20	0.15	-0.51	0.50	0.78	-0.60	1.00	0.40	-0.47	0.70
'St'	0.04	-0.09	0.13	-0.42	-0.19	-0.49	0.66	-0.06	-0.23	0.02	0.08	-0.41	0.05	-0.13	0.25	0.26	-0.15	0.40	1.00	-0.19	0.57
$pc \cdot w_L$	0.88	0.46	0.32	0.25	0.21	0.25	-0.62	-0.16	0.30	0.50	0.51	0.38	-0.35	0.26	-0.29	-0.60	0.66	-0.47	-0.19	1.00	-0.60
$LI \cdot w_L$	-0.54	-0.22	-0.08	-0.12	0.08	-0.20	0.87	0.49	0.10	-0.40	-0.39	-0.50	0.63	-0.30	0.42	0.57	-0.38	0.70	0.57	-0.60	1.00

Table B.2: Correlation overview between parameters. The correlation is between the log value of the parameter. Red cells is where the P-value is smaller than 0.05 and the yellow cells shows where the P-value is between 0.05 and 0.1

P-Value	pc	γ_{peak}	OCR	w_L	w_P	Ip	LI	w	cc	σ'	S_u	S_{ur}	w-w_P	Qualitiy, Δe/ei	a1	a2	b2	Γ	St	$pc \cdot w_L$	$LI \cdot w_L$
pc	1.00	0.00	0.00	0.19	0.23	0.22	0.01	0.00	0.64	0.00	0.00	0.20	0.00	0.00	0.12	0.00	0.00	0.01	0.82	0.00	0.00
γ_{peak}	0.00	1.00	0.00	0.62	0.65	0.64	0.44	0.23	0.67	0.53	0.43	0.34	0.16	0.23	0.00	0.00	0.00	0.01	0.54	0.00	0.15
OCR	0.00	0.00	1.00	0.14	0.32	0.11	0.82	0.10	0.19	0.00	0.48	0.15	0.09	0.01	0.05	0.00	0.00	0.45	0.40	0.02	0.57
w_L	0.19	0.62	0.14	1.00	0.00	0.00	0.00	0.00	0.00	0.72	0.15	0.06	0.00	0.23	0.22	0.07	0.25	0.09	0.00	0.06	0.39
w_P	0.23	0.65	0.32	0.00	1.00	0.00	0.01	0.00	0.00	0.55	0.13	0.30	0.00	0.09	0.85	0.45	0.34	0.78	0.21	0.14	0.55
Ip	0.22	0.64	0.11	0.00	0.00	1.00	0.00	0.00	0.00	0.83	0.20	0.03	0.00	0.38	0.07	0.03	0.25	0.02	0.00	0.07	0.14
LI	0.01	0.44	0.82	0.00	0.01	0.00	1.00	0.90	0.08	0.02	0.10	0.00	0.07	0.24	0.00	0.00	0.01	0.00	0.00	0.00	0.00
w	0.00	0.23	0.10	0.00	0.00	0.00	0.90	1.00	0.00	0.04	0.00	0.77	0.00	0.03	0.99	0.82	0.70	0.58	0.71	0.25	0.00
cc	0.64	0.67	0.19	0.00	0.00	0.00	0.08	0.00	1.00	0.59	0.12	0.16	0.00	0.63	0.95	0.44	0.23	0.26	0.14	0.03	0.48
σ'	0.00	0.53	0.00	0.72	0.55	0.83	0.02	0.04	0.59	1.00	0.00	0.00	0.01	0.00	0.78	0.40	0.15	0.05	0.87	0.00	0.00
S_u	0.00	0.43	0.48	0.15	0.13	0.20	0.10	0.00	0.12	0.00	1.00	0.00	0.00	0.00	0.69	0.18	0.08	0.18	0.62	0.00	0.00
S_{ur}	0.20	0.34	0.15	0.06	0.30	0.03	0.00	0.77	0.16	0.00	0.00	1.00	0.25	0.50	0.68	0.95	0.92	0.19	0.00	0.01	0.00
w-w_P	0.00	0.16	0.09	0.00	0.00	0.00	0.07	0.00	0.00	0.01	0.00	0.25	1.00	0.05	0.89	0.39	0.22	0.32	0.73	0.01	0.00
Qualitiy, Δe/ei	0.00	0.23	0.01	0.23	0.09	0.38	0.24	0.03	0.63	0.00	0.00	0.50	0.05	1.00	0.06	0.01	0.03	0.00	0.39	0.06	0.03
a1	0.12	0.00	0.05	0.22	0.85	0.07	0.00	0.99	0.95	0.78	0.69	0.68	0.89	0.06	1.00	0.00	0.18	0.00	0.10	0.05	0.00
a2	0.00	0.00	0.00	0.07	0.45	0.03	0.00	0.82	0.44	0.40	0.18	0.95	0.39	0.01	0.00	1.00	0.00	0.00	0.08	0.00	0.00
b2	0.00	0.00	0.00	0.25	0.34	0.25	0.01	0.70	0.23	0.15	0.08	0.92	0.22	0.03	0.18	0.00	1.00	0.00	0.32	0.00	0.01
Γ	0.01	0.01	0.45	0.09	0.78	0.02	0.00	0.58	0.26	0.05	0.18	0.19	0.32	0.00	0.00	0.00	0.00	1.00	0.01	0.00	0.00
'St'	0.82	0.54	0.40	0.00	0.21	0.00	0.00	0.71	0.14	0.87	0.62	0.00	0.73	0.39	0.10	0.08	0.32	0.01	1.00	0.21	0.00
$pc \cdot w_L$	0.00	0.00	0.02	0.06	0.14	0.07	0.00	0.25	0.03	0.00	0.00	0.01	0.01	0.06	0.05	0.00	0.00	0.00	0.21	1.00	0.00
$LI \cdot w_L$	0.00	0.15	0.57	0.39	0.55	0.14	0.00	0.00	0.48	0.00	0.00	0.00	0.00	0.03	0.00	0.00	0.01	0.00	0.00	0.00	1.00

Appendix C

Additional Information

This appendix will go through the normalization process step by step, starting with the case of no normalization.

C.1 No Normalization

From the studied graphs in appendix C.1. A trend is found for some of the parameters, but in general there are large spread for all of the parameters. The parameter with clearest trend is γ_{peak}. γ_{peak} is the shear strain at the peak value of the triaxial test. This parameter shows that for small peak shear strain, E_N becomes small and for large peak shear strain E_N becomes large. w and w_P shows a trend with decreasing values from left to right on the graph that indicates that E_R should be multiplied by these values.

While both OCR and S_u shows a small indication of dependency with large values to the left and small values to the right on the graph. This indicates that E_R should be divided by these parameters.

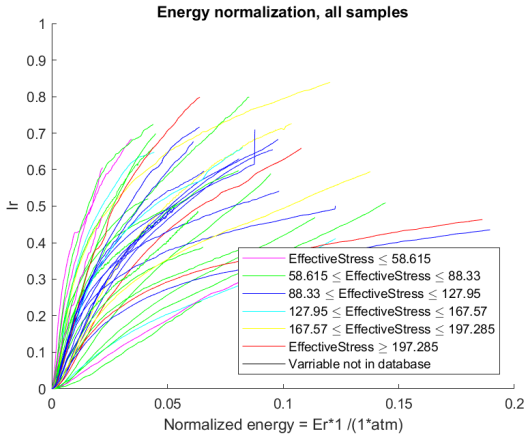

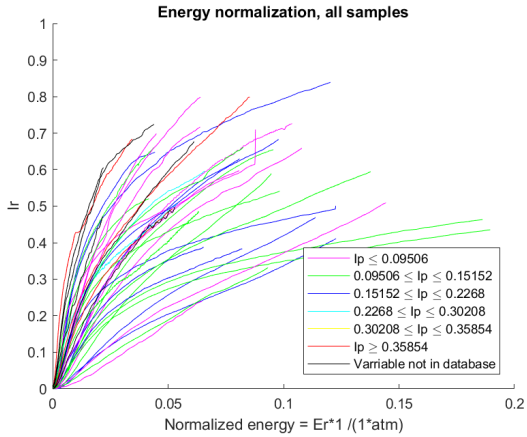

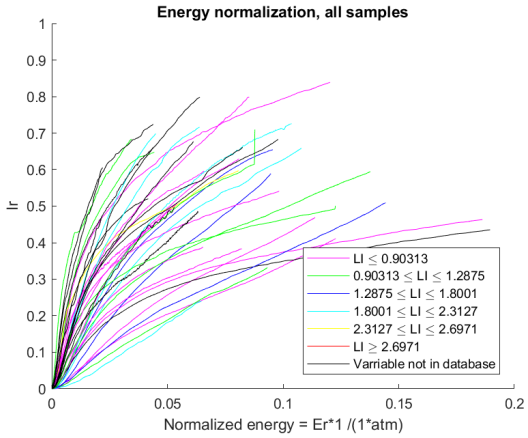
Energy normalization, all samples
Ir
Normalized energy = Er*1 /(1*atm)
LI ≤ 0.90313
0.90313 ≤ LI ≤ 1.2875
1.2875 ≤ LI ≤ 1.8001
1.8001 ≤ LI ≤ 2.3127
2.3127 ≤ LI ≤ 2.6971
LI ≥ 2.6971
Varriable not in database

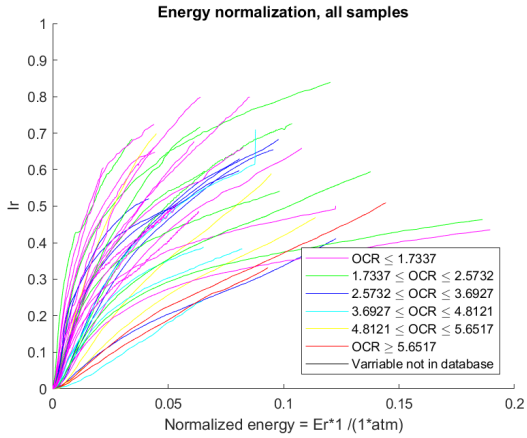
Energy normalization, all samples
Ir
Normalized energy = Er*1 /(1*atm)
OCR ≤ 1.7337
1.7337 ≤ OCR ≤ 2.5732
2.5732 ≤ OCR ≤ 3.6927
3.6927 ≤ OCR ≤ 4.8121
4.8121 ≤ OCR ≤ 5.6517
OCR ≥ 5.6517
Varriable not in database

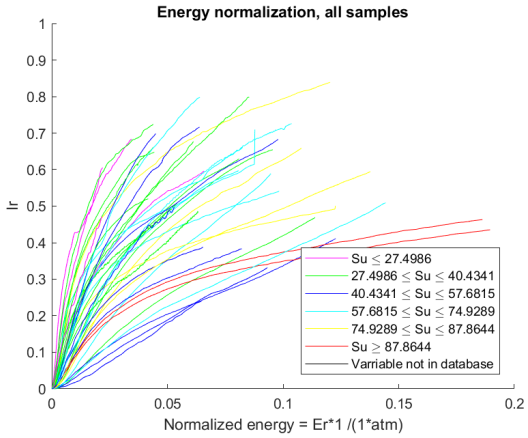
Energy normalization, all samples
Ir
Normalized energy = Er*1 /(1*atm)
Su ≤ 27.4986
27.4986 ≤ Su ≤ 40.4341
40.4341 ≤ Su ≤ 57.6815
57.6815 ≤ Su ≤ 74.9289
74.9289 ≤ Su ≤ 87.8644
Su ≥ 87.8644
Varriable not in database

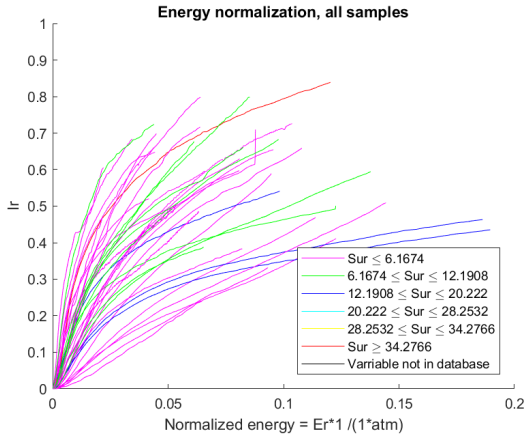
Energy normalization, all samples
Ir
Normalized energy = Er*1 /(1*atm)
Sur ≤ 6.1674
6.1674 ≤ Sur ≤ 12.1908
12.1908 ≤ Sur ≤ 20.222
20.222 ≤ Sur ≤ 28.2532
28.2532 ≤ Sur ≤ 34.2766
Sur ≥ 34.2766
Varriable not in database

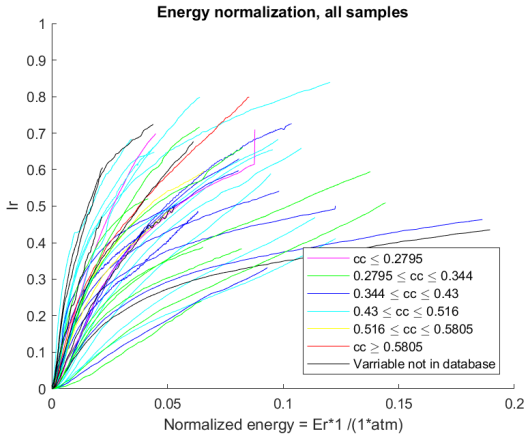
Energy normalization, all samples
Ir
Normalized energy = Er*1 /(1*atm)
cc ≤ 0.2795
0.2795 ≤ cc ≤ 0.344
0.344 ≤ cc ≤ 0.43
0.43 ≤ cc ≤ 0.516
0.516 ≤ cc ≤ 0.5805
cc ≥ 0.5805
Varriable not in database

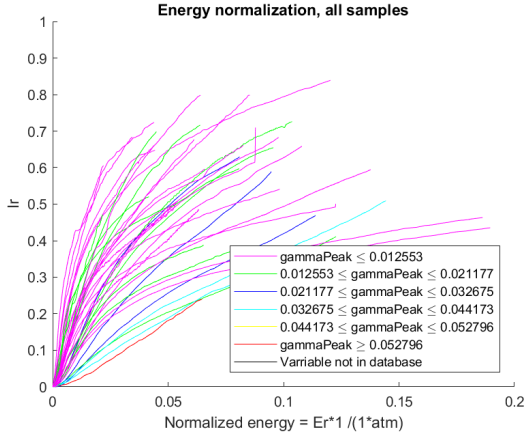
Energy normalization, all samples
Ir
Normalized energy = Er*1 /(1*atm)
gammaPeak ≤ 0.012553
0.012553 ≤ gammaPeak ≤ 0.021177
0.021177 ≤ gammaPeak ≤ 0.032675
0.032675 ≤ gammaPeak ≤ 0.044173
0.044173 ≤ gammaPeak ≤ 0.052796
gammaPeak ≥ 0.052796
Varriable not in database

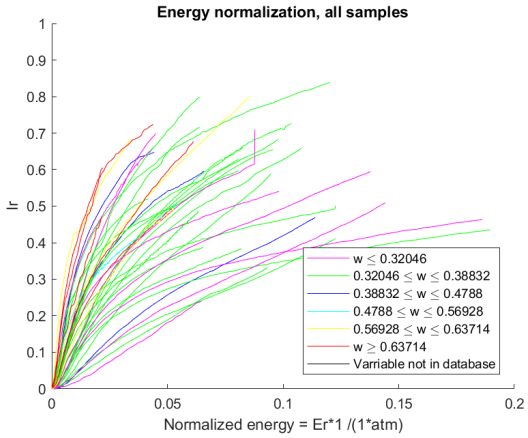

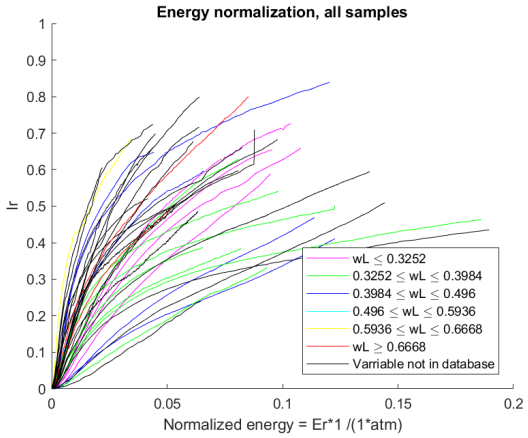

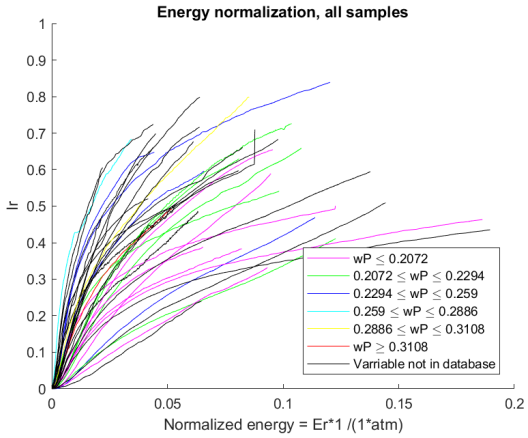

C.2 Normalization with γ_{peak}

Figures in this appendix shows Er/γ_p vs Ir, with the spread of a normalization parameter emphasized in colours.

In this section γ_{peak} was accounted for, so that $N = \sigma_a \cdot \gamma_{peak}$. By studying this section. The parameter with the most dependency was S_u. This parameter had a clear trend. When E_N was large it was large and when E_N was small small S_u was found.

To improve the normalization σ_a had to be exchanged with S_u. This made the new normalization parameter $N = S_u \cdot \gamma_{peak}$. This is further visualized in appendix C.3.

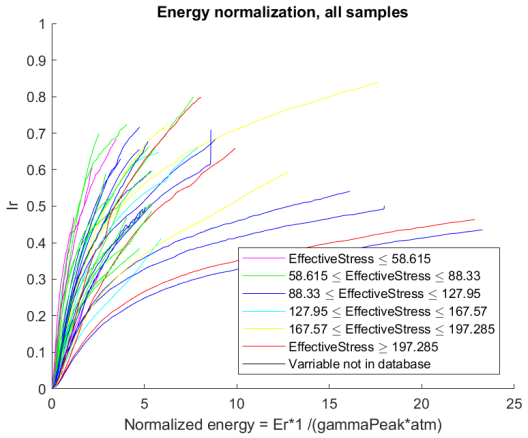
Energy normalization, all samples
Ir
Normalized energy = Er*1 /(gammaPeak*atm)
EffectiveStress ≤ 58.615
58.615 ≤ EffectiveStress ≤ 88.33
88.33 ≤ EffectiveStress ≤ 127.95
127.95 ≤ EffectiveStress ≤ 167.57
167.57 ≤ EffectiveStress ≤ 197.285
EffectiveStress ≥ 197.285
Varriable not in database

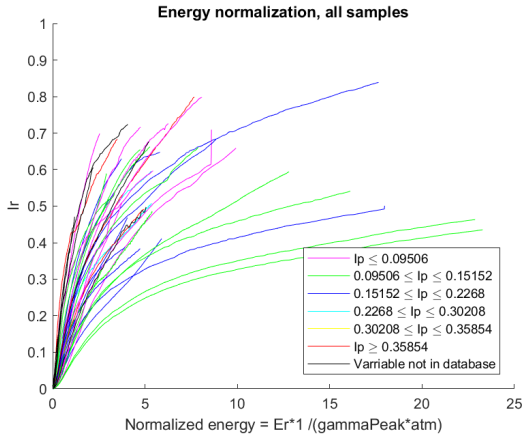
Energy normalization, all samples
Ir
Normalized energy = Er*1 /(gammaPeak*atm)
Ip ≤ 0.09506
0.09506 ≤ Ip ≤ 0.15152
0.15152 ≤ Ip ≤ 0.2268
0.2268 ≤ Ip ≤ 0.30208
0.30208 ≤ Ip ≤ 0.35854
Ip ≥ 0.35854
Varriable not in database

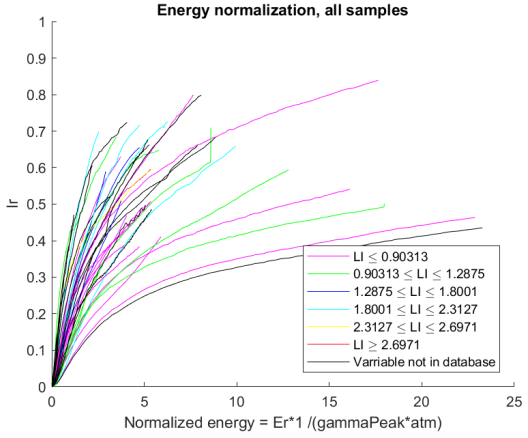
Energy normalization, all samples
Ir
Normalized energy = Er*1 /(gammaPeak*atm)
LI ≤ 0.90313
0.90313 ≤ LI ≤ 1.2875
1.2875 ≤ LI ≤ 1.8001
1.8001 ≤ LI ≤ 2.3127
2.3127 ≤ LI ≤ 2.6971
LI ≥ 2.6971
Varriable not in database

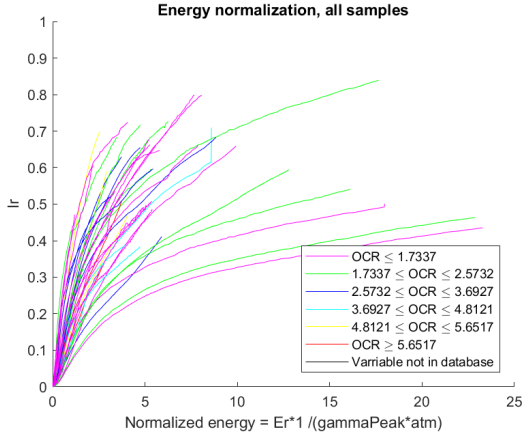
Energy normalization, all samples
Ir
Normalized energy = Er*1 /(gammaPeak*atm)
OCR ≤ 1.7337
1.7337 ≤ OCR ≤ 2.5732
2.5732 ≤ OCR ≤ 3.6927
3.6927 ≤ OCR ≤ 4.8121
4.8121 ≤ OCR ≤ 5.6517
OCR ≥ 5.6517
Varriable not in database

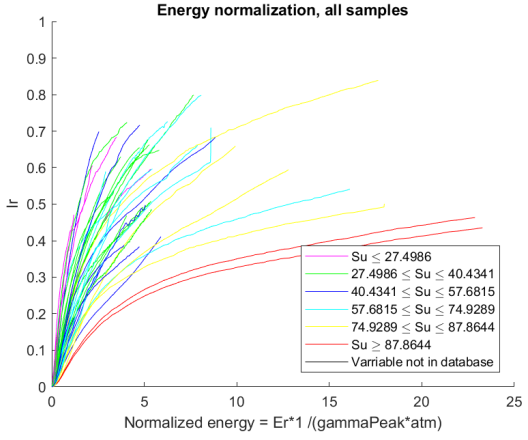
Energy normalization, all samples
Ir
Normalized energy = Er*1 /(gammaPeak*atm)
Su ≤ 27.4986
27.4986 ≤ Su ≤ 40.4341
40.4341 ≤ Su ≤ 57.6815
57.6815 ≤ Su ≤ 74.9289
74.9289 ≤ Su ≤ 87.8644
Su ≥ 87.8644
Varriable not in database

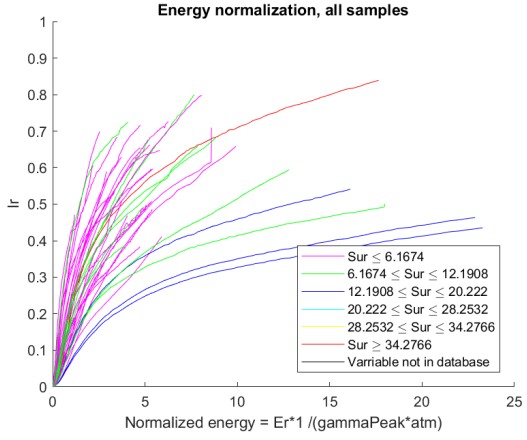
Energy normalization, all samples
Ir
Normalized energy = Er*1 /(gammaPeak*atm)
Sur ≤ 6.1674
6.1674 ≤ Sur ≤ 12.1908
12.1908 ≤ Sur ≤ 20.222
20.222 ≤ Sur ≤ 28.2532
28.2532 ≤ Sur ≤ 34.2766
Sur ≥ 34.2766
Varriable not in database

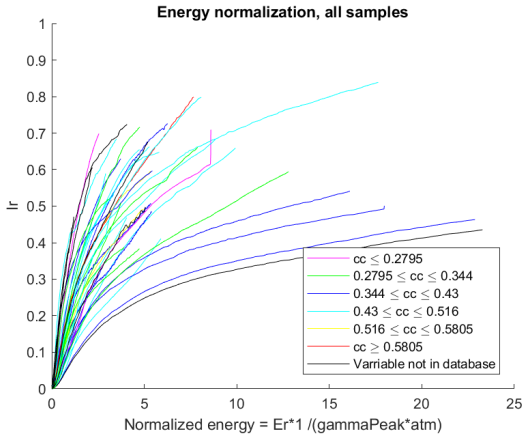

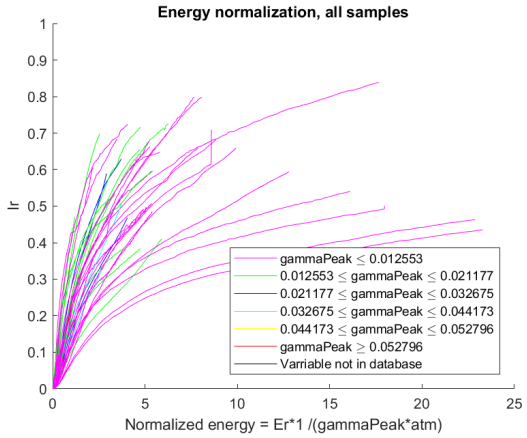

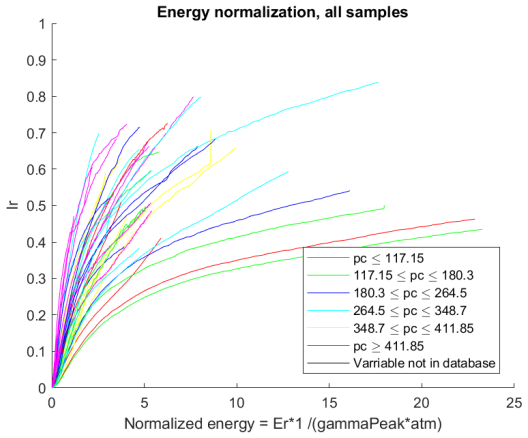

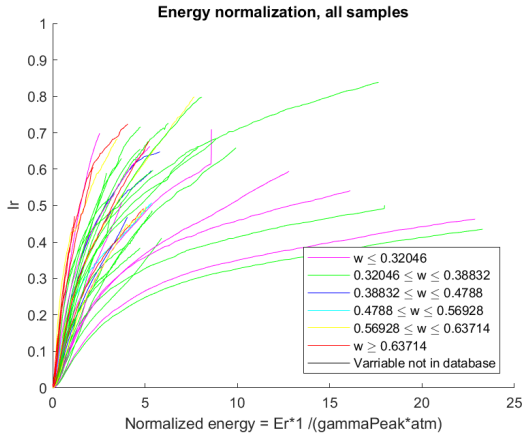

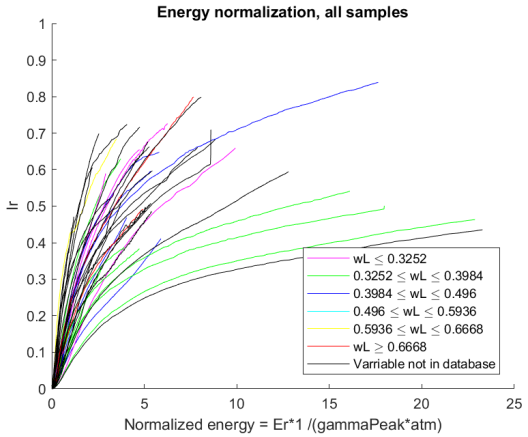

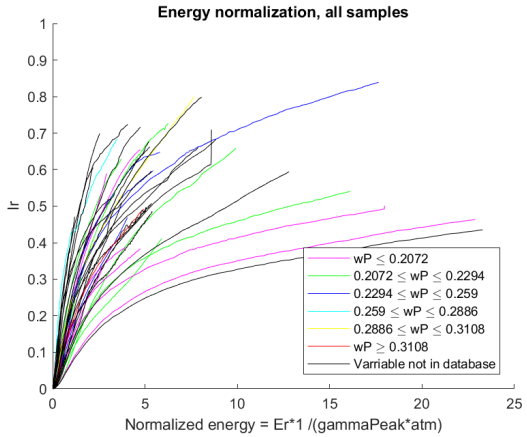

C.3 Adding S_u to Normalization

Figures in this appendix shows $\mathrm{Er}/(\gamma_p \cdot Su)$ vs Ir, with the spread of a normalization parameter emphasized in colours.

A clear trend is now presented for LI, where large LI was found where E_N was small and small LI was found where E_N was large. Therefore LI should be multiplied to E_N to get the graphs closer together. As seen in appendix C.4.

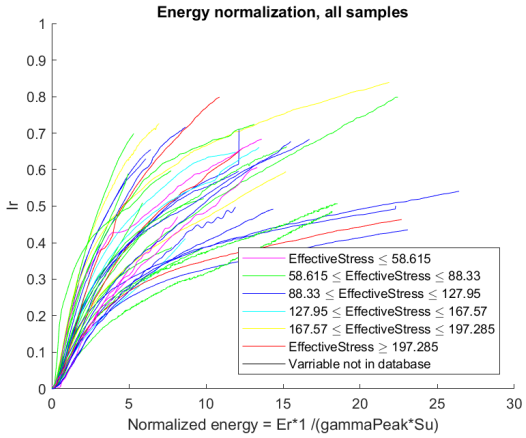
Energy normalization, all samples
Ir
Normalized energy = Er*1 /(gammaPeak*Su)
EffectiveStress ≤ 58.615
58.615 ≤ EffectiveStress ≤ 88.33
88.33 ≤ EffectiveStress ≤ 127.95
127.95 ≤ EffectiveStress ≤ 167.57
167.57 ≤ EffectiveStress ≤ 197.285
EffectiveStress ≥ 197.285
Varriable not in database

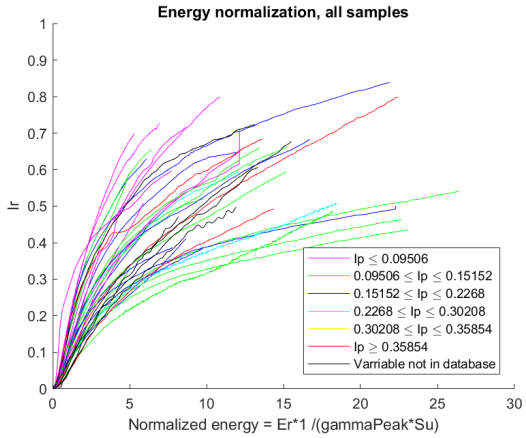
Energy normalization, all samples
Ir
Normalized energy = Er*1 /(gammaPeak*Su)
Ip ≤ 0.09506
0.09506 ≤ Ip ≤ 0.15152
0.15152 ≤ Ip ≤ 0.2268
0.2268 ≤ Ip ≤ 0.30208
0.30208 ≤ Ip ≤ 0.35854
Ip ≥ 0.35854
Varriable not in database

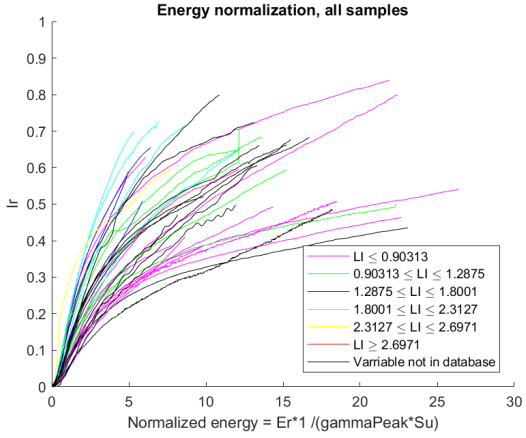
Energy normalization, all samples
Ir
Normalized energy = Er*1 /(gammaPeak*Su)
LI ≤ 0.90313
0.90313 ≤ LI ≤ 1.2875
1.2875 ≤ LI ≤ 1.8001
1.8001 ≤ LI ≤ 2.3127
2.3127 ≤ LI ≤ 2.6971
LI ≥ 2.6971
Varriable not in database

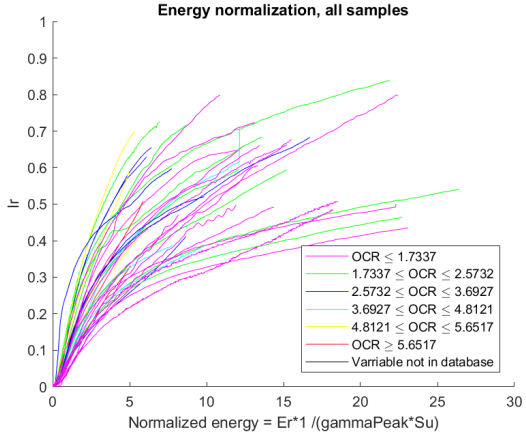
Energy normalization, all samples
Ir
Normalized energy = Er*1 /(gammaPeak*Su)
OCR ≤ 1.7337
1.7337 ≤ OCR ≤ 2.5732
2.5732 ≤ OCR ≤ 3.6927
3.6927 ≤ OCR ≤ 4.8121
4.8121 ≤ OCR ≤ 5.6517
OCR ≥ 5.6517
Varriable not in database

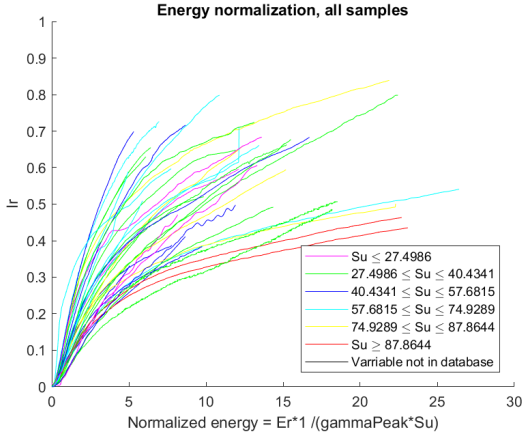
Energy normalization, all samples
Ir
Normalized energy = Er*1 /(gammaPeak*Su)
Su ≤ 27.4986
27.4986 ≤ Su ≤ 40.4341
40.4341 ≤ Su ≤ 57.6815
57.6815 ≤ Su ≤ 74.9289
74.9289 ≤ Su ≤ 87.8644
Su ≥ 87.8644
Varriable not in database

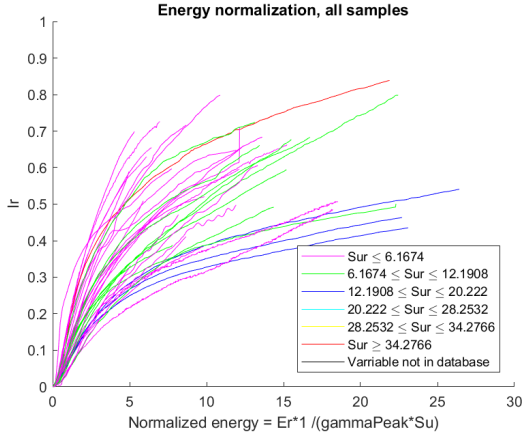
Energy normalization, all samples
Ir
Normalized energy = Er*1 /(gammaPeak*Su)
Sur ≤ 6.1674
6.1674 ≤ Sur ≤ 12.1908
12.1908 ≤ Sur ≤ 20.222
20.222 ≤ Sur ≤ 28.2532
28.2532 ≤ Sur ≤ 34.2766
Sur ≥ 34.2766
Varriable not in database

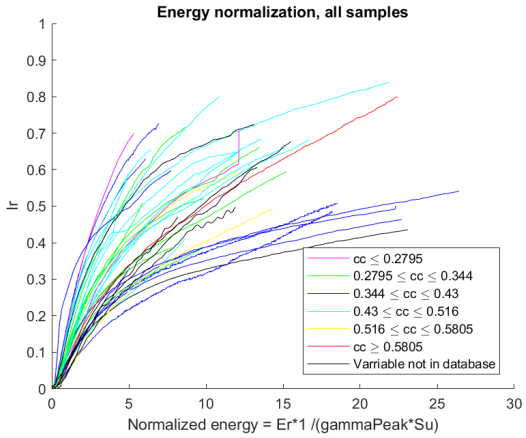

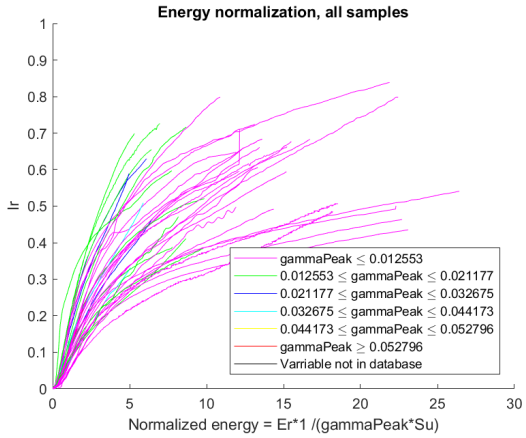

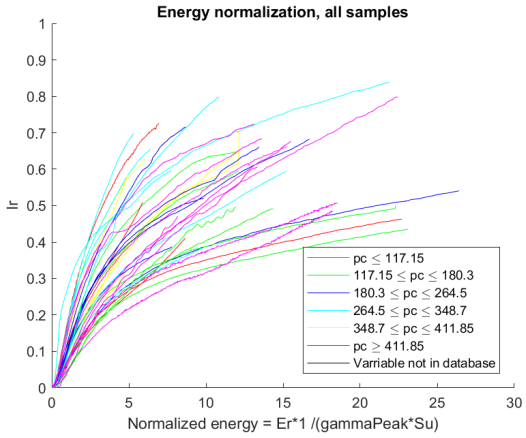

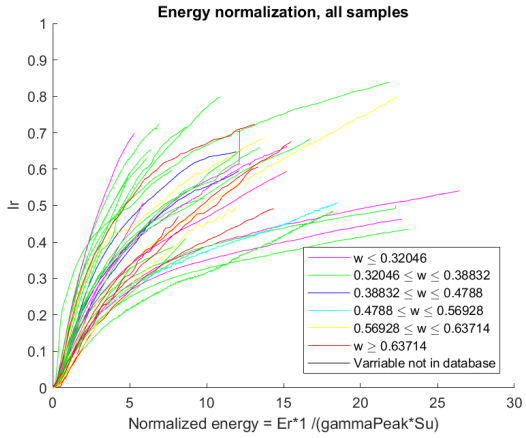

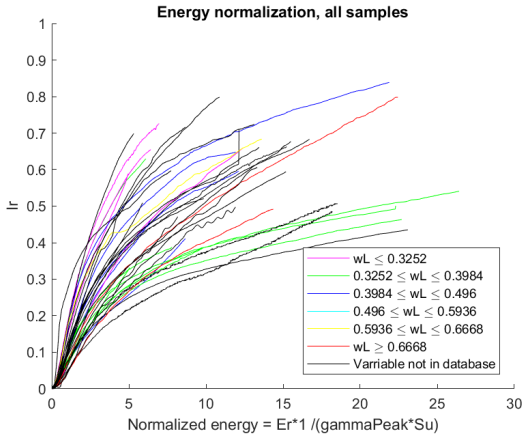

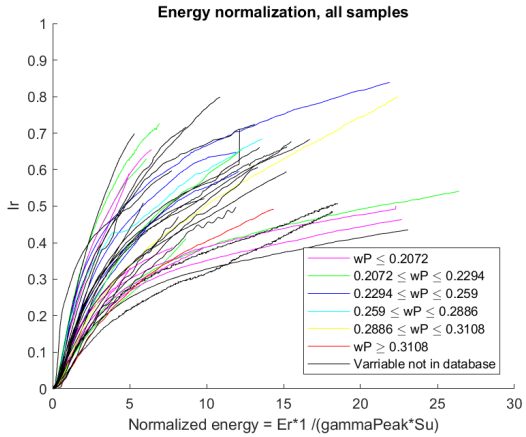

C.4 Adding LI to Normalization

Figures in this appendix shows $\mathrm{Er} \cdot \mathrm{IL}/(\gamma_p \cdot Su)$ vs Ir, with the spread of a normalization parameter emphasized in colours.

In appendix C.3 the clearest trend in with the parameter LI. LI overestimates so that the trend is in the opposite direction. A correction to LI was made by taking the square root of LI instead. The result of this can be seen in C.5.

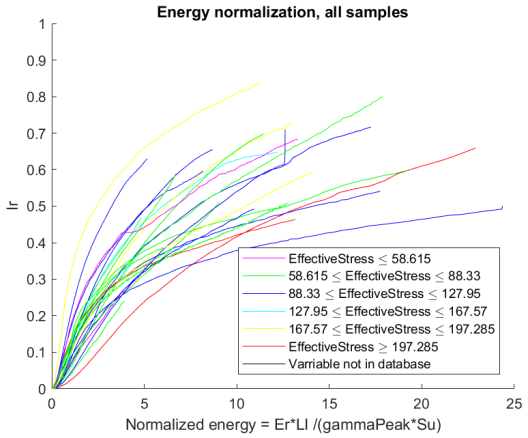
Energy normalization, all samples
Ir
Normalized energy = Er*LI /(gammaPeak*Su)
EffectiveStress ≤ 58.615
58.615 ≤ EffectiveStress ≤ 88.33
88.33 ≤ EffectiveStress ≤ 127.95
127.95 ≤ EffectiveStress ≤ 167.57
167.57 ≤ EffectiveStress ≤ 197.285
EffectiveStress ≥ 197.285
Varriable not in database

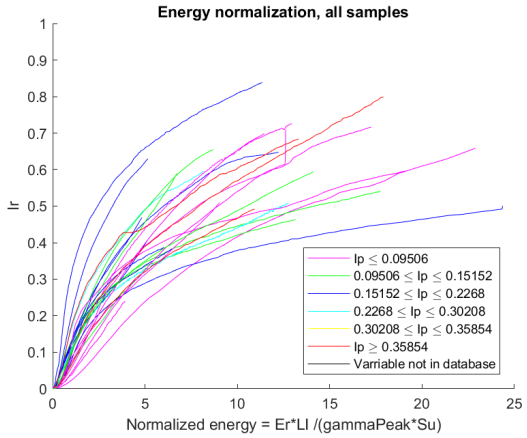
Energy normalization, all samples
Ir
Normalized energy = Er*LI /(gammaPeak*Su)
Ip ≤ 0.09506
0.09506 ≤ Ip ≤ 0.15152
0.15152 ≤ Ip ≤ 0.2268
0.2268 ≤ Ip ≤ 0.30208
0.30208 ≤ Ip ≤ 0.35854
Ip ≥ 0.35854
Varriable not in database

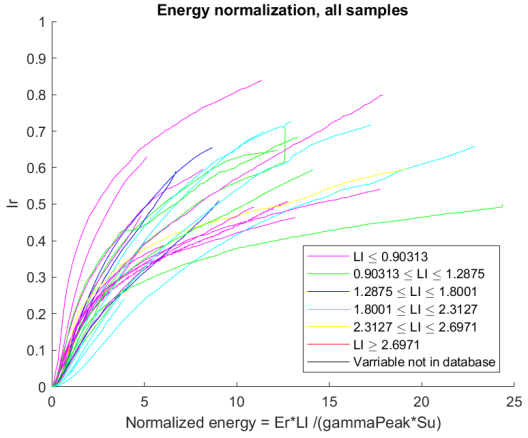
Energy normalization, all samples
Ir
Normalized energy = Er*LI /(gammaPeak*Su)
LI ≤ 0.90313
0.90313 ≤ LI ≤ 1.2875
1.2875 ≤ LI ≤ 1.8001
1.8001 ≤ LI ≤ 2.3127
2.3127 ≤ LI ≤ 2.6971
LI ≥ 2.6971
Varriable not in database

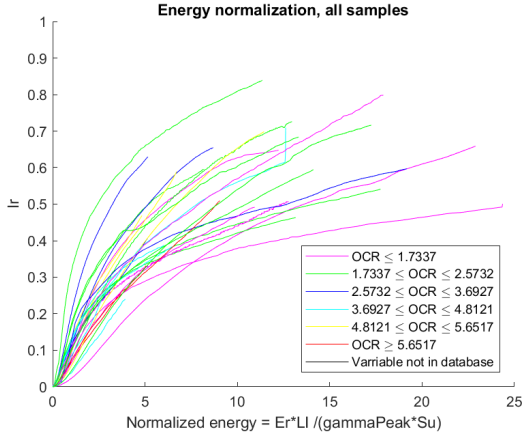
Energy normalization, all samples
Ir
Normalized energy = Er*LI /(gammaPeak*Su)
OCR ≤ 1.7337
1.7337 ≤ OCR ≤ 2.5732
2.5732 ≤ OCR ≤ 3.6927
3.6927 ≤ OCR ≤ 4.8121
4.8121 ≤ OCR ≤ 5.6517
OCR ≥ 5.6517
Varriable not in database

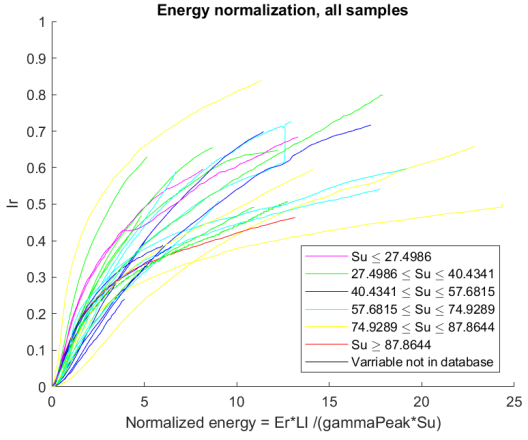
Energy normalization, all samples
Ir
Normalized energy = Er*LI /(gammaPeak*Su)
Su ≤ 27.4986
27.4986 ≤ Su ≤ 40.4341
40.4341 ≤ Su ≤ 57.6815
57.6815 ≤ Su ≤ 74.9289
74.9289 ≤ Su ≤ 87.8644
Su ≥ 87.8644
Varriable not in database

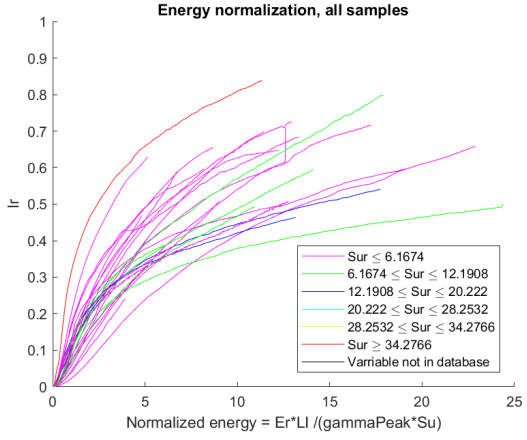
Energy normalization, all samples
Ir
Normalized energy = Er*LI /(gammaPeak*Su)
Sur ≤ 6.1674
6.1674 ≤ Sur ≤ 12.1908
12.1908 ≤ Sur ≤ 20.222
20.222 ≤ Sur ≤ 28.2532
28.2532 ≤ Sur ≤ 34.2766
Sur ≥ 34.2766
Varriable not in database

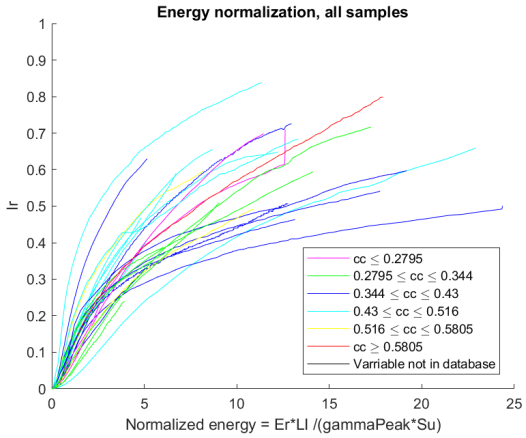

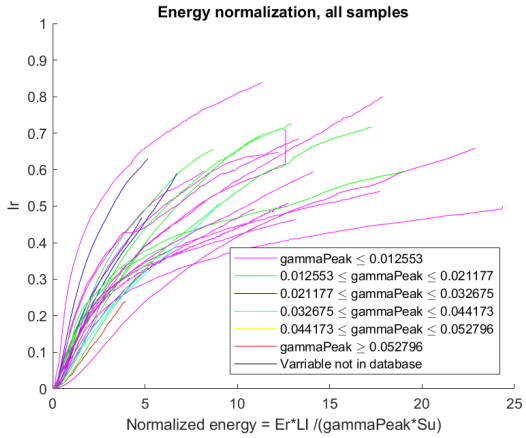

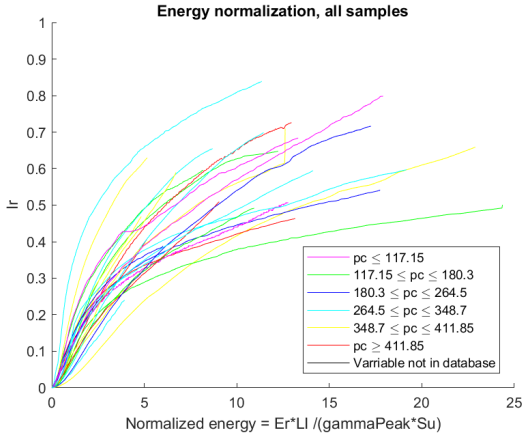

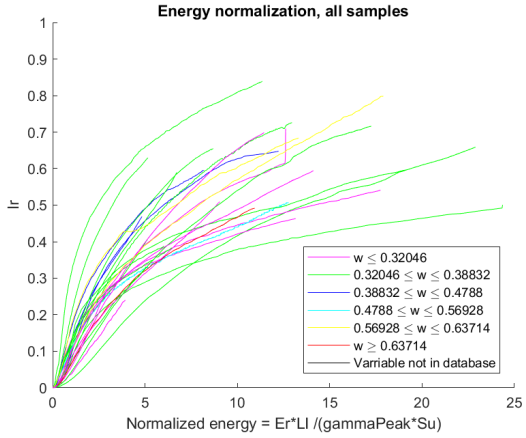

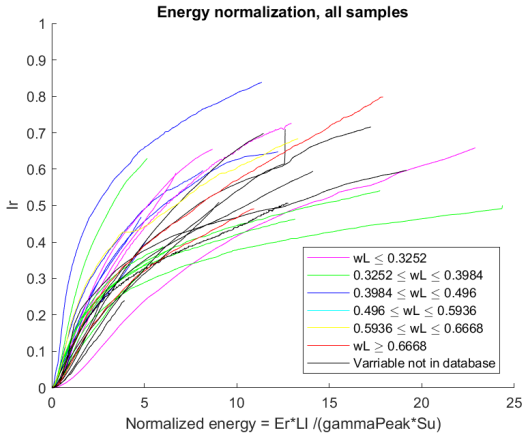

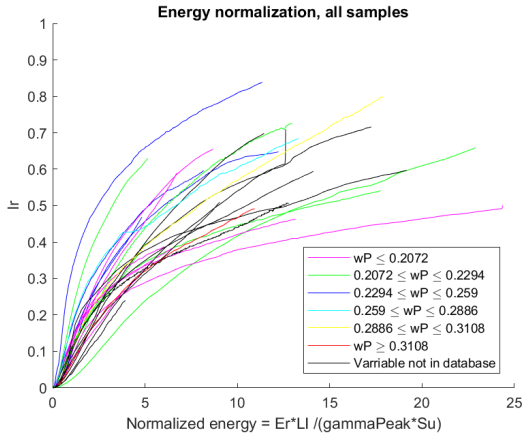

C.5 Final Normalization

Figures in this appendix shows Er $\cdot$ $IL^{0.5}/(gamma_p \cdot Su)$ vs Ir, with the spread of a normalization parameter emphasized in colours.

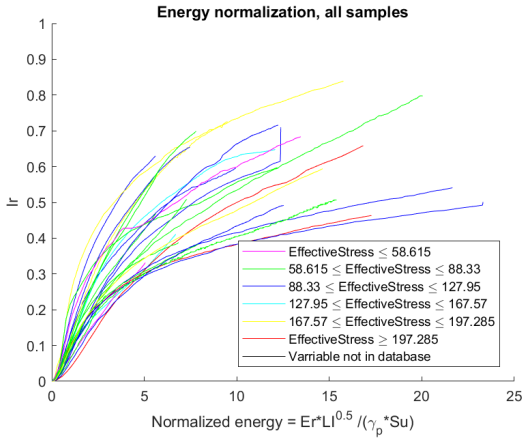
Energy normalization, all samples
Ir
Normalized energy = Er*LI^0.5 /(γp*Su)
EffectiveStress ≤ 58.615
58.615 ≤ EffectiveStress ≤ 88.33
88.33 ≤ EffectiveStress ≤ 127.95
127.95 ≤ EffectiveStress ≤ 167.57
167.57 ≤ EffectiveStress ≤ 197.285
EffectiveStress ≥ 197.285
Varriable not in database

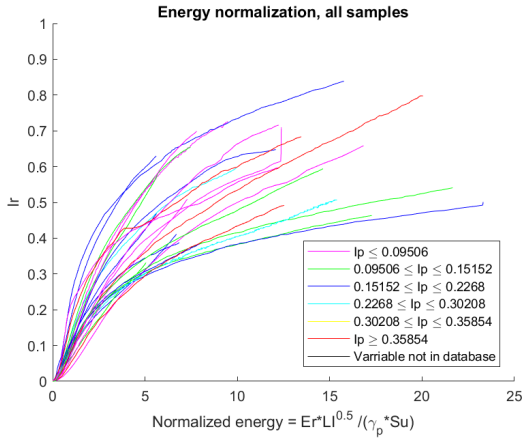
Energy normalization, all samples
Ir
Normalized energy = Er*LI^0.5 /(γp*Su)
Ip ≤ 0.09506
0.09506 ≤ Ip ≤ 0.15152
0.15152 ≤ Ip ≤ 0.2268
0.2268 ≤ Ip ≤ 0.30208
0.30208 ≤ Ip ≤ 0.35854
Ip ≥ 0.35854
Varriable not in database

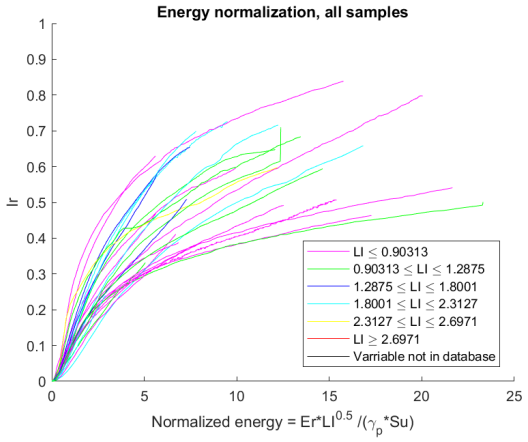
Energy normalization, all samples
Ir
Normalized energy = Er*LI^0.5 /(γp*Su)
LI ≤ 0.90313
0.90313 ≤ LI ≤ 1.2875
1.2875 ≤ LI ≤ 1.8001
1.8001 ≤ LI ≤ 2.3127
2.3127 ≤ LI ≤ 2.6971
LI ≥ 2.6971
Varriable not in database

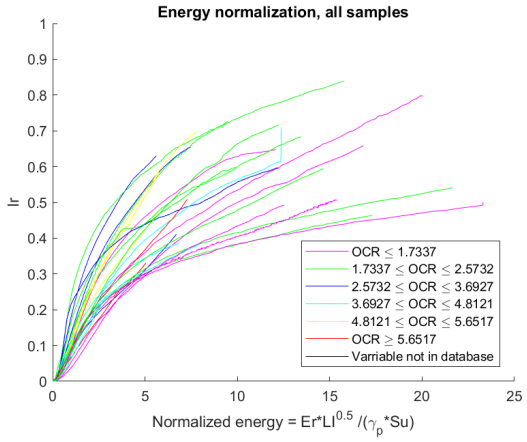
Energy normalization, all samples
Ir
Normalized energy = Er*LI^0.5 /(γp*Su)
OCR ≤ 1.7337
1.7337 ≤ OCR ≤ 2.5732
2.5732 ≤ OCR ≤ 3.6927
3.6927 ≤ OCR ≤ 4.8121
4.8121 ≤ OCR ≤ 5.6517
OCR ≥ 5.6517
Varriable not in database

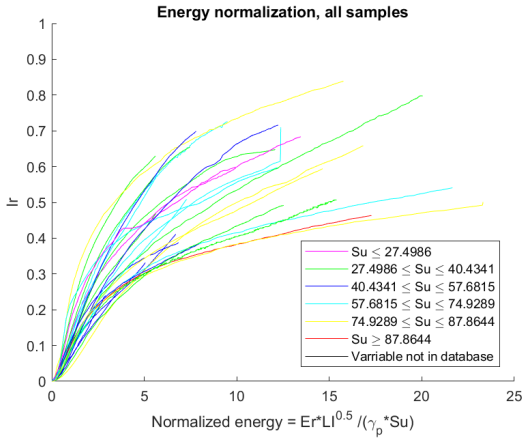
Energy normalization, all samples
Ir
Normalized energy = Er*LI^0.5 /(γp*Su)
Su ≤ 27.4986
27.4986 ≤ Su ≤ 40.4341
40.4341 ≤ Su ≤ 57.6815
57.6815 ≤ Su ≤ 74.9289
74.9289 ≤ Su ≤ 87.8644
Su ≥ 87.8644
Varriable not in database

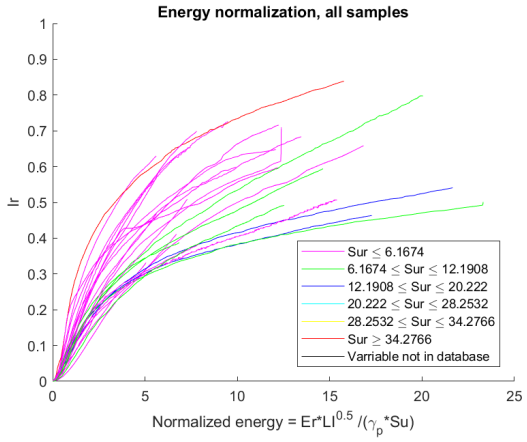
Energy normalization, all samples
Ir
Normalized energy = Er*LI^0.5 /(γp*Su)
Sur ≤ 6.1674
6.1674 ≤ Sur ≤ 12.1908
12.1908 ≤ Sur ≤ 20.222
20.222 ≤ Sur ≤ 28.2532
28.2532 ≤ Sur ≤ 34.2766
Sur ≥ 34.2766
Varriable not in database

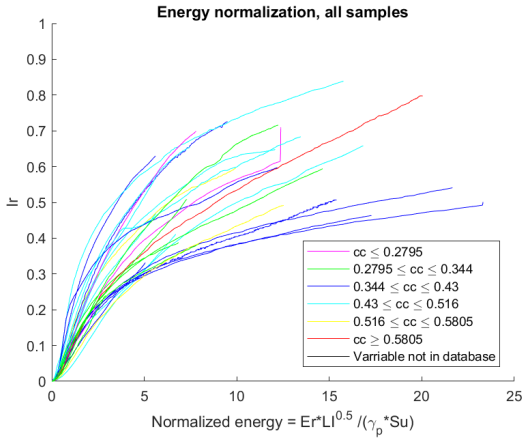
Energy normalization, all samples
Ir
Normalized energy = Er*LI^0.5 /(γp*Su)
cc ≤ 0.2795
0.2795 ≤ cc ≤ 0.344
0.344 ≤ cc ≤ 0.43
0.43 ≤ cc ≤ 0.516
0.516 ≤ cc ≤ 0.5805
cc ≥ 0.5805
Varriable not in database

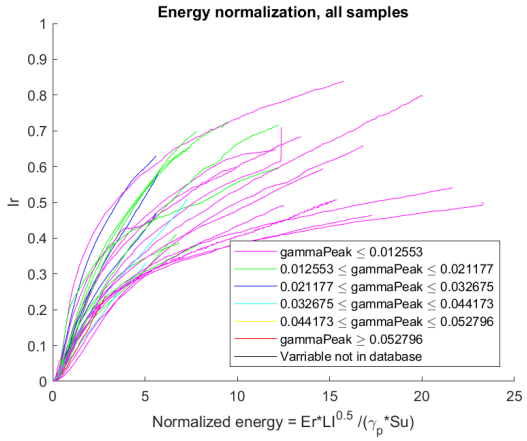
Energy normalization, all samples
Ir
Normalized energy = Er*LI^0.5 /(γp*Su)
gammaPeak ≤ 0.012553
0.012553 ≤ gammaPeak ≤ 0.021177
0.021177 ≤ gammaPeak ≤ 0.032675
0.032675 ≤ gammaPeak ≤ 0.044173
0.044173 ≤ gammaPeak ≤ 0.052796
gammaPeak ≥ 0.052796
Varriable not in database

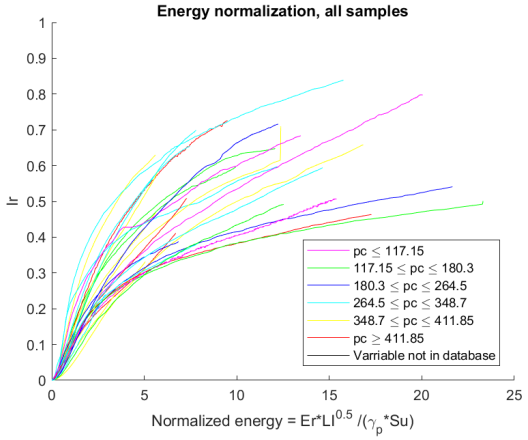
Energy normalization, all samples
Ir
Normalized energy = Er*LI^0.5 /(γp*Su)
pc ≤ 117.15
117.15 ≤ pc ≤ 180.3
180.3 ≤ pc ≤ 264.5
264.5 ≤ pc ≤ 348.7
348.7 ≤ pc ≤ 411.85
pc ≥ 411.85
Varriable not in database

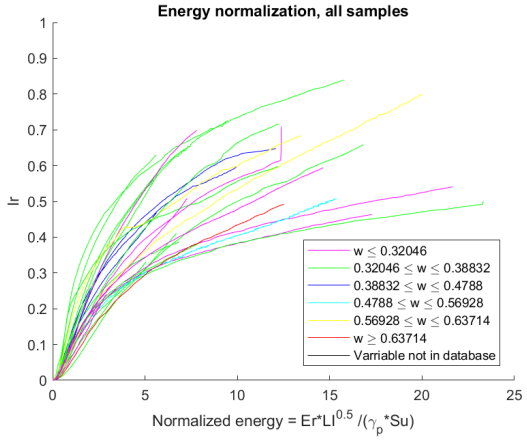
Energy normalization, all samples
Ir
Normalized energy = Er*LI^0.5 /(γp*Su)
w ≤ 0.32046
0.32046 ≤ w ≤ 0.38832
0.38832 ≤ w ≤ 0.4788
0.4788 ≤ w ≤ 0.56928
0.56928 ≤ w ≤ 0.63714
w ≥ 0.63714
Varriable not in database

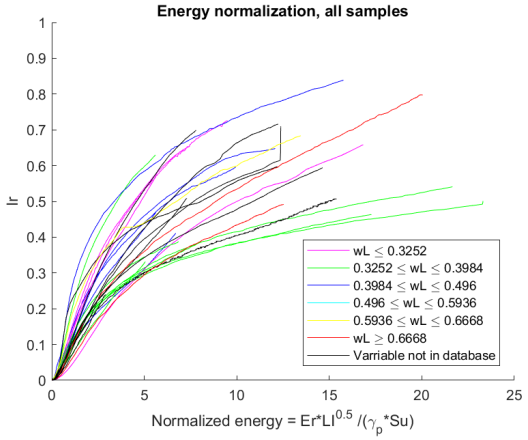
Energy normalization, all samples
Ir
Normalized energy = Er*LI^0.5 /(γp*Su)
wL ≤ 0.3252
0.3252 ≤ wL ≤ 0.3984
0.3984 ≤ wL ≤ 0.496
0.496 ≤ wL ≤ 0.5936
0.5936 ≤ wL ≤ 0.6668
wL ≥ 0.6668
Varriable not in database

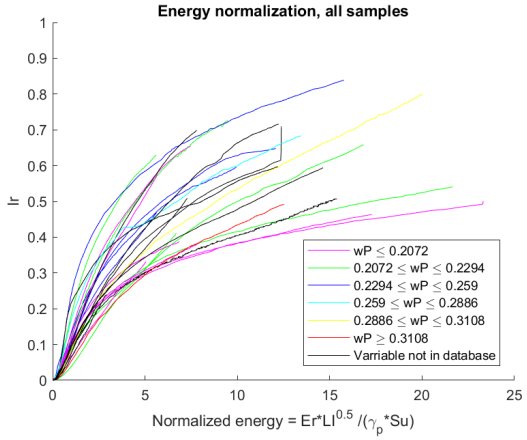
Energy normalization, all samples
Ir
Normalized energy = Er*LI^0.5 /(γp*Su)
wP ≤ 0.2072
0.2072 ≤ wP ≤ 0.2294
0.2294 ≤ wP ≤ 0.259
0.259 ≤ wP ≤ 0.2886
0.2886 ≤ wP ≤ 0.3108
wP ≥ 0.3108
Varriable not in database